Resonant Tunnelling Diodes for Millimetre and Sub-Millimetre Wave Mixing Applications

Mussa Farag Mussa Elsaadi

Submitted in accordance with the requirements for the degree of

Doctor of Philosophy

The University of Leeds
Institute of Microwaves and Photonics
School of Electrical and Electronic Engineering

June 2016

Declaration of Academic Integrity

The candidate confirms that the work submitted is his own, except where work which has formed part of jointly authored publications has been included. The contribution of the candidate and the other authors to this work has been explicitly indicated below. The candidate confirms that appropriate credit has been given within the thesis where reference has been made to the work of others.

The down conversion mixing design, shown in Chapter 4, was presented in the following paper:

- *M. Elsaadi, D. P. Steenson, I. D. Robertson, and V. Doychinov, "A 320GHz low drive level sub-harmonic mixer based on quantum barrier junctions," in Infrared, Millimeter, and Terahertz waves (IRMMW-THz), 2015 40th International Conference on, 2015, pp. 1-2.*

The up conversion mixing design, shown in Chapter 5, was presented in the following paper:

- *D.P. Steenson, M. Elsaadi, I. D Robertson, V. Doychinov ''Sub-Harmonic Upconversion Mixers Based on Resonant Tunnelling Diodes at W-Band and G-Band'', in IET Colloquium on millimetre-wave Terahertz Engineering & Technology 2015, UK.*

For both papers, the author's contribution was to design the mixer circuit, present the design methodology, simulate and optimise the mixer performance, interpret the results in the form of figures and tables, and write the consistent discussion. The contribution of V. Doychinov was to provide the measured data of the RTDs, with valuable discussion regarding the simulated results. The contribution of Dr. D.P.Steenson and Prof. I.D.Robertson (author's supervisors) was to suggest the initial circuit design, provide discussions and guidance, and to revise the paper text before submitting the finial paper.

ACKNOWLEDGEMENTS

First of all, my deepest gratitude goes to Dr. DP Steenson who was my supervisor during the course of this PhD program. Many thanks to Dr.Steenson for providing me the unique opportunity to study high frequency engineering at the University of Leeds, and for all the support and guidance, including the weekly meetings and the associated valuable comments, and many others.

I would like to thank Dr.Li Chen for the cleanroom training. Likewise, I would like to express my thanks to Mr. Hamza Patel who provided the measured RTDs data. Warm thanks go to Dr.Victor Doychinov for his discussions regarding the stimulation on joint research interests, and for his help with the 3D split-blocks design.

Many thanks to all IMP PhD students for the great time throughout my PhD program. I would like to thank my parents for their unlimited support during my study. Also, my gratitude goes to my wife for her patient and daily support.

ABSTRACT

This Thesis primarily aims to explore potential applications of Resonant Tunnelling Diodes (RTDs) as non-liner elements in sub-harmonic millimetre and sub-millimetre wave mixing circuits.

The primary intention of this research work was to evaluate a topology for a sub-harmonic down conversion mixer exploiting the fourth harmonic of a LO signal. Designs were evaluated by simulation at 640GHz and 320GHz with the aim of exploring the potential of a RTD based down-converter at 640GHz, in the 580-750GHz atmospheric window, with an intermediate frequency signal in the range around 2GHz by mixing with the fourth harmonic of a 159.5GHz LO signal. Related design studies were undertaken at 320GHz which gave a simulated single side band (SSB) conversion loss of 5.7dB, and with a LO power requirement of less than -9.5dBm which vindicated the principle, as far as the design stage is concerned, of using RTDs as the non-linear mixing element, where the layer design can be tailored to favour very low pump powers.

The other, related, target of the current PhD work was to also explore the potential for high LO drive level mixers and their up-conversion efficiencies using the same novel devices, i.e. RTDs, but with a different layer design, better suited to support high pump powers in this instance. For achieving the latter goal, two different sub-harmonic up-conversion mixers employing a single RTD and using the second harmonic of an LO signal were designed and evaluated at two different frequencies. The first mixer design was aimed at 180 GHz providing -7.5dBm of output power while the second one should work at 110GHz showing output power in the range of -4dBm, and was used to initially evaluate the approach and which could, in principle, be later fabricated and measured.

All these down and up-conversion mixers were carefully designed using ADS and HFSS and evaluated using two different technologies, microstrip and Grounded Coplanar Waveguide (GCPW), and both compared with a nearest Schottky diode based approaches, and also their physical mask was produced in anticipation of a later fabrication stage.

Table of Contents

List of Figures

List of Tables

List of Abbreviations

ADS	Advanced Design System.
APDP	Anti-parallel diode pair.
CAD	Computer-aided design.
CL	Conversion Loss.
DBQW	Double Barrier Quantum Well.
E_C	Conduction Band Energy.
E_V	Valence Band Energy.
E_F	Fermi-level.
EM	Electromagnetic.
F_{IF}	Output signal (intermediate frequency).
F_{LO}	Local oscillator frequency.
FIR	Far-infrared.
F_{RF}	Signal frequency (Radio frequency).
GCPW	Grounded Coplanar Waveguide.
HBT	Heterojunction bipolar transistor.
HFSS	High frequency structural simulator.
HEB	Hot-electron bolometers.
HEMT	High electron mobility transistors.
I_S	Saturation current.
IMPATT	IMPact ionization Avalanche Transit-Time.
LO	Local Oscillator.
MBE	Molecular Beam Epitaxy.

NDR	Negative Deferential Resistance.
QBDs	Quantum Barrier Devices.
QCL	Quantum Cascade Laser.
RF	Radio Frequency.
RWG	Rectangular Waveguide.
RTD	Resonant Tunneling Diode.
SIS	Superconductor- insulator-superconductor.
SDD	Symbolically-Defined Device.
TD	Tunnelling Diode.
TE	Transverse Electrical.
TM	Transverse Magnetic.
TUNNETT	Tunnel injection transittime.
THz	Terahertz.
n	Mixing order.
V_{th}	Thermal voltage of the diode.
V_{RF}	Signal frequency voltage.
V_{LO}	Local oscillator voltage.
V_{bias}	Bias voltage.
VNA	Vector Network Analyser.
Z_0	Characteristic impedance.

Chapter 1 Introduction

1.1 A brief Overview

Millimetre waves (mm waves) are located within the 30GHz-300GHz frequency band, between 10mm-1mm wavelengths. These are followed by the sub-mm wave region, commonly referred to as the lower end of the terahertz (THz) gap, which extends from 300 to 3000GHz, and the wavelength correspondingly ranges from 1mm to 0.1 mm, and are surrounded by the microwave and the far-infrared region on the electromagnetic spectrum. Although appreciable advances have already been achieved covering a wide range of potential applications, this interesting frequency region still merits more systems development not only in terms of generating signals from solid state sources with adequate power, but detecting signals at low Local Oscillator (LO) pump powers as well. Especially low LO powers, in the presence of typically weak signals such that the high power end of the dynamic range is not an issue, consequently favour systems using multi-element detection for faster scanning in either imaging or beam-steering applications. For such crucial reasons the THz gap is being extensively exploited by decreasing and increasing the wavelength of electronics and photonic devices respectively.

The mm waves, more relevant to the current work, have different atmosphere attenuation rates at different wavelengths (frequencies), resulting in various applications such as communications, scientific research, imaging for security applications, radar, atmospheric sensing, medical and other potential applications. For mobile communication, for example, the demand of wireless technology and related area networks has increased throughout the last three decades, and its performance in terms of the data rates was noticeably improved every single decade from the beginning of 1980's as shown in Table 1.1 starting at the first generation 1G to 4G and the potential upcoming 5G[1]. The Bluetooth and standards such as IEEE802.11a/b/g and ultra-wideband (UWB) are typically operated below 10GHz where the spectrum is likely to be congested in near future[2]. Furthermore, very high capacity is required for multimedia communications, therefore the need to move up to the mm wave lengths is required to contend with such requirements. Exploiting the mm wave band in applications such as data transmission and sensing systems has some advantages[3] such as: wide bandwidth leading to high data rates; penetration through snow, dust and fog, which is significantly better than for the optical wave lengths; compact systems with high beam resolution are possible since these shortwave lengths result in a reasonable size antenna with a high directivity and, lastly, transceivers within mm wave band can be adapted to monolithic and integrated design approaches, resulting in compact systems at inexpensive costs.

Table 1.1: The improvement technologies of mobile wireless communication.

Technology Generation	Speed (kbps)	Year
1G	2.4	1980
2G	64	1990
3G	200	2000
4G	100,000	2011
5G	Expected a few Gbps	Expected in 2020

Although there is still available space in the spectrum within the mm wave range, some factors should be considered such as the rainfall and atmospheric gases absorption, regarding the propagation of line of sight and the free space loss[4].

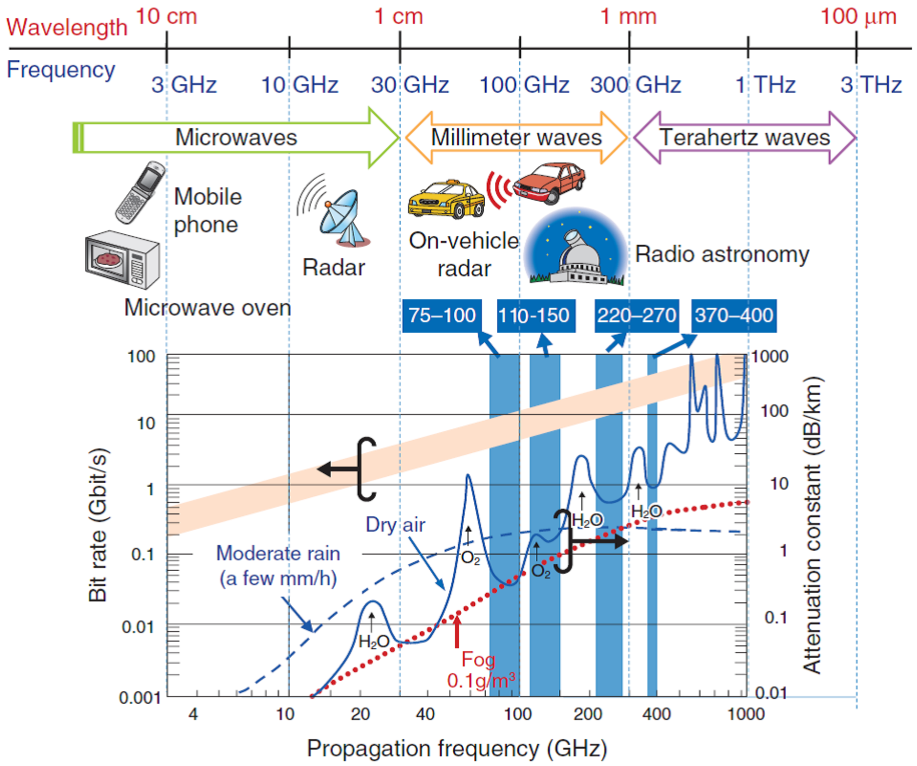

Figure 1.1: mm wave attenuation by water vapour and atmospheric oxygen[4].

Unlike the microwave range of signals, as shown in Figure 1.1, the mm wave signals are greatly affected by the absorption of atmospheric gases rain and water vapour at which the operating frequency of radar or communication systems is determined by the transmission distance, leading to short and long-range communications. For instance the rain drop dimension at this band is comparable to the wavelength, and the energy loss is a strong function of the rainfall magnitude[5]. Although the attenuation is very high, it can be a key benefit to provide further spatial isolation and higher implicit security. This also permits the control of the transmission range by adjusting the frequency without causing interference. Windows with low attenuation at 35GHz, 94GHz, 140GHz, 220GHz and 340 GHz can be exploited for large range transmission such as satellite communications, mm wave backhaul and point to multi-point communications. Among these bands, the 60 GHz unlicensed frequency band has occupied a great place for short range communications where the available bandwidth is wider when compared to microwave systems. Figure 1.2 shows the unlicensed band around 60 GHz in different countries, whereas The Table 1.2 summarizes the main differences between the radio and the mm channels in terms of some figure of merits such as path losses, output power, antenna performance and the related bandwidth and data rates.

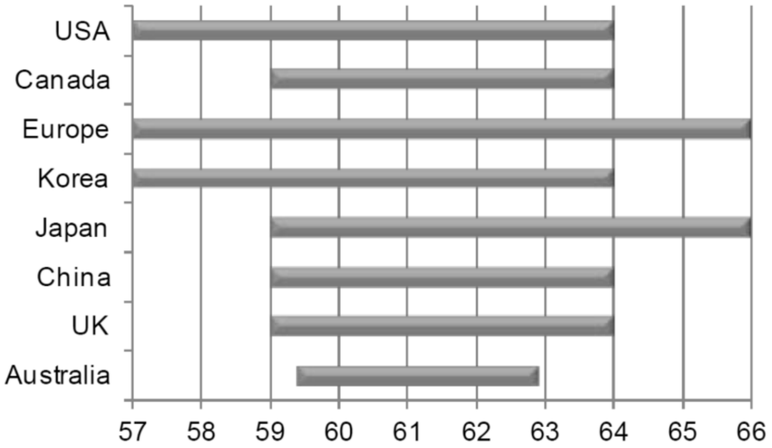

Figure 1.2: The unlicensed band around 60 GHz at different countries[6].

Table 1.2: The differences between the conventional and the mm communication[7].

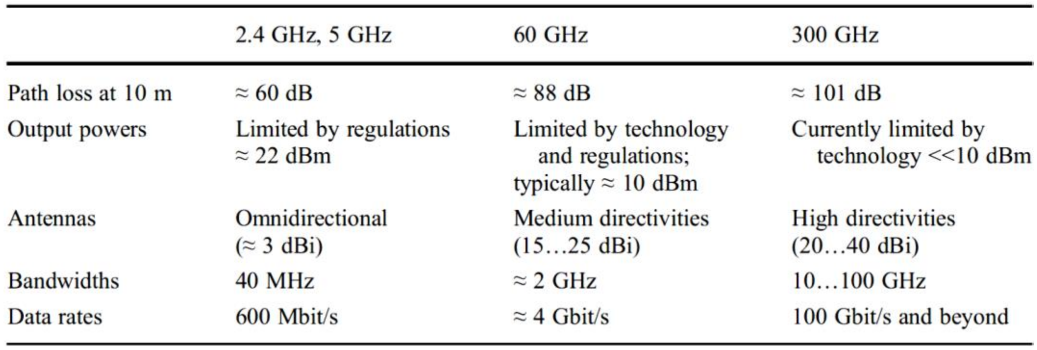

	2.4 GHz, 5 GHz	60 GHz	300 GHz
Path loss at 10 m	≈ 60 dB	≈ 88 dB	≈ 101 dB
Output powers	Limited by regulations ≈ 22 dBm	Limited by technology and regulations; typically ≈ 10 dBm	Currently limited by technology <<10 dBm
Antennas	Omnidirectional (≈ 3 dBi)	Medium directivities (15…25 dBi)	High directivities (20…40 dBi)
Bandwidths	40 MHz	≈ 2 GHz	10…100 GHz
Data rates	600 Mbit/s	≈ 4 Gbit/s	100 Gbit/s and beyond

For scientific research applications, the operating frequency for both radio astronomy and remote sensing is typically in the millimetre wave range, i.e. for investigating star formation and space research[8]. Radio astronomy based in ground stations is strongly affected by the site's altitude because of atmospheric absorption, while some remote sensing satellites, however, are capable of determining the upper atmosphere temperature by taking the measurement of oxygen molecule radiation as a function of both pressure and temperature. The climate sensing and meteorological applications, also, find millimetre wave range useful for atmospheric monitoring purposes[9]. For imaging and security purposes, different mm wave bands with both low and high atmospheric attenuation, as shown in Figure 1.1, are employed for active and passive systems. The major exploited frequencies are around 183GHz, 94GHz and 77GHz where the signals have specific properties leading to the penetration of some materials such as clothing, plastic, and also through rain and fog. A clear example of the mm wave image systems are the body scanners in airports to provide physical security[10]. As the mm waves are naturally non-ionizing, they also find some use in biology and medicine where the low intensity waves with frequencies around 42.2 GHz, 53.6GHz, and 61.2 GHz are commonly used for tumour treatment using radiation therapy, hyperthermia[11].

1.2 Literature review

Technologically speaking, in order to effectively build ultra-high frequency systems, the dimensions of a device structure need to be scaled down to the micron or sub-micron range at which the quantum mechanical regime may become important. From a classical physics point of view, when the kinetic energy of a particle (i.e. an electron) is higher than a potential barrier, this electron is capable of overcoming that barrier. In contrast to this classical view, in quantum mechanics there is still a probability for electrons to tunnel through one side of a thinner potential barrier, and then appear on the other side; even if these electrons have energy less than the barrier height.

Likewise, semiconductor devices with ultra-thin barriers can trace similar non-linear behaviour if two different band gap materials are layered on top of one another. Alternatively, ultra-thin potential barriers in semiconductors can be created using abrupt doping, such as a p^+- n^+ homo-junction. Basically, this tunnelling behaviour in semiconductor tunnel diodes can be one of two main types, namely inter-band tunnelling and intra-band tunnelling. The first type implies that electrons flow into valence band from the conduction band; such type of tunnelling can be realized in bipolar devices with both n-type and p-type doping. In the second case, intra-band tunnelling, the tunnelling is from/to the same band, i.e., electrons tunnel from states in the conduction band to unoccupied states in the conduction band. This type of tunnelling is the mechanism of Double Barrier Quantum Well Resonant Tunnelling Diodes (DBQW-RTDs) which gives rise to the non-linear current voltage behaviour and is the heart of non-linear elements on which this thesis is focused. More details regarding intra-band tunnelling will be given in Chapter 2 when the RTD's operation principle is described. As the current research work was intended to explore the design of high frequency mixers for both down and up-mixing purposes, a literature review will present some related device reviews reserved either for generating or detecting high frequency signals.

It is a useful and informative step to firstly take a closer look at the available output powers at the mm and sub-mm wave regions since the major objective of this thesis is to explore high drive level mixers and high conversion efficiencies through designing millimeter up-conversion RTD mixers which may be used occasionally as signal sources or receivers in communication systems, and where amplifiers do not yet commonly exist.

In the literature there are numerous devices exploited to detect and generate mm wave and sub-mm wave signals, which are required for a wide range of potential applications. For generating a high power signal, various common techniques are in use such as lasing, free electron lasers, frequency multiplication or negative deferential resistance (NDR).

A high power source based on the principles of Lasing is an optical amplification process, i.e., stimulated emission of energy generating electromagnetic radiation, where an electron is emitted from a higher to a lower energy state, accompanying photon (light) at the similar frequency and phase[12]. The two most used lasers are far-infrared (FIR) gas laser and quantum cascade lasers (QCLs). A commercial sub-type of FIR pumped gas laser is a carbon dioxide (CO_2) laser at which a tube filled with methanol molecules (CH_3OH) is stimulated by a CO_2 laser to generate signals in the range of FIR frequencies[13]. The FIR gas laser is capable of generating a signal of 2.5THz with output power of 100mW. This result requires liquid cooling of the CO_2 and FIR cavities[14], inherently causing higher cost and bulky physical size. However, more recently the QCL can be a substitute for the FIR gas laser in many occasions. QCLs are solid state laser devices based on a set of quantum wells to confine particles. In 2004, Williams[15] introduced a QCL operating at 2.1THz, the lowest frequency to bridge the THz gap, with a power of 1.2mW at a temperature around 17K. Similar to FIR lasers the QCLs require a bulk cooling-in their case cryogenic-temperature system, which limits their use in some applications where portable devices are required.

Another method to generate THz radiation is to exploit vacuum tube based approaches such as free electron and slow wave devices such as the Gyrotron and backward wave oscillators (BWOs). Using a Gyroton, signals in the range of mm frequencies can be generated by stimulating charged particles under the influence of a heavy-duty magnetic field. A high power on order of kilowatts and even up to Megawatts can be offered by the Gyroton[16]. The other traveling-wave tube sources are BWOs at which a heated cathode radiates a beam of electrons that are collimated by a high magnetic field, and typically with applied accelerating voltage in range of 1-10 kilowatts. The resultant BWO’s output power is around 1mW at THz frequencies[17]. In general, free electron devices require strong electro and magnetic fields and are physically large and heavy as well.

Alternatively for very compact systems, high frequency signals can be generated by frequency multiplication in such a way that higher power low microwave frequency signals are up-converted using non-liner elements used typically as doublers, triplers or cascaded multipliers, up to about the 9th harmonic. These non-liner devices (varactors or varistors) exploit the high power low frequency input signals to produce high frequency signals used as effective local oscillator power sources, each conversion stage is only around 1-2% efficient. Although for zero biased Schottky based mixers the output powers are usually in the range of 1-10mW. The most widely used non-linear devices in THz range are planar Schottky diodes, which are capable of delivering around 0.5µW at 2THz based on a tripler circuit[18], but the phase noise is high as corresponding to the frequency multiplication factor, and also they suffer from lower power efficiency and their lifetime can be relatively short[19], if the first diode is driven very hard.

Other THz sources can be produced using two terminal negative deferential resistance (NDR) electronic devices. These comprise both fundamental and harmonic power generators such as tunnel injection transit-time (TUNNETT) diodes[20], impact avalanche transit-time (IMPATT) diodes and transferred electron (Gunn) diodes[21]. Other three terminal devices are predominantly used for amplification at lower frequencies such as high electron mobility transistors (HEMT)[22] and heterojunction bipolar transistors (HBT)[23]. With sufficient positive feedback then these three terminal devices can be deliberately made to become unstable and thus generate mm-wave power. At lower frequencies (below 100GHz) these three terminal devices are sometimes used as harmonic converters and mixers with conversion gain, but at higher frequencies because of the complexity and degree of difficulty in making the three terminal devices then two terminal mixers or multipliers based on Schottky diodes are commonplace[24].

Previously Esaki tunnel diodes (which will be discussed more fully in chapter 2) were preferred for very low power signal detection. However their high specific capacitance and the link between high doping levels and the tunneling characteristic meant that their use was often restricted to the threshold of mm wave frequencies. Other quantum barrier devices such as resonant tunneling diodes (RTDs), also discussed in Chapter 2, offer all the strengths of the Esaki tunnel diodes but with a much lower specific capacitance and independent control of the tunneling characteristics and the doping, which is why they feature in this study.

As an overview of the available power from different semiconductor devices at millimeter wave frequencies and beyond, Figure 1.3 shows the output power levels previously achievable. The typical wall plug efficiency of these devices is in the range of 2-4%[25], excluding QCLs which are below 2% in continues-wave (CW) operation and with very low cooling temperature requirements[26]. Among all these, the highest frequency produced so far is by RTDs as fundamental oscillators, efficiently operating at room temperature.

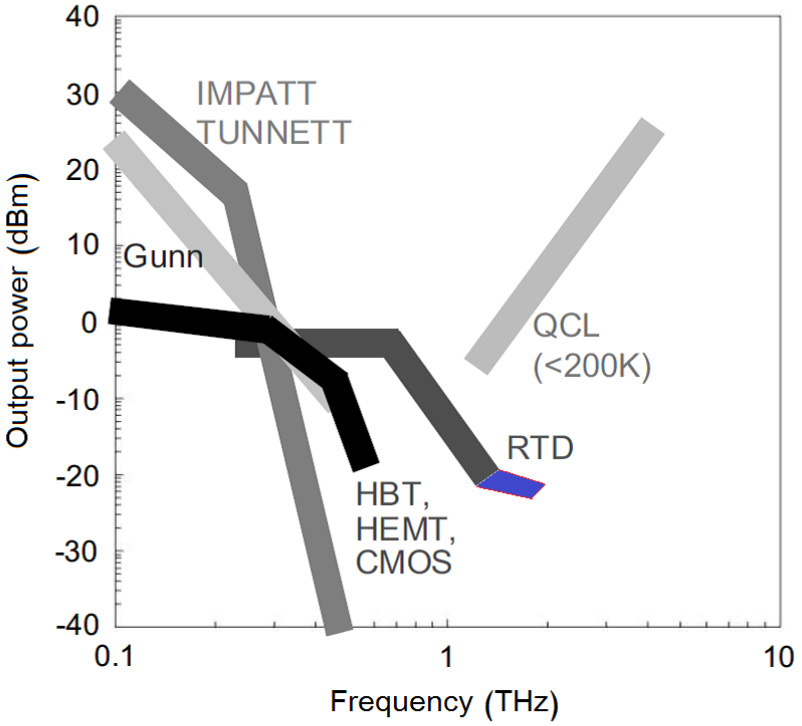

Figure 1.3: RF power levels for various electronic devices, adapted from[27].

Back in the beginning of the 1980s, the RTD's operating frequency was expected to reach around 2.5THz[28], and ten years later, it was mentioned they could operate at around 4THz[29]. The achieved frequencies, however, were 56GHz and 712GHz in 1987[30] and 1991[31] respectively. After these two initial experimental results and for twenty-year gap, many scientific efforts could not extend the RTD's operating frequency. However, the RTDs were recently improved by focusing on the planner embedding circuit and integrated antenna, and demonstrated up to 1THz in 2010[32] and the operating frequency was rapidly increased through the most recent five years, as shown in Table 1.3.

Table 1.3: The recent advancement frequency of RTD.

Frequency (THz)	Year	Reference
0.056	1987	[30]
0.712	1991	[31]
1	2010	[32]
1.1	2011	[33]
1.31	2012	[34]
1.42	2014	[35]
1.92	2016	[36]

However, from a detection perspective, the most common mixing devices used for sensitive heterodyne receiving applications are hot-electron bolometers (HEB), superconductor- insulator-superconductor (SIS) and Schottky diodes. SIS[37] and HEB[38] based mixers show excellent sensitivity and dominate ground based radio astronomy applications, but their super-cooled nature makes them expensive, power hungry and difficult to use. SIS tunnel junction was presented for the first time by Dayem in 1962[39], basically created by aluminium oxide insulator layer surrounded by two superconducting layers of niobium. SIS mixers have occupied a great place in high frequency receiving applications, mainly for heterodyne spectroscopy. This superconducting device has proven to be indispensable for use in the millimeter-wave region and up to 1.4THz[40] . Alternatively, HEB mixers, which depend on the bolometric effect that employs the highly non-linear relationship between the resistance and the temperature of a superconductor whilst held at just below the critical temperature, have presented great performance compared to SIS tunnel junctions in THz region, in that, a frequency of 2.8THz was reported[41] with noise temperature of 1050K, and a receiver operating at 4.3THz with noise temperature of 1300K was demonstrated as well[42]. However, at room temperature and for millimeter-wave signals Schottky diode based mixers are the work-horse of super-heterodyne detection, even though they typically have less sensitivity and require very significantly larger LO power, they are ultimately capable of providing frequency conversion up to 5THz[43] which tends to be limited more by the LO power and frequency. Historically GaAs whisker contacted Schottky diodes were widely employed as non-linear elements in high frequency mixing applications. The main obstacle with whisker Shottky diodes is their susceptibility to vibration and the lack of integration with other structures, and for this key reason the planer technology has been introduced and optimized for more than twenty years now. Typically, a conversion loss on the order of 8dB at room temperature can be offered by Schottky mixers at 0.5THz with around 1800K noise temperature[44]. Recent operating frequencies for Schottky diodes as sub-harmonic mixers were demonstrated at 2.5THz[45] and 4.7THz[46].

This thesis aims to explore the potential applications of Resonant Tunnelling Diodes (RTDs), as non-linear elements in mm and sub-mm wave mixing circuits, where the I-V characteristic can be intrinsically anti-symmetric and where the degree of nonlinearity can be controlled using several parameters. This approach can be based largely on similar anti-parallel Schottky diode pair approaches (detailed in subsection 4.2.2). A reconsideration of previous published work based on anti-parallel Schottky diode pair is a reasonable step to set the scene and validate the RTD’s performance. Table 1.4 summarizes Schottky diodes in terms of the conversion loss (power efficiency) as a function of local oscillator (LO) pumped power for a range of different frequencies.

Table 1.4: Sub-harmonic Schottky mixers performance at high frequencies.

Frequency (GHz)	CL (dB) *simulated	LO Harmonic number (n)	LO Power (dBm)	Reference
182	12.7	n=2	+6.5	[47]
170 - 210	16-12	n=2	+10	[48]
215 - 225	8.2*	n=2	-	[49]
230	10.9	n=2	4.7	[50]
320	9	n=2	6	[51]
330	6.3	n=2	5	[52]
330	10	-	20	[53]
340	10.1/7.3* SSB	n=2	6	[54]
361	15*	n=2	6	[55]
366	6.9	n=2	8.7	[56]
380	8	n=2	-	[57]
400	8	n=2	7	[58]
520	7.7	-	-	[59]
540	12	-	-	[59]
590	14	n=2	6	[60]
600	15*	n=4	-	[61]
614	12	n=2	-	[62]
640	9	n=2	-	[51]
650	10	n=2	-	[62]

As can be obviously realized from this table, the typical conversion loss at sub-mm wave frequencies is around 8 dB below 500GHz and 10-12dB above, while the pumped LO power is on order of 6 dBm. These values will serve as a reference level when the RTD results are presented and evaluated later in this thesis.

1.3 Thesis objectives

Apart from the fundamental frequency generation (sources), a non-linear element with an anti-symmetric I-V characteristic is required to provide efficient sub-harmonic mixing. For a long time, the only alternative for realizing an anti-symmetric I-V characteristic was a Schottky diode pair, forming a linked back-to-back structure with the anode of one diode connected to the cathode of the other. However, a certain type of quantum barrier device (QBD), known as a resonant tunnelling diode (RTD), has a single junction, or more correctly a series of hetero-structure barriers, which are capable of producing the same anti-symmetric I-V curve, and whose performance in the context of a sub-harmonic down conversion mixer is investigated in this thesis, and with the primary aim of exploring efficient mixing with very low LO powers. A sub-harmonic number of four (n=4) was chosen as a compromise between n=2 and higher even harmonics and to favour pumping by a much lower LO frequency where ample power is readily available yet still be extended to signal frequencies of 500-1000GHz. The ultimate goal of the work is to realize a mixer design which is capable of detecting signals in the 580-750GHz atmospheric window, whilst using a 150-190GHz LO, and where x’s 3 varactor multipliers are able to supply 10’s of mW’s of pump power. The investigation in this thesis is to study the design of a scaled version at 320GHz in the first instance. The other main goal of the work reported herein primarily investigates the design and potential applications of Resonant Tunnelling Diodes (RTDs) as non-liner elements in mm wave up-conversion circuits based on the 2nd sub-harmonic of a Local Oscillator (LO) pumping signal. Of primary interest in this case is the maximum power handling of the RTD based up conversion mixers which, it is hoped, will favour vacuum tube driven sub-mm wave communication systems, where output amplification is almost non-existent, and high mixing efficiency and output powers may provide a valid substitute. All these down and up-conversion mixers share similar underlying layer and device structures but the layers and conductivity profiles are optimized for either low or high pump power operation, respectively. The circuits themselves are carefully designed using Advanced Design

System (ADS) and High Frequency Structural Simulator (HFSS) and evaluated using two different technologies, microstrip and Grounded Coplanar Waveguide (GCPW), and both are compared with the nearest Schottky based approach.

1.4 Thesis organisation

This thesis is structured by chapter. Following chapter 1, the introduction, which provides a general review of mm and sub-mm devices, different applications of the RTDs are individually explored throughout the remaining chapters.

Chapter 2 gives a simple overview of the established theory behind the basic structures of Esaki tunnelling diode (ETD) and resonant tunnelling diodes (RTDs), alongside their key differences and the principle of operation and their modelling within a simulation environment.

Chapter 3 focuses on the design of transitions and device embedding structures such as antipodal finline transitions from microstrip lines to rectangular waveguides (RWG) and microstrip-to-GCPW transitions as well as GCPW-to-GCPW transitions, for use with waveguide split blocks for assembly and testing of these transitions. This work is necessary to achieve an efficient low loss broadband transition from the spatially large RWG mode to the microscopic planar modes in order to couple the EM radiation into the mixing junction. Moreover, this chapter demonstrates the design of calibration pieces for the GCPW and microstrip lines.

Chapter 4 introduces the mathematical description of mixing signals, the most common configuration of mixers, their features and common modes of operation, namely fundamental and sub-harmonic mode, including the benefits and drawbacks behind the back-to-back configuration of a Schottky diode pair. This chapter also presents the design and the results of two-different topologies of sub-harmonic down conversion mixer based on the fourth harmonic of a LO signal.

Chapter 5 explores the potential of using RTDs in a x3 frequency multiplier using polynomial-type approach in MATLAB. Furthermore, this chapter presents the design of two different sub-harmonic up-conversion mixers incorporating a single RTD with the second harmonic of a pumped LO signal, based on both the use of ADS and HFSS software.

Chapter 6 summarizes the progress made on the whole of the current work and suggests some possibilities for future related research.

1.5 Summary

This chapter presented a brief introduction on the issues related to the sub-mm wave or THz gap region of the EM spectrum, and also gave a review of the most common devices and corresponding techniques used for generating and detecting high frequency signals. However, all aforementioned devices are beyond the scope of this thesis, except the Double Barrier Quantum Well Resonant Tunnelling Diodes (DBQW-RTDs), which will be discussed more in the next chapter. Furthermore this first introductory chapter summarised previous published performance of back-to-back Schottky diodes mixers in terms of conversion loss and local oscillator power requirements, which will serve as a benchmark for the RTDs comparisons presented in this research work, as both antiparallel Schottky diode pairs and single junction RTDs exhibit similar anti-symmetric I-V characteristics.

Chapter 2 RTD Theory and Background

2.1 Chapter Objective

As the subject of the current research is concerned with the use of quantum barrier devices (i.e. RTDs), a useful step is to review some of the most relevant basic concepts, used to create and exploit such high frequency semiconductor devices, such as heterostructures, quantum well construction, tunnelling and the type of contact used between semiconductors and metals, i.e. Schottky contacts and ohmic contacts. This chapter reviews these attributes along with the growth of the structures after introducing the background theory of both Tunnel diodes (TDs) and RTDs, and ends by briefly discussing the commonly used models for representing the RTDs in simulation environments.

2.2 Tunnel diode

The p-n tunnel diode or Esaki tunnel diode (ETD) is a two-terminal semiconductor device invented in 1958 at Sony Corporation, or Tokyo Tsushin Kogyo, by Leo Esaki who received the Nobel Prize in Physics in 1973 for the first experimental demonstration of tunnelling. Historically, the current-voltage (I-V) characteristic of an Esaki's diode exhibits a unique characteristic, well-known as negative differential resistance (NDR) region. The physical structure is shown in Figure 2.1(a), where the ETD was built using different types of semiconductor materials, i.e., germanium p-n junction, with a very high doping concentration ($\geq 10^{19}$cm^{-3})[63]. At a zero-bias condition as shown in Figure 2.1(b), the states in the conduction band are filled with electrons resulting in the Fermi level moving up and into the conduction band. Likewise, the states near the top of the valence band are not filled with electrons (i.e., holes), and consequently the Fermi level goes down towards and into the valence band. As soon as a forward bias is applied, a number of electrons will have enough energy to tunnel through the barrier between the conduction band bottom of n-type to the valence band top of p-type material. A further increase of the forward bias, Figure 2.1(c), will cause more current to tunnel through the junction until a peak value (I_P) is reached, at which the bias is called peak voltage (V_P) shown in Figure 2.2. Following this peak point, any increase in the bias causes the current to decrease because there are no longer any states to tunnel into, and thus an NDR is exhibited, where at another higher bias the current has a smaller value, which is called valley current (I_V), as shown in Figure 2.2.The current after its valley point behaves as a normal current or so-called thermionic emission current. Under reverse bias condition, however, the conduction band of the n-type material has empty states permitting electrons in the p-type valence band to tunnel through the thin junction, which will create a large reverse current, depending on how much a revers bias voltage is applied. There is no NDR in this bias direction.

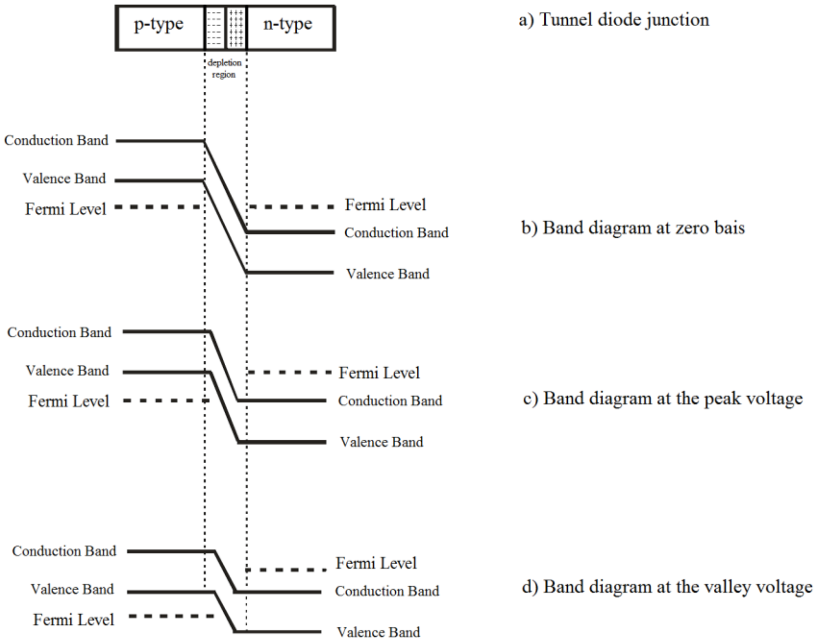

Figure 2.1: A tunnel diode band diagram.

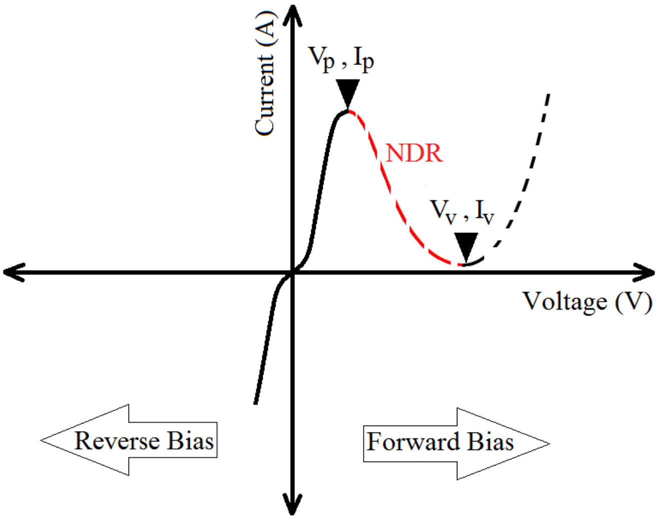

Figure 2.2: An Esaki tunnel diode current-voltage characteristic.

As a benefit of the NDR region, the ETD was employed in a number of applications such as an amplifier, oscillator and logic circuits. However, Esaki diodes in the form of a back diode are primarily used for detecting very low power signals. Their inherently high specific capacitance restricts their use at higher frequencies, i.e., millimeter wave frequencies and beyond. This was part of the motivation for Esaki and Tsu to explore in 1973[64] a superlattice's properties in terms of electrical transportation. This theoretically predicted a novel behavior resulting in electrons tunnelling inside a double barrier quantum well (DBQW) in the form of thin GaAs well surrounded by two AlGaAs barriers. This original phenomenon (quantum confinement at certain energy values related to the well bottom) indicates that the transmission coefficient exhibits resonances which are reflected electrically in the form of the I-V characteristic. A year later, the Esaki team confirmed the theoretical result by demonstrating a practical quantum barrier device, currently well known as resonant tunnelling diode or RTD[65]. The following section will outline the structure and principal of operation of this device.

2.3 Resonant tunnelling diodes

The RTD in its simplest form has several benefits compared to Esaki diodes, and its structure could be broadly divided into three main regions:

- An emitter region functioning as an electron source, followed by a spacer layer.
- A quantum well of a low band gap material surrounded by two different materials with a high band gap to establish the key structure, the double-barrier quantum-well (DBQW).
- A spacer layer followed by a collector region for attracting tunnelled electrons.

The key difference compared to an Esaki p-n tunnel diode is that each of these three regions can be adjusted largely independently of one another, which favours precise engineering of the electrical characteristics. How some of these factors influence microwave and mm wave mixing is the subject of this work.

An example of the common structure of an RTD, along with the corresponding I-V characteristic, is depicted in Figure 2.3 and Figure 2.4 respectively. There are a number of resonant levels inside the quantum well, and as soon as the energy level of electrons coming from the left emitter region are in alignment with these quantised states, the electrons can easily tunnel through the structure. As shown in Figure 2.3(b), there is no possibility of current to flow through the structure without an appropriate applied bias. As a result of a small applied forward bias an accumulation layer forms near the barrier, neighbouring the emitter region, and electrons are thus capable of aligning with resonant levels inside the quantum well. They then tunnel through the whole structure with a high probability, resulting in the flow of current. Further increasing the applied bias boosts the current due to rise in the stream of electrons from the emitter region towards to the collector side, and the current thus reaches its peak value, Ip. Again, the number of electrons which tunnel through the barriers is limited and by further increasing of the voltage; the current therefore goes down to reach its valley value, Iv, since there is no longer alignment with the resonate states inside the well. Once the current and the voltage pass the valley value, the normal thermionic current over the barrier, or through the 1st excited state takes place. However, considering the reverse bias voltage, the current behaves in a similar way to the forward one to produce the anti-symmetric I-V characteristic if the barriers and other regions are made identical, i.e., from the same materials and doping. The application of this anti-symmetric I-V curve in sub-harmonic mixers is of key importance, which will be discussed in section 2.5.

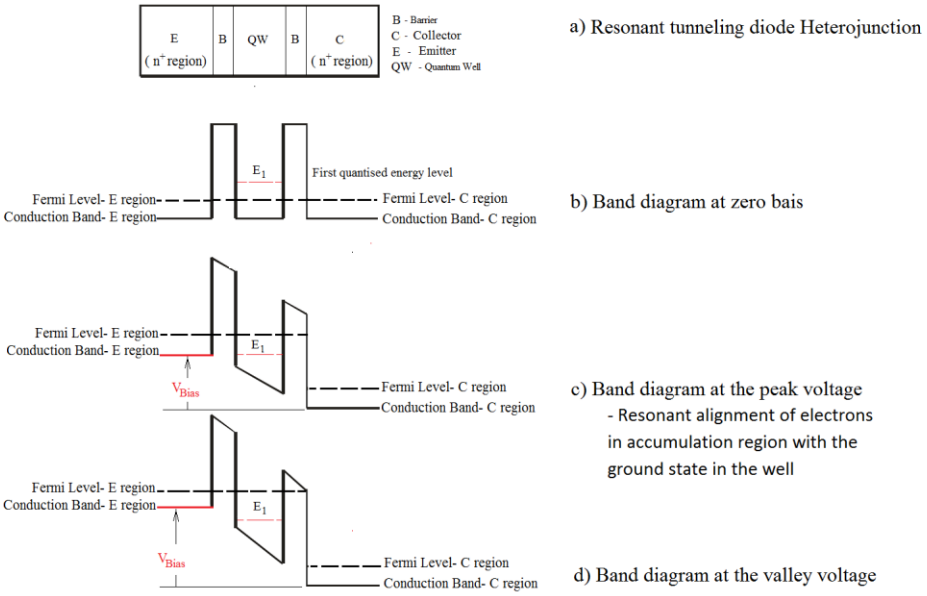

Figure 2.3: A resonant tunneling diode structure.

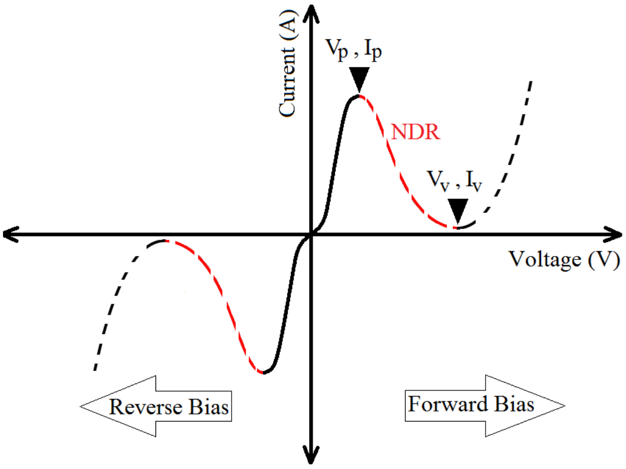

Figure 2.4: A resonant tunneling diode current-voltage characteristic.

From the perspective of RTDs' applications, the NDR portion (red-dashed line shown in Figure 2.4) is the key feature behind using RTDs as high frequency oscillators. In such cases, the peak (Ip) to valley current (Iv) ratio, (PVCR=Ip/Iv), is required to be high, as is the peak to valley voltage, for achieving a maximum power range. The current thesis focuses on mixing applications where the NDR and peak voltage region are beyond the voltage swing (max excursion of the applied signals) resulting from the mixer pump signal with zero DC bias. In other words, the exploited area for mixing purposes is up to the first non-linear portion of the I-V characteristic (black-solid line in Figure 2.4) between the current peaks on either side of the origin of the I-V characteristic. For the down conversion case, this region is preferred to be as close as possible to the origin, favouring detection of high frequency signals using very low amounts of the LO power. Alternatively for the up conversion case, the region between the peaks should be at a reasonable distance from the origin in such a way that much more input power can be applied or pumped (maximum dynamic range) to achieve a good output power at the high frequency. The potential of RTDs in down and up mixing applications at mm and sub-mm signals will be explored by designing different sub-harmonic mixers, which are presented in detail in next chapters, while the next section will review some basic concepts used to create such high frequency semiconductor devices.

2.4 Basic Concepts for RTDs

From a basic-perspective point of view, when a device's structure comprises two or more heterojunctions, the device is specified as heterostructure. The heterojunction itself is simply the interface produced due to the contact of two dissimilar band gap semiconductor materials, such as GaAs with 1.4eV and AlAs with 2.4eV, which suddenly causes alterations in terms of the ground-state energy in both the conduction band and the valence band. This consequently results in band discontinuities which largely determine the electrical properties of the heterojunction. For more clarification, Figure 2.5 illustrates the energy band diagram of two dissimilar band gap semiconductor materials, where E_V and E_C are the energies of the valence and conduction band respectively while the energy band gap between them is denoted as E_g and the Fermi level is signified as E_F for both type of the semiconductors. Likewise, the electron affinities of the first wider band gap and the second narrower band gap semiconductor are χ^1 and χ^2 respectively. ΔE_C is the conduction band discontinuity between these two different materials while the valence band discontinuity between them is denoted as ΔE_V.

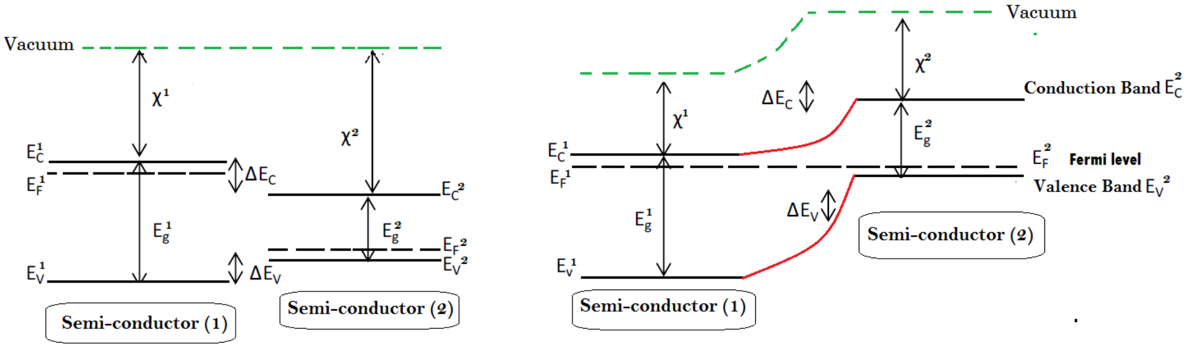

a): before the contact. b): after the contact.

Figure 2.5: The energy band diagrams of two-dissimilar band gap semiconductor materials.

Referring to Figure 2.5, the difference between the band gaps of these two dissimilar semiconductors is expressed as:

$$\Delta E_g = \Delta E_C + \Delta E_V \tag{2.1}$$

where ΔE_C and ΔE_v can be individually introduced as follows:

$$\Delta E_C = \chi^1 - \chi^2 \tag{2.2}$$

$$\Delta E_V = (E_g^1 - E_g^2) - (\chi^1 - \chi^2) \tag{2.3}$$

By combining Equation 2.2 and Equation 2.3, the band gap of these two semiconductors can be rewritten as:

$$\Delta E_g = E_g^1 - E_g^2 \tag{2.4}$$

In order to reduce the mechanical and electrical disturbance due to mismatch in bond lengths at the interface, materials with matched or close enough lattice constants should be employed. A good example of the most common III-V lattice matched system is GaAs/$Al_xGa_{1-x}As$, where the aluminium composition is represented by what is referred to as the mole fraction (x).

As an overview of different energy band gaps and lattice constants, Figure 2.6 shows some matched lattice materials such as AlAs and GaAs at which the lattice constants are 5.6605Å and 5.6533Å respectively with a band gap difference of 1eV. With the advent of Molecular Beam Epitaxy (MBE) the precise control of such materials and interfaces characteristics (band offset) becomes possible leading to a wide range of related device structures. These epitaxy layers are deliberately made very thin corresponding to the de Broglie wavelength[66], or with respect to the average travelled distance of electrons between collisions, the so-called electron mean free path. The de Broglie wavelength can be expressed as:

$$\lambda = \frac{h}{p} \tag{2.5}$$

where Plank's constant, h, equals 6.62607 x 10^{-34} joules, and p is the electron momentum. This results in quantisation of the energy states inside the quantum well, which are confined in the growth direction and electrons can only move in the perpendicular plane.

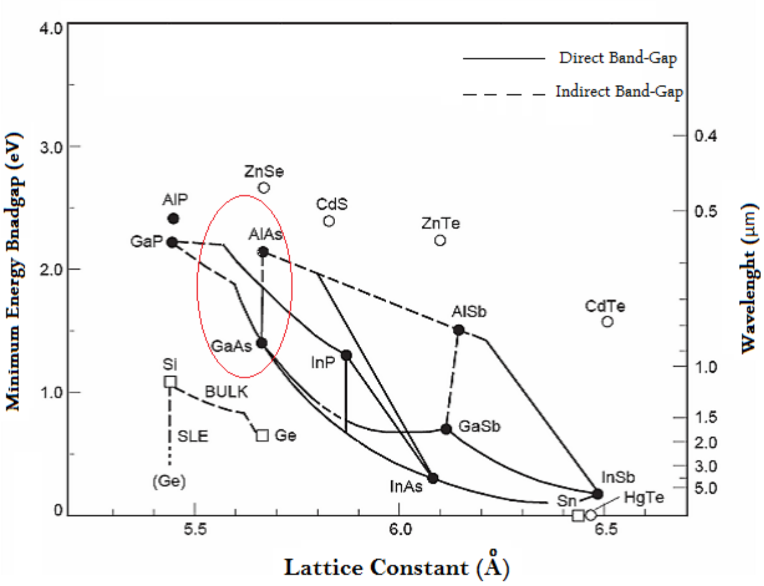

Figure 2.6: Energy band gaps and lattice constants of III-V and II-VI semiconductors at room temperature, adapted from[67].

Figure 2.7 shows a quantum well made by GaAs surrounded by two $Al_xGa_{1-x}As$ barriers. The conduction band diagram is sufficient to explain the behaviour since the quantum tunnelling mechanism in this case is intra-band, as discussed in Chapter (1). According to[68], the energy level of these quantised states is given by:

$$E_n = \frac{1}{8m^*}\left(\frac{hn}{W_w}\right)^2 \tag{2.6}$$

where W_w is the well width, and m* is the effective mass while n is the quantised energy level inside the quantum well, e.g., 1, 2… and so on.

According to Fermi-Dirac distribution, the electron spectrum in the emitter contact can be considered in thermal equilibrium because of the electrons' interaction with their adjacent environment, which is the same view at collector side. Since the electrons are inherently treated as waves in quantum domain, these electrons experience reflections due to the hetero-structure interfaces, and eventually leading to resonant tunnelling process. The dimensionality across these interfaces is not of the same order, i.e., the states's density in the emitter side is in three dimensions (3D), whereas in quantum well it is two dimensional (2D). This leads to different types of transmissions, for example, considering the transport through the resonant states, the reflections from the interface depend on wavelength of the incident electron coinciding with the resonant energy of the ground state level (E_1) where these energies align and can attain the highest theoretical transmission probability of one.

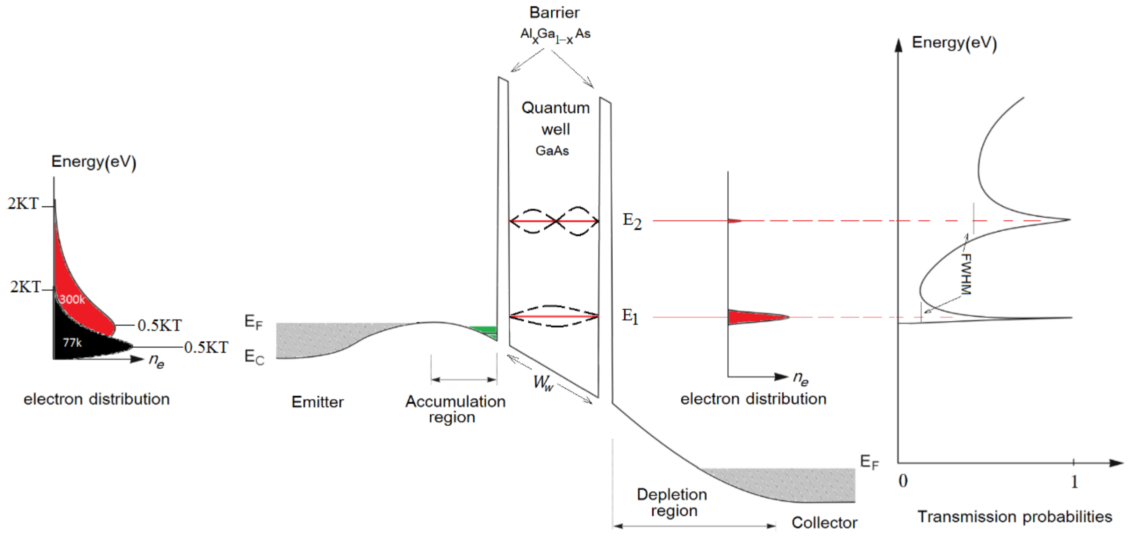

Figure 2.7: The quantum well band diagram of a GaAs/AlGaAs system, not to scale.

Another type of tunnelling can be involved where electrons are firstly scattered into a certain level in the 2D accumulation region, green portion on Figure 2.7 and sequentially tunnel when coincident with the E_1 level inside the quantum well. Additionally, higher energy incident electrons can cross over the barrier by thermionic emission or by tunnelling through the next energy level. In principle, the number of electrons tunnelling through the structure is determined by the electron distribution/concentration in the emitter where its shape is governed by temperature, as shown on the left side of the Figure 2.7. The black distribution reflects the electron spread and number at 77K (liquid nitrogen) while the red distribution is for 300K (room temperature). The electrons at 77K will require a small range of bias to be aligned with the ground resonant state inside the well, correspondingly leading to a sharp nonlinear region within the I-V curve and the resultant current density is higher compared to the 300K where the nonlinear region is relatively smooth and wider and the current density is lower, reflecting the lower number of electrons available for tunnelling. Figure 2.8 shows the effect of the temperature on the I-V characteristic of a RTD, fabricated and measured by the group led by Dr. Steenson at the University of Leeds. More detail will be presented later in Chapter 5.

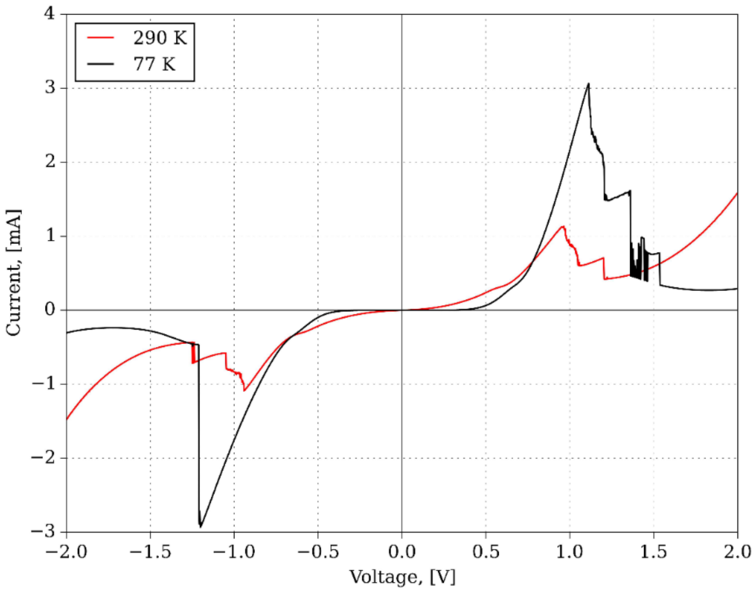

Figure 2.8: The temperate effect on the current–voltage characteristic[69].

Indeed, the actual physical process describing the operation of RTDs is more complicated as the electrons' energies are changed with not only the external applied voltage (making the device no longer isolated quantum structure, alternatively opening to the outside environment), but also the interaction with impurities, vibration of lattice, roughness of interfaces and the electrons interactions themselves[70].

Figure 2.9 shows the mechanical motion of an electron in the tunnelling direction, at a given position of space, which can be defined by the 1-D time independent Schrödinger equation as follows:

$$\left[-\frac{\hbar^2}{2m^*}\frac{d^2}{dx^2}+V(x)\right]\psi(x) = E\psi(x) \tag{2.7}$$

where $\psi(x)$ is the wave-function that defines the electron probability in the x-direction, and $\hbar = \frac{h}{2\pi}$ is the reduced Plank constant, while $V(x)$ is the potential energy with respect to $V(x) = 0$ and E is the system energy.

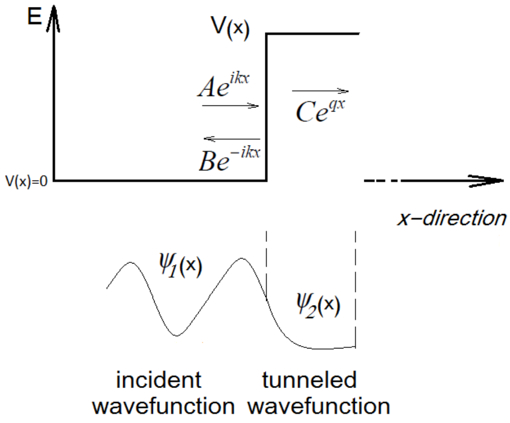

Figure 2.9: The wave-function of electrons.

At the regions adjacent to the interface where $V(x) = 0$ as shown in Figure 2.8, Equation 2.7 can be reduced to be as:

$$\frac{d^2\psi}{dx^2} = -\frac{2Em^*}{\hbar^2}\,\psi = -k^2\psi \tag{2.8}$$

where $k = \sqrt{\frac{2Em^*}{\hbar^2}}$ presenting the wave vector inside the barrier. The general solution of this 2nd order differential equation, incident wave function, can be written as:

$$\psi_1(x) = Ae^{ikx} + Be^{-ikx} \tag{2.9}$$

where A is the incident wave amplitude while B is the reflected one. Similarly, at the interface where $V(x) \neq 0$, the Schrödinger equation is:

$$\frac{d^2\psi}{dx^2} = -\frac{(E-V_o)2m^*}{\hbar^2}\,\psi = -q^2\psi \tag{2.10}$$

where $q = \sqrt{\frac{(E-V_o)2m^*}{\hbar^2}}$, and the general solution of Equation 2.10 at the interface can be written as:

$$\psi_2(x) = Ce^{iqx} \tag{2.11}$$

Equation 2.11 obviously indicates that the electrons decay exponentially inside the potential barrier. This means that the transmission probability of the electron on the other side depends on the height and the width of the barrier. By finding the solution of the preceding equations, using common methods such as transfer matrix or computer based approach, the whole electron wave function can be defined in the RTD's structure.

To gain a practical benefit from such a heterostructure, a low resistance metal contact to the semiconductor device is needed. Metal-semiconductor junctions can be one of two common types, depending on the interface characteristics, namely Schottky contact or ohmic contact. The metal-semiconductor junctions are implicitly barrier-height dependent and that determines the flow and directionality of electrons resulting from an applied bias. To tackle the barrier, electrons should be associated with a certain emission process or carrier-transport mechanism defined largely by the doping concentration. This emission can be a thermionic emission using low doping, thermionic field emission resulting from moderate doping or field emission (or tunnelling) using heavily doping[71]. The thermionic emission is the dominant mechanism when the barrier height is relatively high at which a thermal excitation is required for charge carriers (electrons) to overcome the barrier, and this is the case when using the Schottky-type contact. Field Emission, on the other hand, is where the electrons can tunnel through a thin barrier resulting from a heavy concentration of doping; this type of emission is involved with the ohmic contacts.

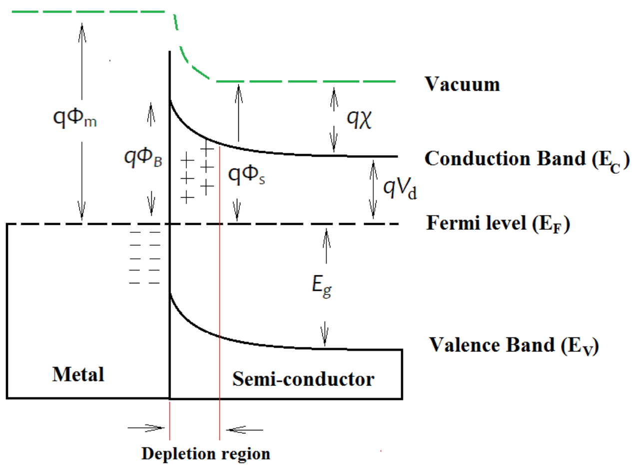

Figure 2.10: The band diagram of metal- semiconductor in contact with a zero-bias condition.

A metal-semiconductor Schottky contact can be understood by looking at the Schottky-Mott principle[72]. Figure 2.10 schematically shows the corresponding band diagram when a metal and a semiconductor are brought together without an applied bias. As shown on this Figure, $q\phi_s$ and $q\phi_m$ represent the work functions of semiconductor and metal respectively. The work function itself is the difference between the vacuum level and the Fermi level. The energy difference between the vacuum and the conduction band is defined as the electron affinity and denoted as $q\chi$. The gap between the semiconductor conduction band (E_C) and the Fermi level (E_F) denoted as qV_d, while the valence band is denoted as E_V.

Contacting the semiconductor to the metal, electrons can flow from the conduction band of the semiconductor into the metal until thermal equilibrium is reached at which the Fermi level of both the semiconductor and metal are aligned, resulting in a depletion region next to the interface in the semiconductor due to the accumulation, i.e., negative electrons at the interface of the metal and positive donors at the interface of the semiconductor. An electric field is inherently induced as a result of this carrier redistribution. As a consequence a built-in potential barrier will affect the flow of electrons coming from the metal into the semiconductor. Similarly the built-in potential will be greater in resisting the flow of electrons coming from the semiconductor into the metal. Thus, the built-in potential can be defined as the difference between the metal and the semiconductor in terms of their work function, and contributes to the zero bias junction capacitance which is proportional to the length of this depletion region.

By considering the forward-bias condition as presented in Figure 2.11(a), the metal’s Fermi level is lower than the Fermi level in the semiconductor (n-type material), and consequently a small potential drop across the semiconductor is caused. Furthermore, the barrier is reduced as seen by electrons coming from the semiconductor side, and therefore more electrons flow into the metal resulting in a high current. On the other hand, when a negative bias is applied to the metal as illustrated in Figure 2.11(b), the Fermi level of the metal is higher compared to the semiconductor’s Fermi level and only small leakage current flows. The potential is increased across the semiconductor due to the applied external voltage (but no voltage drop across the metal in this case), causing not only the depletion region to be wider (lowering the capacitance) at the interface but the corresponding electric field is large as well. This means that the electrons from the semiconductor intended to move into the metal will be restricted by the increased barrier height, resulting in a small amount of current flowing into the metal.

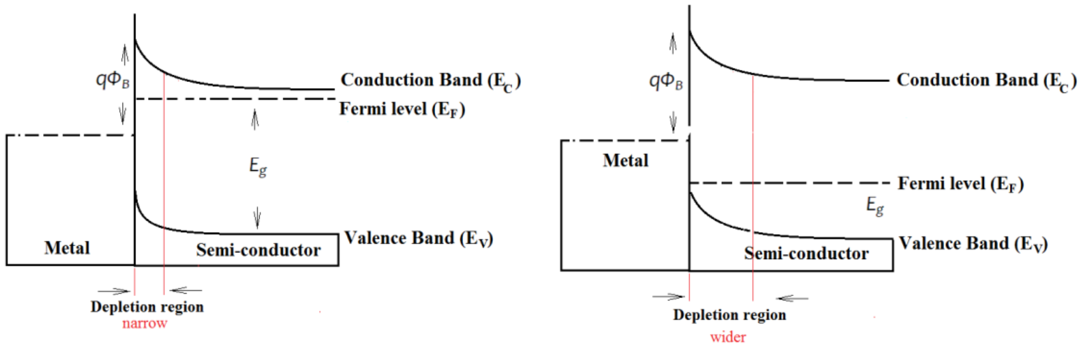

a): Forward bias.

b): Reverse bias.

Figure 2.11: Schottky contact band diagram, (a) Forward bias, and (b) Reverse bias.

This bias direction dependent behaviour is referred to as Schottky rectifying which is based on the thermionic emission mechanism; again, in a lightly doped semiconductor (< $1x10^{17}cm^{-3}$) which is a key condition[73].

As mentioned previously for ohmic (low and linear resistance) contacts, a different mechanism called field emission is used instead of the thermionic emission where electrons tunnel through a deliberately thin potential barrier. Unlike a Schottky, an ohmic contact has a non-rectifying behaviour resulting in linearity in terms of the I-V characteristic, similar to Ohm’s law, in both the forward and the reverse bias condition. The most often used technique to create an ohmic contact is to introduce a very highly doped layer adjacent to the metal, reducing the depletion region width at the interface to <10nm. Consequently electrons can tunnel through the barrier even when a small external bias is applied. Technologically, ohmic contacts are in the form of an alloyed (based on a reasonable high doped semiconductor, <$1x10^{18}$ cm^{-3}) or non-alloyed (based on a very highly doped semiconductor, >$1x10^{19}$ cm^{-3}). For the alloyed contact, the contact needs to be thermally annealed where a set of metals are employed, and one of them is used as an acceptor or a donor to ensure the diffused doping at the semiconductor interface has the necessary heavy concentration. In that, the heated metal diffuses into the semiconductor to build a region with a very high concentration of doping, resulting in an extremely narrow depletion region and consequently providing a low resistance tunnelling path for electrons to move in either direction, i.e., a low resistance ohmic contact. However, the ohmic contacts formed without alloying are inherently based on a very highly doped semiconductor to begin with; consequently there is no need to provide thermal annealing[74].

In order to put all the previous considerations into context, Table 2.1 depicts the typical double barrier RTD growth structure while Figure 2.12 shows the physical cross section structure of the RTD fabricated here in Leeds, alongside a SEM picture. In Table 2.1 considering from the bottom to the top in terms of growth direction, the semi-insulating GaAs (III-V material) is the substrate on which the other epitaxial layers are built. The heavy doped n region (GaAs n+ contact) serves as an alloyed type of ohmic contact to provide an electrical path between this heterostructure and the outside world. The graded n layer comes with a relatively low doping, and its function is to increase the depletion region width, i.e., lower junction capacitance, and consequently the NDR is shifted to a higher voltage, if this is required, but as a trade-off the undesired series resistance of any un-depleted region is increased. This graded layer is followed by a spacer layer ensuring that the tunnel barriers (i.e., the two barriers and the single quantum well) are protected from dopant dependent scattering from the high energy electrons coming from the heavy n+ layer, where the spacer layer is usually formed by a thin intrinsic GaAs layer typically in range of 5-10nm. As can be seen from this Table, the RTD structure is a mirror heterostructure (or identical on both sides of the well) where the two barriers and the single quantum well is placed. The undoped GaAs quantum well is sandwiched between undoped double barriers of $Al_xGa_{1-x}As$ where aluminium (Al) is simultaneously introduced along with the growing of the GaAs through MBE process, in that the Al should satisfy the ratio x: x-1 by replacing some As atoms, where x is the aluminium fractional amount. The main reason for not doping the barriers and quantum well is to avoid the presence of impurity atoms which contribute to the scattering inside this area.

Table 2.1: A typical double barrier RTD growth structure.

Layer	**Material**	**Doping**
Top n^+ Contact	GaAs	doped
Graded n Layer	GaAs	doped
Spacer Layer	GaAs	Un-doped
Barrier	$Al_xGa_{1-x}As$	Un-doped
Quantum Well	GaAs	Un-doped
Barrier	$Al_xGa_{1-x}As$	Un-doped
Spacer Layer	GaAs	Un-doped
Graded n Layer	GaAs	doped
Bottom n^+ Contact	GaAs	doped
Substrate	GaAs	-

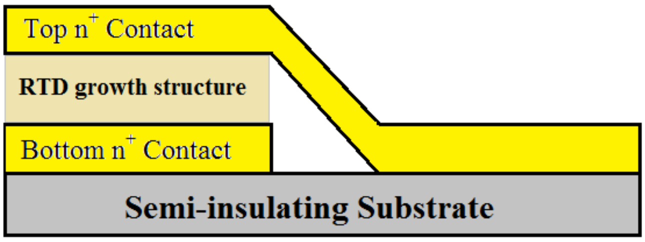

a): A cross-section.

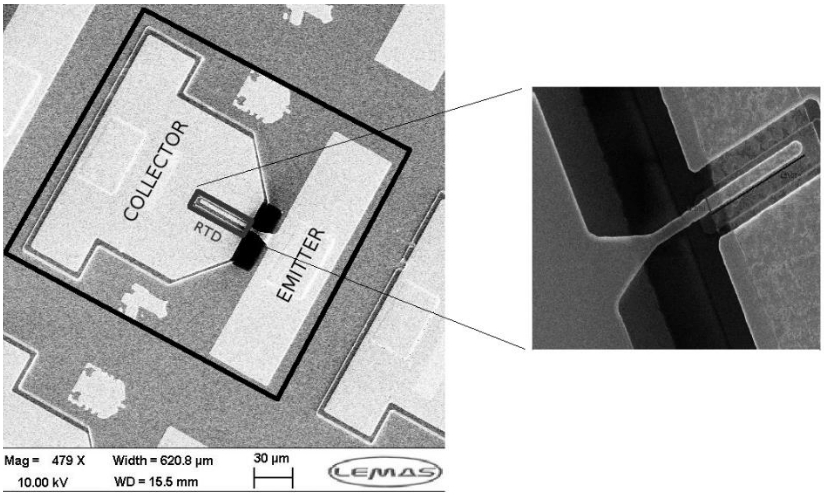

b): a SEM picture showing the finger.

Figure 2.12: The physical structure of the RTD fabricated at the University of Leeds a): a cross-section, b): a SEM picture.

Once more, the RTD's multiple layer structure can be adjusted largely independently to generate a specific I-V characteristic for a certain application such as up or down mixing, which is the main focus of this thesis. The barrier thickness' effect on the current density can be distinguished by observing the transmission probability where the current density increases through thinner barriers [75], which can be effortlessly adjusted through the MBE growth. Recalling Equation 2.6, the effect of the quantum well width on its quantised energies can be observed, where the state energy levels increase when the well width decreases. As a consequence of the well width decreasing, the peak in the voltage of the first current maximum is shifted to a higher level responding to the applied bias that needs to be increased as well, thinner barriers lead to high transmission probabilities (high resonant current)[76]. Furthermore, the peak-to-valley current ratio (PVCR) is increased, corresponding to the separation increasing among the quantised energy levels inside this thinner well. According to the Wentzel–Kramers–Brillouin (WKB) approximation[77], the resonant level at the full-width at half-maximum (FWHM), which indicates the peak current, can be defined as:

$$\Delta E_n = E_n\, e\left(-2t_B\sqrt{\frac{2m^*(V_0-E_n)}{\hbar^2}}\right) \tag{2.12}$$

where t_B is the barrier thickness. Figure 2.13 shows theoretically how the difference in terms of the layer structure, such as the barrier material and its thickness, can affect the transmission probability of electrons, and correspondingly on the experimental I-V characteristic as shown in Figure 2.14.

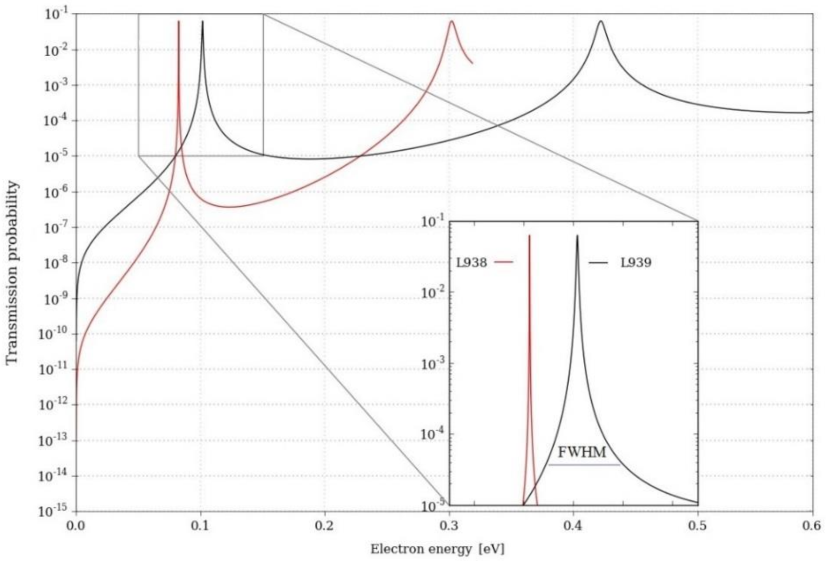

Figure 2.13: The transmission probability of two different structure RTDs[69].

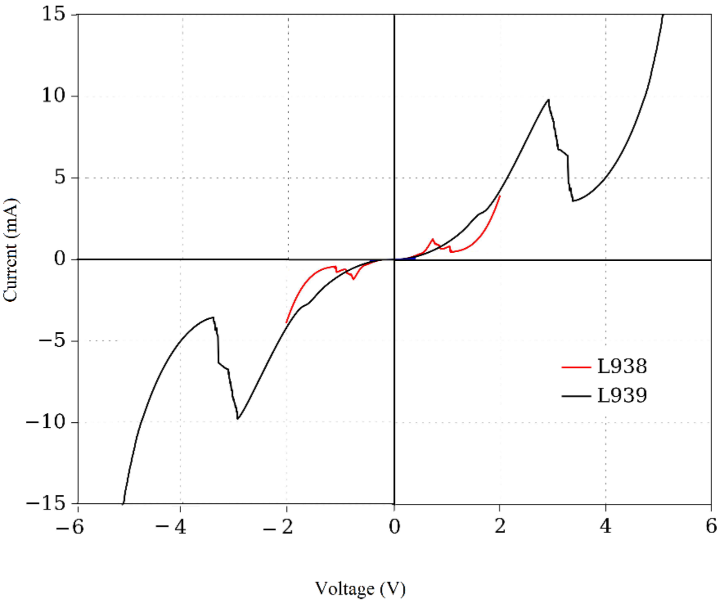

Figure 2.14: The I-V characteristic of two different structure RTDs, L938 and L939[69].

The transmission probability of two different RTDs, designated as L938 and L939, is shown in Figure 2.13. They have the same area of 30µm^2, but the L938 has $Al_{0.4}Ga_{0.6}As$ barriers with 5nm thickness while L939 has AlAs barriers with 1.7nm thickness, and for both the well width is 5nm. The ground state resonant energy of the L939 is also higher compared to L938, and this results in occurring the NDR at higher applied bias as shown in Figure 2.14. The L939 also provides a wider FWHM leading to a significantly higher current density compared to L938 as shown on the same figure.

These RTDs, L938 and L939, were fabricated at the University of Leeds, and FORTRAN program was written by Dr DP Steenson to calculate their transmission probabilities. The detailed growth structure of these RTDs and the resulting potential for use in high frequency mixing applications will be presented in Chapter 4 and Chapter 5, while the next section will only discuss the common presented methods used to model these non-liner elements (RTDs) in a CAD environment.

2.5 RTD modelling

In order for RTD characteristics to be used in a circuit simulator, a model of their structure is required which relates their I-V and C-V to a form that can be used in a time domain model. Following the tunnel diode model proposed by Esaki and Tsu, several different models have been proposed in the literature, [78-91], for detailed exploration the potential use of RTDs in various applications. These models represent the numerical and analytical simulation of the I-V and/or C-V characteristic of given RTDs in a form which is compatible with the CAD software. As a benefit for this, the non-linear device circuits using RTDs, such as mixers, oscillators, power amplifiers and others, can be designed and hence their potential performance prior to the fabrication stage can be assessed. These common methods can be based on three distinct approaches, namely physics and analytic models, SPICE models or equivalent circuit models.

In the literature there are a number of physics based models of this semiconductor device, using different mathematical approaches representing the physical energy-band parameters that are of relatively limited practicality for high frequency modelling. Principally the physics based approaches exploit both the physical dimensions and the electrical properties of RTDs by using a single, or a set of, empirical equation(s), which inherently requires a physical understanding of electron behaviour such as the transmission of electrons, electron reflection, and the particles' scattering inside a double barrier quantum well structure. In such case, the current as a function of the voltage (I-V curve) of a given device can be represented in the form of empirical equations with multiple tuneable terms, which is more useful for layer design than for high frequency modelling use. The recalculation of which would greatly slow down the frequency domain circuit modelling.

SPICE based models fundamentally employ an ideally continuous (or discontinuous) function which relatively simply describes three-distinct regions of the I-V characteristic of the RTD, namely first Positive Differential Resistance (PDR1) which appears before the tunnelling effect (less than Vp), Negative Differential Resistance (NDR) and second Positive Differential Resistance (PDR2) where the current behaviour is normal thermionic emission over the barriers. In that way, a piecewise-linear technique, proposed in [78], individually represents the linearity of these three different regions to represent them as elements such as switches, voltage dependent resistors and so on. However, the obvious drawback of this methodology lies in fact that these three dissimilar regions are not in practice piecewise or linear in the actual device, meaning this type of approach is unable to satisfy the desired modelling. Likewise, an alternative method was employed in[79] known as piecewise-nonlinear using a switch and two different diodes to present both positive regions (PDR1 and PDR2). In order of the PDR1 to be presented, the switch is used to turn on the diode at a voltage below the V_p of the RTD, again for this work this approach is not deemed appropriate.

The other modelling type, equivalent semi-analytic circuit based models, is frequently considered as an effective technique for employing the RTD in a frequency domain environment. On the whole, the simplest equivalent circuit representing the main double barrier RTD structure is shown in Figure 2.15. This lumped element based model was proposed by Gering et al [80] as an improved version of the Esaki tunnel diode.

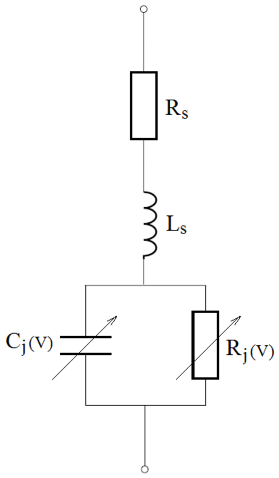

Figure 2.15: A typical equivalent circuit of a double barrier RTD[80].

As shown in the above circuit, a resistor (R_s) and an inductor (L_s) are in a series connection, and both are connected in series with the device junction represented by a capacitor (C_j) and resistor (R_j) in parallel. The R_s embodies the entire resistance of the contacts and different layers of the device, excluding the active tunnelling junction (i.e., the double barrier region). The L_s introduces the potential inductive effect caused by the bond wire. The C_j represents the nonlinear voltage-dependent capacitance of the device junction, which can be expressed and calculated as a parallel plate capacitor. The other voltage dependent element is the Rj, which represents the nonlinear junction resistance reflecting the nonlinear relationship of the current and voltage.

Figure 2.16 shows an alternative common equivalent circuit introduced by Brown et al[81], where a series circuit in the form of a non-linear resistor R_j with an inductor L_s is in parallel with a non-linear capacitor C_j, and all are connected with a resistor R_s in series. The L_s here signifies T_n/R_j where T_n defines the lifetime of a given resonant state inside the quantum well, such that, the inclusion of experimentally measured S-parameters, impedance and DC current–voltage curve are the main principle of this approach. As a result, the equivalent circuit elements of a given diode are obtained with respect to the desirable application, giving a limitation of this approach at different operating frequencies.

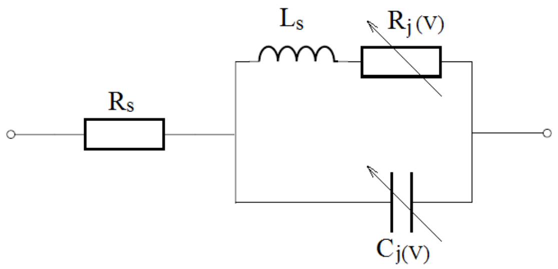

Figure 2.16: A modified equivalent circuit of a double barrier RTD[81].

Considering the package effect, an accurate equivalent circuit proposed by Miles et al is shown in Figure 2.17. The C_A and C_W are a function of the applied voltage and represent the capacitance of the accumulation region and quantum well respectively, while the R_B

and R_C represent the barrier resistance and the resistance path over the device respectively. The voltage independent parasitic elements are represented by R_P, L_P and C_P, which are associated with the package effect.

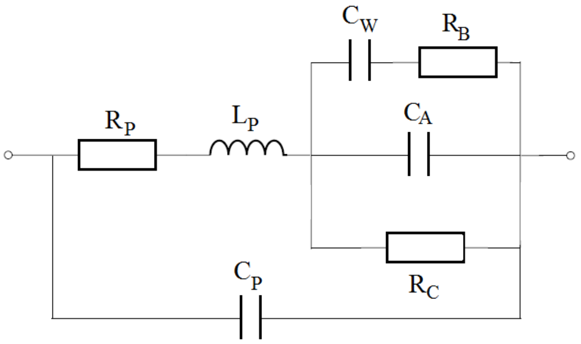

Figure 2.17: An accurate equivalent circuit of double barrier RTD[82].

For the current thesis the RTDs, whose simple equivalent circuit is similar to that of Gering shown previously in Figure (2.15), are modelled using a fitting approach that represents the measured I-V characteristic of these RTDs in form of polynomial equations using MATLAB software, and in turn, these fitted polynomial equations can be employed at high frequencies using the Symbolically-Defined Device (SDD) model capability provided in Keysight ADS. For the current work, the potential performance of different layers of RTDs can be investigated by fitting a polynomial of the first part of the I-V characteristics, i.e., the nonlinear region before the peak voltage. Since there is already a built-in model of the Schottky diode in ADS package, this built-in model and an SSD model description of a Schottky diode are compared, as shown in Figure 2.18, in order to prove the validity of the fitted polynomial-type method. From this Figure, there is good agreement between these two models; more discussions are presented in chapter

4 and chapter 5 when it comes to clearly estimating the potential performance for the complete mixer design.

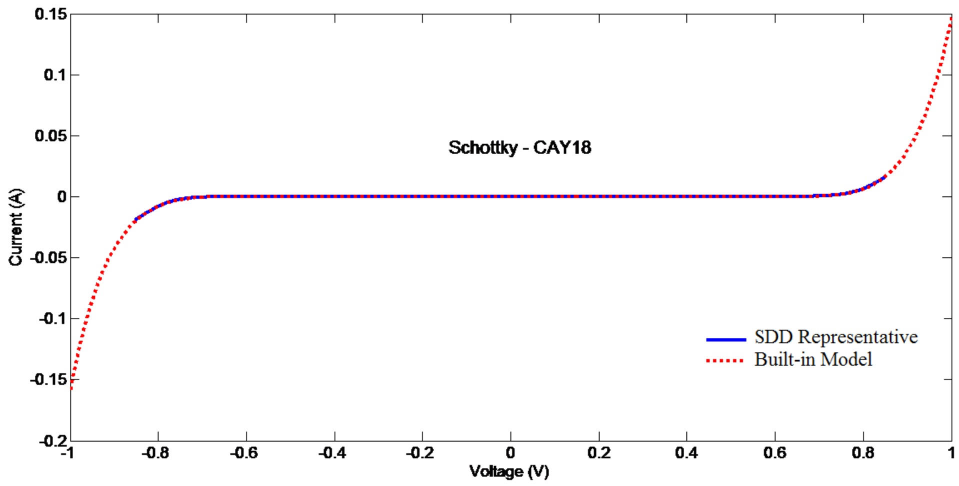

Figure 2.18: The measured and fitted I-V curve of a commercial Schottky diode.

For the complete mixer sub-system, it is necessary to include the input and the output transmission lines, and for frequencies above 110GHz wafer probes tend to be prohibitively expensive and system designers tend to be use low loss rectangular waveguides (RWG) connectors. Therefore the next chapter will present and develop the background for the transitions between RWG and planer waveguides which are featured in chapter 4 and chapter 5.

2.6 Summary

This chapter described the basic theory and served to provide the background to these high frequency semiconductor devices (RTDs), by quickly looking at heterostructures, quantum wells and the contacts between semiconductor devices and metals, and which underpin the high frequency model. Also this chapter introduced the different effects of temperature on the carrier-transport mechanism and thus the I-V characteristic, and likewise the barrier and the well effects on the I-V characteristic. Following this, the chapter reviewed the widely used modelling approaches for the RTDs within simulation environments to point the way towards the high frequency mixer modelling discussed later.

Chapter 3 Transitions and Calibration Pieces

3.1 Chapter objective

This chapter covers the design of transitions and calibration pieces, which are required for the sub-harmonic mixers presented in chapter 4 and chapter 5, and form an integral part of the mixer sub-system. These transitions are not the main focus of this thesis, and they can be the subject of study on their own. However, to effectively estimate the potential of the whole mixer, the transition losses should be considered first.

Firstly two different antipodal finline transitions, favoured because of their broadband nature, between rectangular waveguide (RWG) and microstrip line are designed and simulated at W-band and G-band, such that the LO and the RF of the 180GHz sub-harmonic mixer (discussed in chapter 5) can be respectively pumped and extracted. To validate the performance of these transitions, back-to-back E-plane split RWG blocks are designed. Additionally, a transition from microstrip to GCPW is designed at W-band to suit a CPW probe to rapidly evaluate the design at the measurement stage instead of using RWG. Also, the design of a GCPW to GCPW transition is also carried out to facilitate the measurement of the 110GHz sub-harmonic mixer presented in chapter 5. This mixer is designed with a relatively small GCPW dimension when compared to that of the available CPW probes at the University of Leeds. To validate the results of all the mixers presented in this work, this chapter ends with the design of a set of calibration pieces at W-band and G-band, using GCPW and RWG technology respectively. This is required to properly evaluate and diagnose each part of the design, i.e. separate out any losses associated with the transitions and evaluate the embedding structure.

3.2 Introduction

In order for the electromagnetic (EM) waves to keep propagating from one transmission line to another, a certain type of transitions is required, depending on the desired characteristics and the operating frequency. For example, at higher frequencies the RWGs are the ideal low loss option, requiring planar transitions between microstrip lines, coplanar waveguides, slot, strip-line or coaxial cables, which can be frequency dependent and at risk of generating undesired modes[92]. As the current work is intended for high frequency mixing applications, these planar transitions will not be presented in the later designs, instead, the emphasis will be on the RWG to strip-line ones. Unlike the aforementioned transitions, the RWG has a single conductor, permitting both transverse electrical (TE) and transverse magnetic (TM) modes to be introduced, i.e. no existence of transverse electrical and magnetic (TEM) mode. Therefore for EM propagation, the operating frequency must be higher than the low cut-off frequency of the TM and TE modes of the RWG, and the TE_{10} is the desired mode. The cutoff frequency is the lowest frequency at which these modes can propagate through the RWG. In terms of performance, the EM wave transition can be generally characterised by insertion loss, return loss or scattering matrix (S-parameters) at which the field matching and impedance matching are the two main aspects through the modal transition between RWGs and planar transmission lines. The field matching implies that EM fields are adapted with boundary conditions of the lines. The the impedance matching concept is the ability to connect two different lines whilst keeping the reflections as low as possible. However, it is not a straightforward task to reshape the EM field lines during the transition between a RWG and a planar transmission line, and this in turn gives rise to several different transitions such as ridge-waveguide transitions, in-line transitions, transverse transitions and aperture-coupling transitions[93]. The ridge-waveguide and in-line transitions involve the reshaping of the EM field through a transition process while the function of the others is to match the impedance. However, these transitions are outside the scope of the current work, as the finline transition is considered to be the most practical alternative. There are four common types of finlines, namely unilateral, bilateral, coupled and antipodal [94]. Among these, antipodal finlines are the optimum choice for microstrip because of their convenient layout, allowing, direct broadband transition between RWG and microstrip or CPW. Furthermore, antipodal finline parameters can be controlled in a way that a desired performance can be easily accomplished.

3.3 Transition design

In order for HFSS results to be efficiently considered, Figure 3.1 demonstrates the 3D design of a RWG- unilateral finline at Ka-band using finline taper with characteristics and conditions identical to the taper presented by Olsen[94]. The main purpose behind reproducing Olsen's transition is only to confirm that the current HFSS setup such as boundary conditions, port size, integration line and others are properly achieved, which is the most important step for EM designs. Results show that, the performance of this design is well matched with the Olsen one as illustrated in Figure 3.2. Based on this, the next two subsections will introduce the design of different frequency transitions that are served to the mixer circuits, presented in chapter 4 and chapter 5.

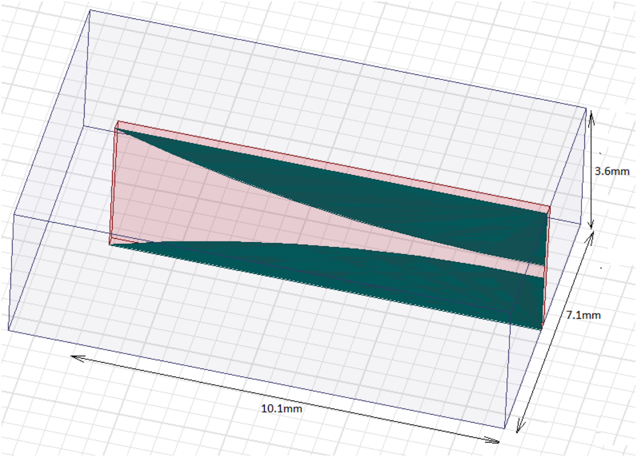

Figure 3.1: RGW- unilateral Finline at Ka-band using finline taper.

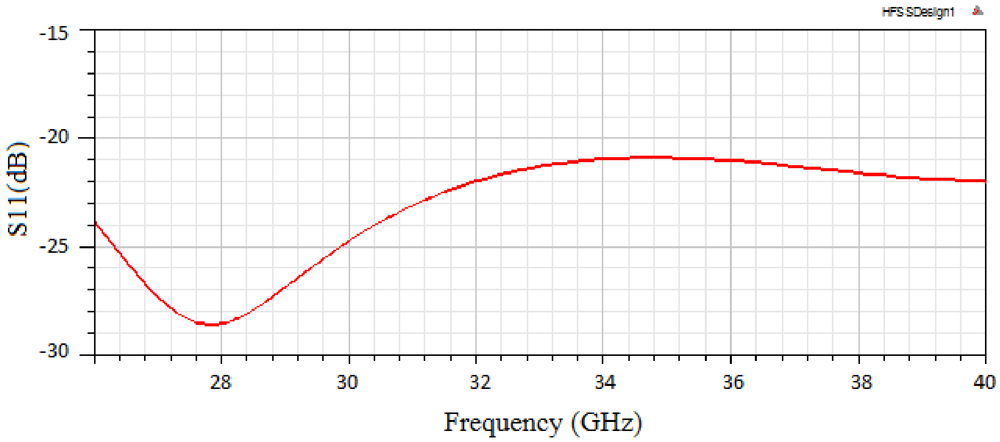

a): Current work

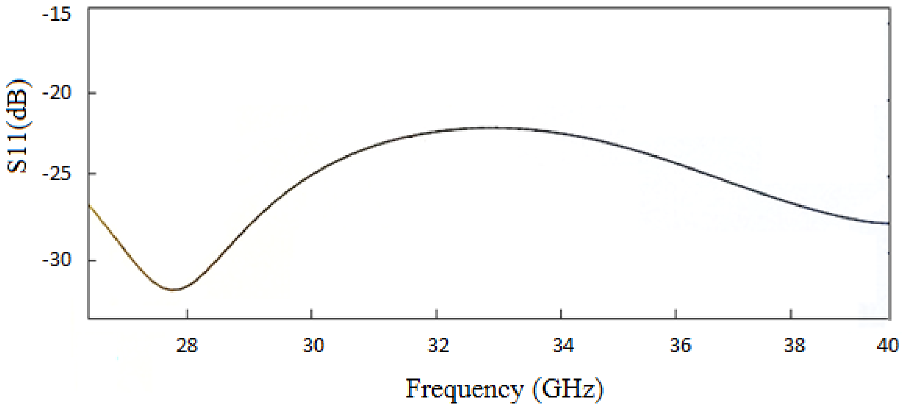

b): Olsen's work.

Figure 3.2: The reflection loss simulation at Ka-band frequency.

3.3.1 RWG to microstrip transition

A proposed antipodal finline, inserted into a RWG to offer a transition to microstrip line, is presented in Figure 3.3. Among all of the antipodal finline parameters illustrated on this Figure, the transition length, L, plays a key role in achieving the optimum performance (least loss and lowest reflection coefficient) at different frequency bands. The first antipodal finline is designed to be operated at W-band frequency, where the standard dimensions of the associated RWG are a = 2.54mm and b = 1.27mm as shown on Figure 3.3 . By selecting constant values 0.5mm, 0.05mm and 0.1mm for A, B and C respectively, the optimum length of the finline transition is found to be in the range of 3mm. In a similar way the second transition operated at G-band (a =1.3mm and b =0.65mm), is designed with constant values of A = 0.15mm, B = 0.051mm and C = 0.35mm, yielding an optimum length of the transition in the range of 2mm. For verification purposes, these two transitions should be measured in a back-to-back configuration.

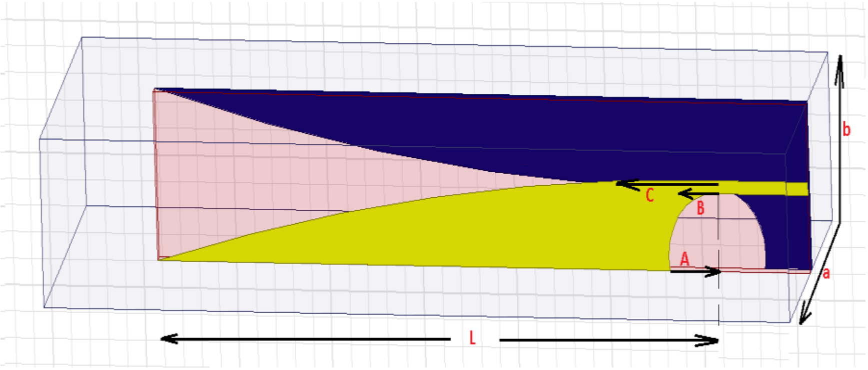

Figure 3.3: Antipodal finline taper inserted to RGW.

By using SOLIDWORKS, the E-plane split blocks of these transitions are designed as shown in Figure 3.4 and Figure 3.5. More CAD details such as their mechanical dimensions are presented in Appendix-V. The potential performance of these two different band transitions is presented in Figure 3.6, alongside their performance in a back-to-back configuration. From this Figure, it is obvious that the potential return losses are better than 15dB and 10dB over the whole W-band and G-band respectively.

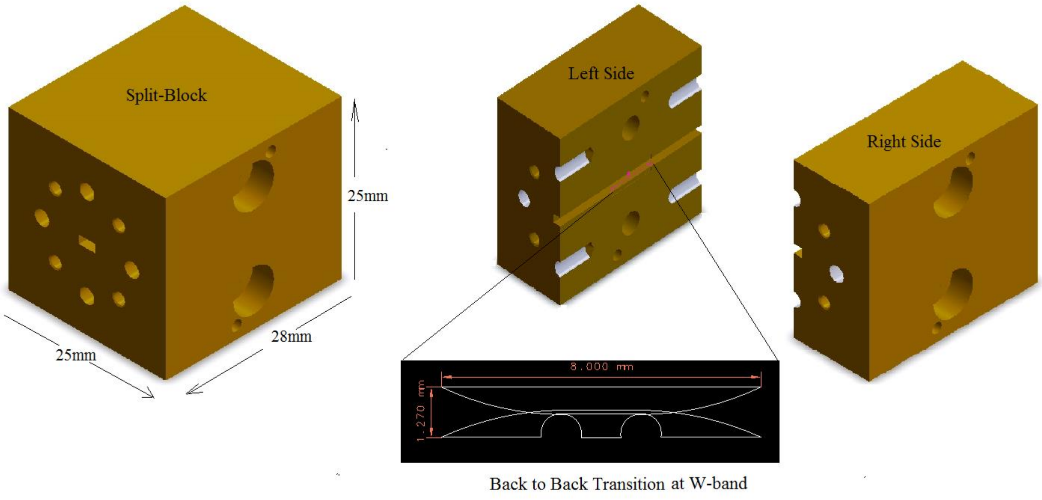

Figure 3.4: A 3D W-band back to back transition mounted in split-block.

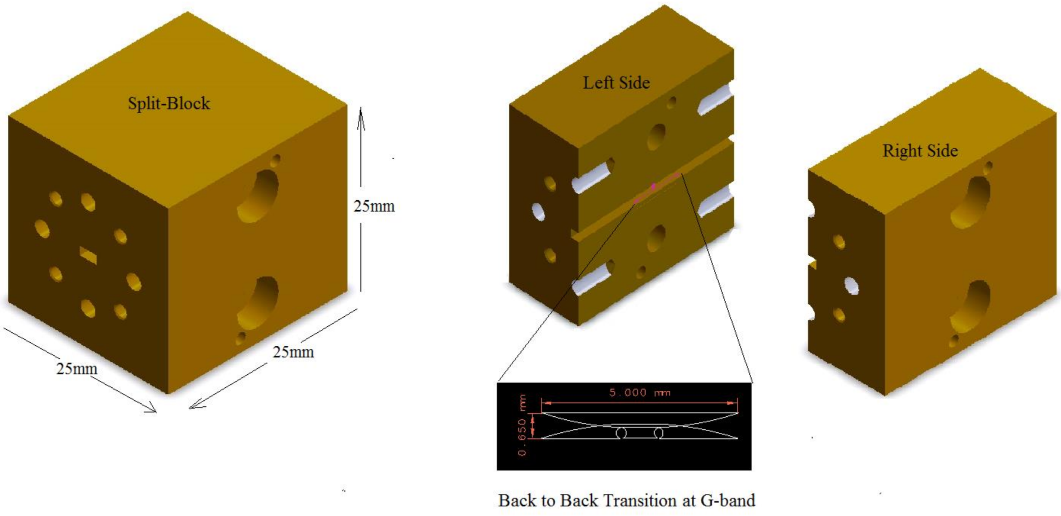

Figure 3.5: A 3D G-band back to back transition mounted in split-block.

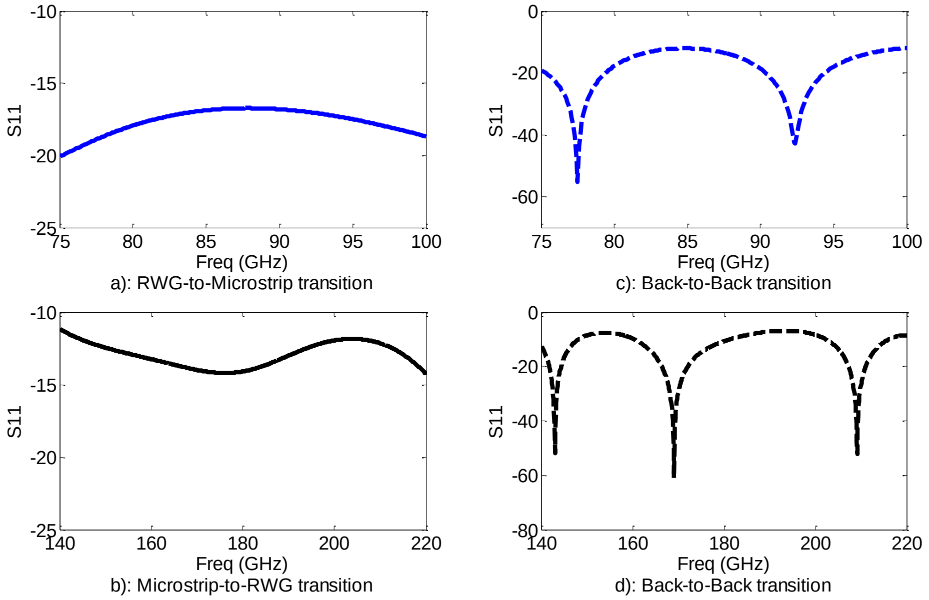

Figure 3.6: The return loss performance at different frequency bands.

3.3.2 Planar to planar transition

A simple transition from a microstrip line to GCPW is shown in Figure 3.7.This transition is designed to achieve reasonable performance at W-band, specifically at 85GHz. It is intended as an alternative for coupling the LO signal to the 180GHz sub-harmonic up conversion mixer. This transition offers adequate performance in terms of return loss, which is better than 16dB over the whole W-band, as shown in Figure 3.8.

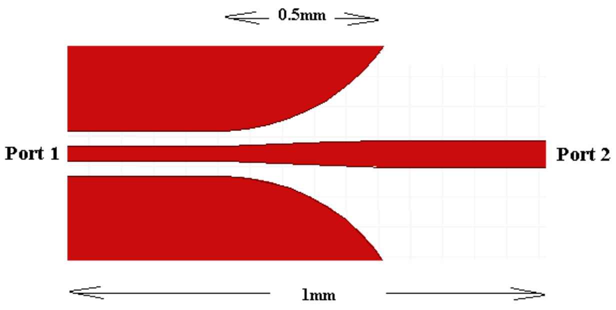

Figure 3.7: Microstrip -to- CPW transition layout.

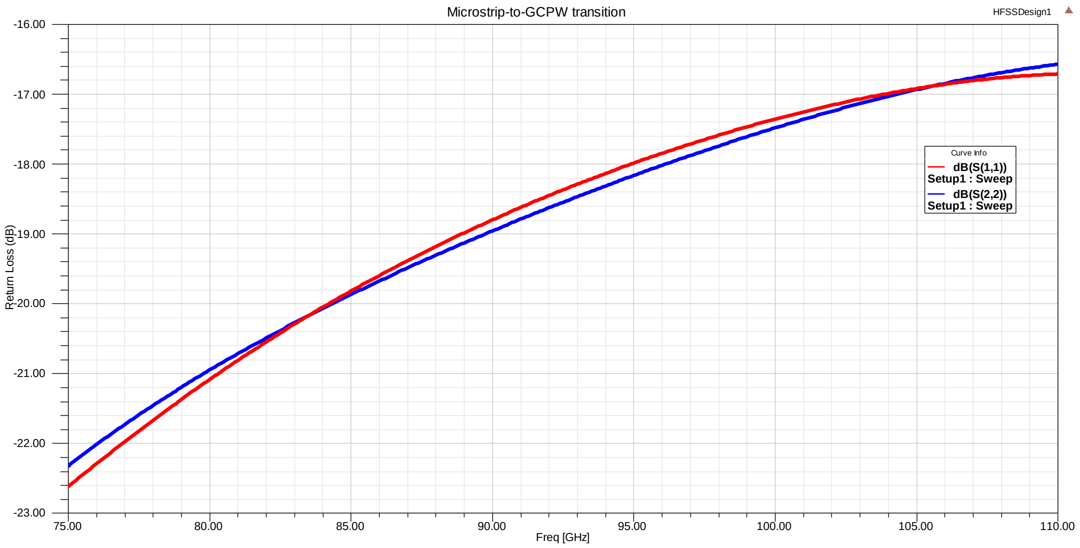

Figure 3.8: Microstrip -to- CPW Transition return loss performance.

On the other hand, Figure 3.9 depicts a simple layout of a GCPW to GCPW transition, while Figure 3.10 presents the simulated performance in terms of return loss, which is better than 15dB from DC up to the end of W band frequency.

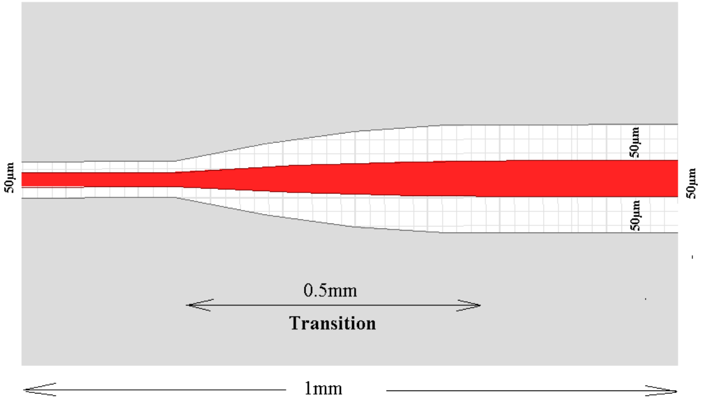

Figure 3.9: CPW-to-CPW transition layout.

These constant impedance transitions are designed and simulated to serve as end connectors of the 110GHz mixer circuit in such a way that IF, LO and RF ports can be conveniently adapted for the CPW wafer probe dimensions, which is the currently available measurement approach.

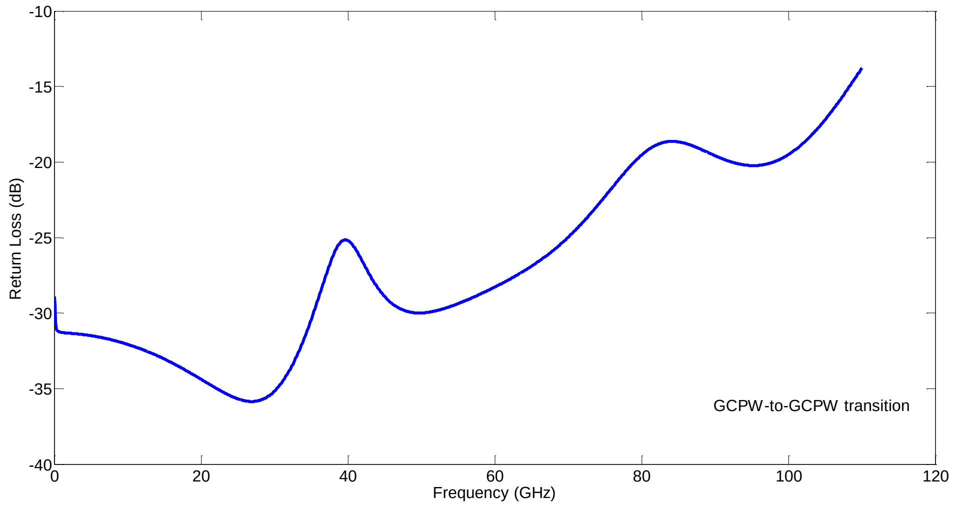

Figure 3.10: CPW -to- CPW transition return loss performance.

3.4 Calibration pieces design

The high frequency devices will be characterised by measuring their S-parameters using a vector network analyser (VNA). Consequently an accurate calibration process is required to validate the actual performance of the device under test (DUT). The aim of calibration is to eliminate errors caused by the fixtures, connected cables or probes used for on-wafer measurement. These errors are well-known as systematic errors which are involved once S-parameters are measured. However, unpredicted errors such as cable repeatability, noise and others cannot be removed by the calibration process. In this case, calibration standards having known values are mounted and measured firstly instead of the DUT. The most used calibration standards can be combination of thru, line, delay, reflect. The thru is a typical 50 Ω zero-length transmission line providing, a direct connection between the two test ports. For on wafer measurements a non-zero length is employed, where its centre defines the reference plane for the DUT. The line is a typical 50 Ω short-length transmission line, which defines the normalisation impedance. The delay is a typical 50 Ω transmission line with 20° - 160° electrical length with respect to the thru. The reflect line can be in the form of open or short transmission line, keeping the same reflection coefficient at the test ports. In general, there are several different calibration methods, such as short-open-load-thru (SOLT), line-reflect-reflect-match (LRRM) and Thru-Reflect-Line (TRL) [95]. With the exception of TRL, these are beyond the scope of this work. TRL can be directly based on the waveguide, while the others use the load standard that is undesired for the thesis's DUTs. Also using the TRL based RWG, the signals' propagation can be distinguished through the back to back configuration of the designed RWG. In the following subsections a set of TRL calibration pieces are designed in HFSS at W-band and G-band frequencies using CPW and RWG technology to ensure the accuracy and performance of the mixer circuits designed in chapter 4 and chapter 5.

3.4.1 TRL design at W-band

These calibration pieces are designed for the110GHz sub-harmonic up conversion mixer. The substrate used is semi-insulating GaAs of 100µm thickness based on GCPW to avoid the mismatch with the mixer circuit. Figure 3.11 depicts the physical layout of the TRL while the performance in terms of return loss (S11) and insertion loss (S21) is presented in Figure 3.12 and 3.13 respectively.

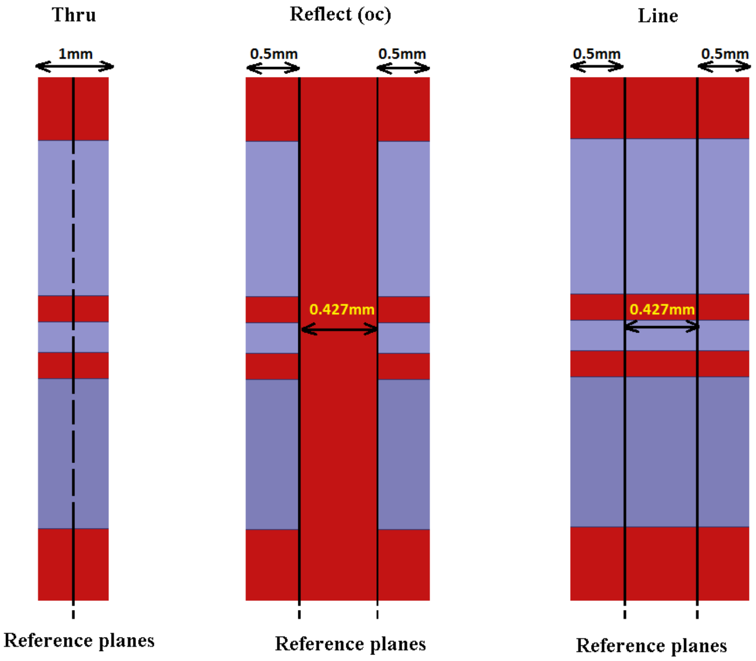

Figure 3.11: On wafer TRL at W-band based CPW / GaAs 100µm thickness.

It should be noted that the return loss of the Reflect line/ open circuit is expected to be naturally small (ideally zero), and therefore its S11 is deliberately presented in Figure 3.13 beside the insertion loss of the Thru and Line, while its inherently high S21 is shown in Figure 3.12. As can be seen from Figure 3.12 the potential return loss for both Thru and Line is below 15dB while the insertion loss of Reflect is below 30dB at the end of W-band. On the other hand, the insertion loss of Thru and Line, as well as the return loss of Reflect are all less than 3dB. Figure 3.14 shows the expected TRL impedance which is kept 50Ω over the whole band. The phase difference between Thru and Line is between 20° - 160° with respect to 20GHz and 110GHz, as shown in Figure 3.15.

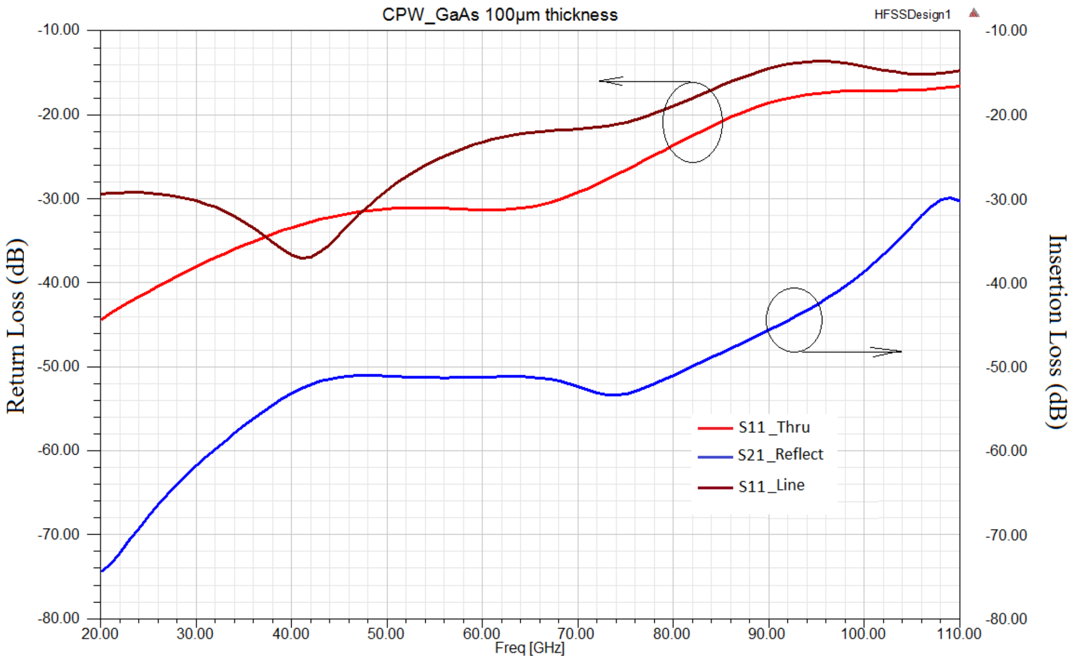

Figure 3.12: The return loss of TRL at W-band based CPW / GaAs 100µm thickness.

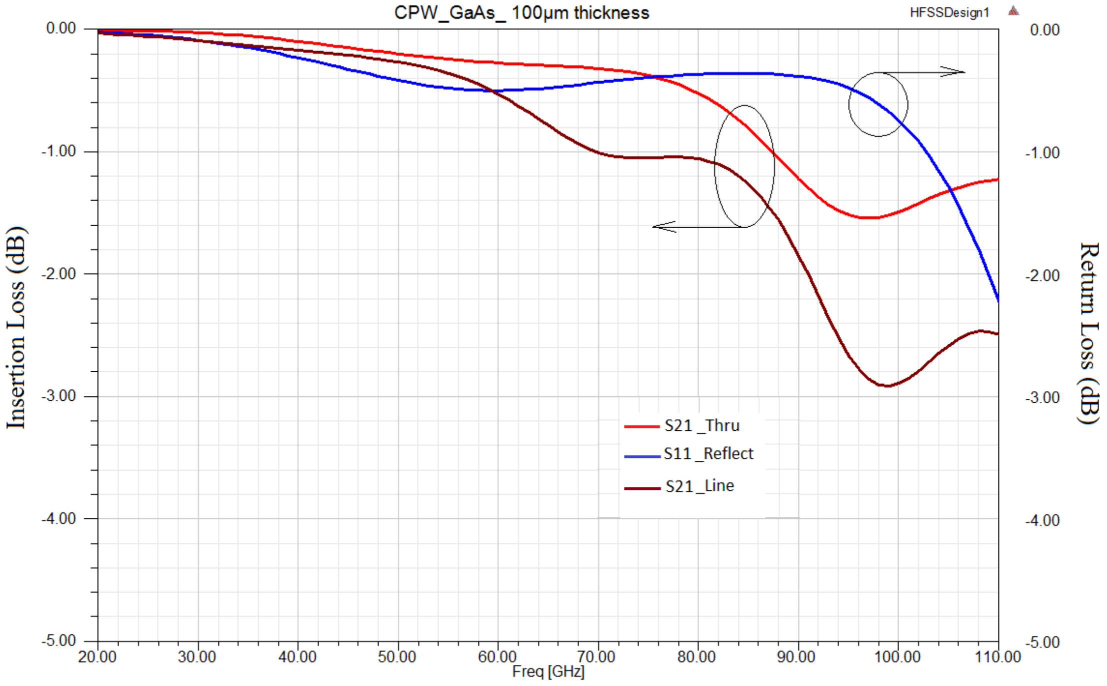

Figure 3.13: The insertion loss of TRL at W-band based CPW / GaAs 100µm thickness.

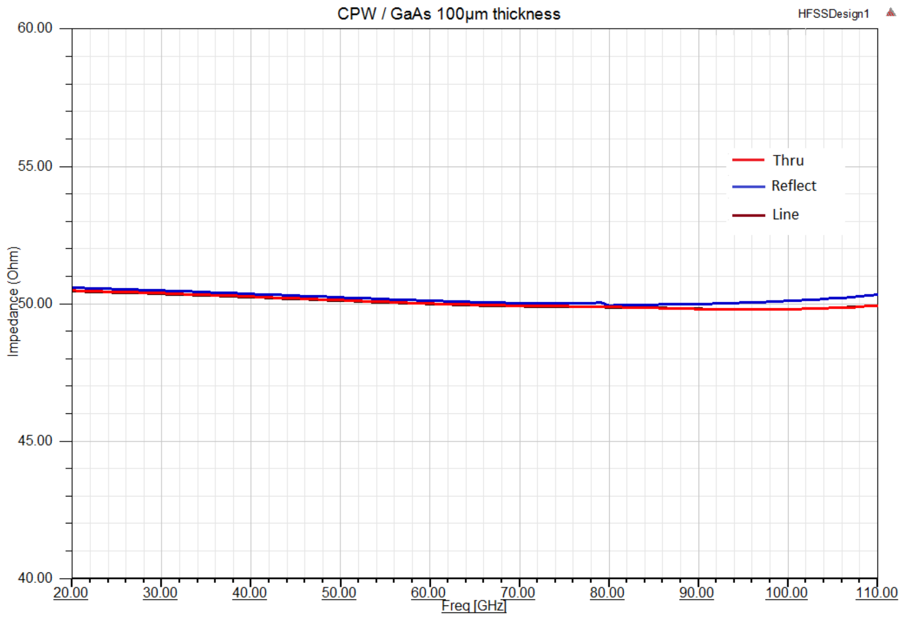

Figure 3.14: The impedance of TRL at W-band based CPW / GaAs 100µm thickness.

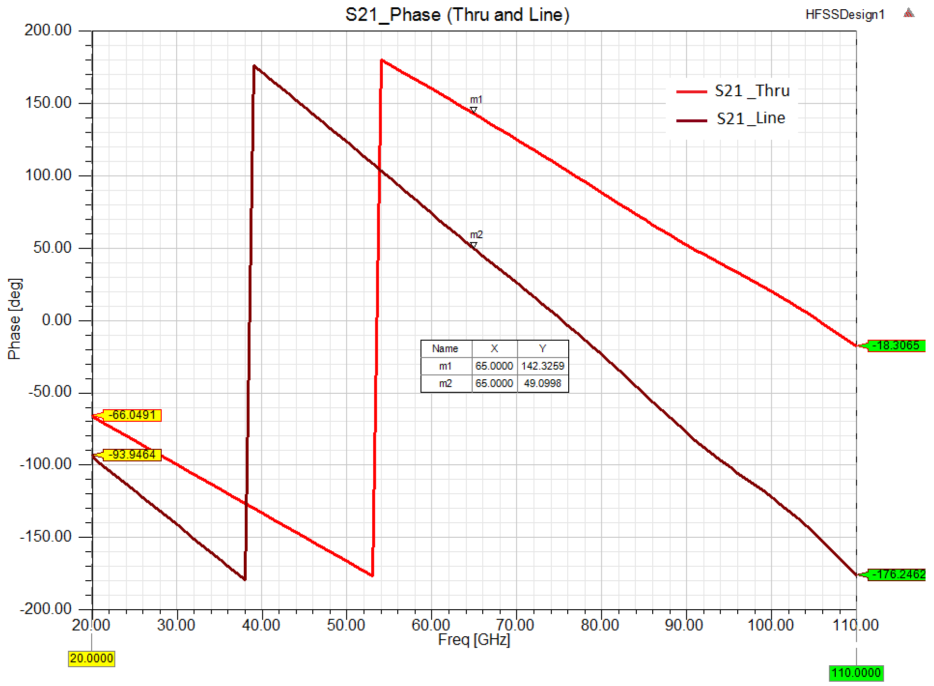

Figure 3.15: The phase difference between Thru and Line at W-band based CPW / GaAs 100µm thickness.

Likewise, similar procedures are employed to design a TRL for the 180GHz sub-harmonic mixer, using a GCPW LO signal at W-band frequency. These TRL elements are based on Quartz with 50µm thickness and use GCPW, similarly to the 180GHz mixer circuit (chapter 5). The TRL layout is illustrated in Figure 3.16, which exhibits a reasonable performance, as shown in Figure 3.17 and Figure 3.18.

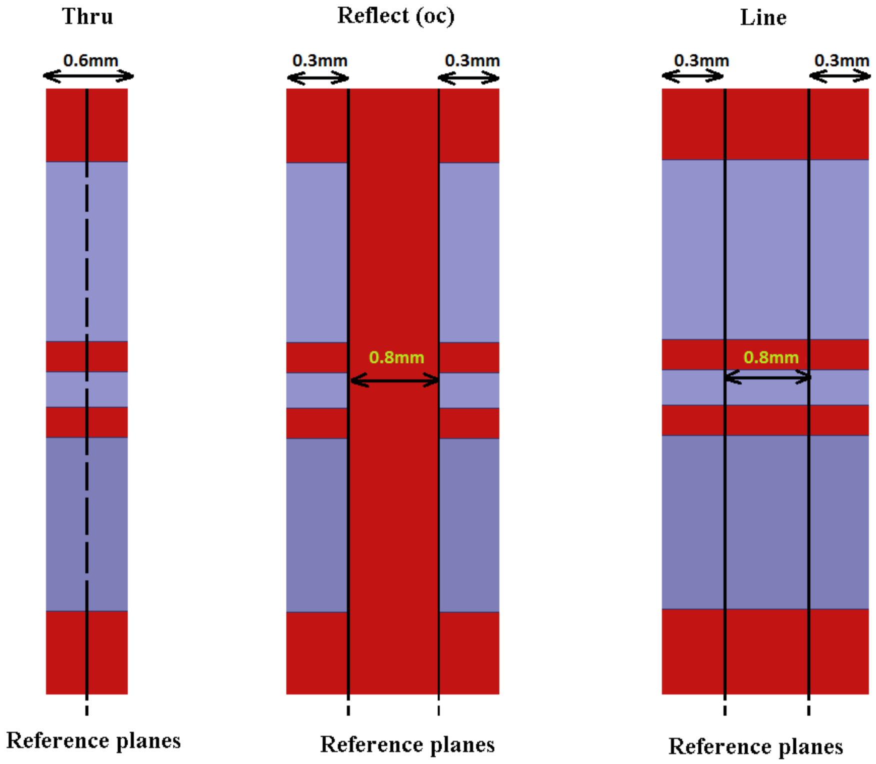

Figure 3.16: on wafer TRL at W-band based CPW / Quartz 50µm thickness.

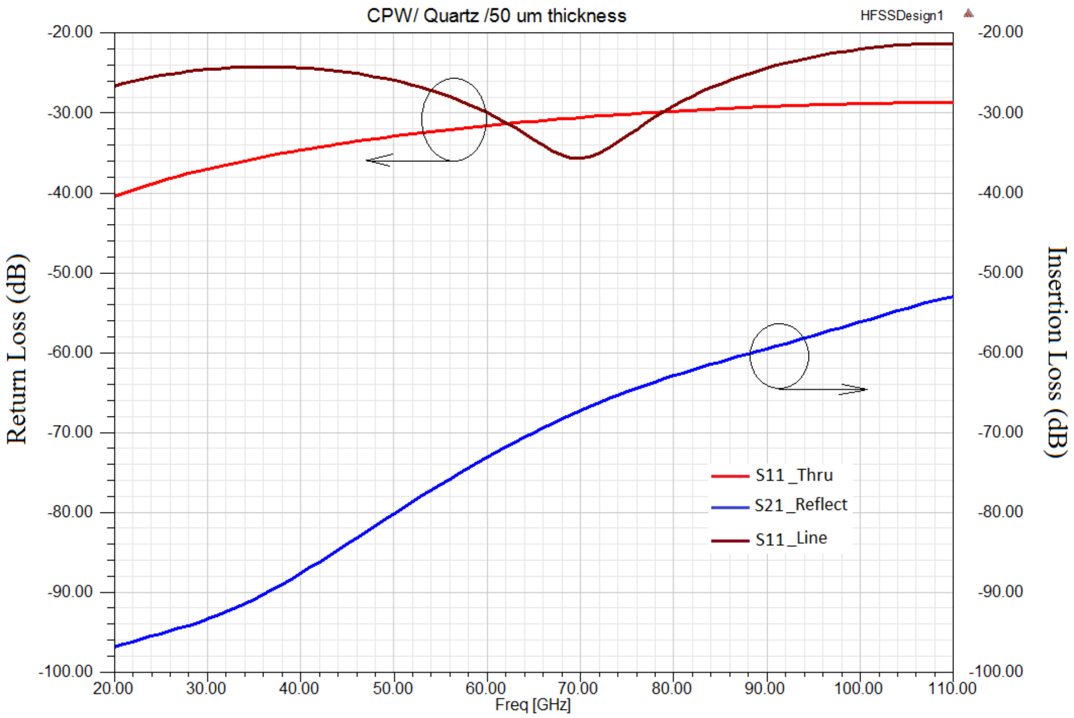

Figure 3.17: The return loss of TRL at W-band based CPW / Quartz 50µm thickness.

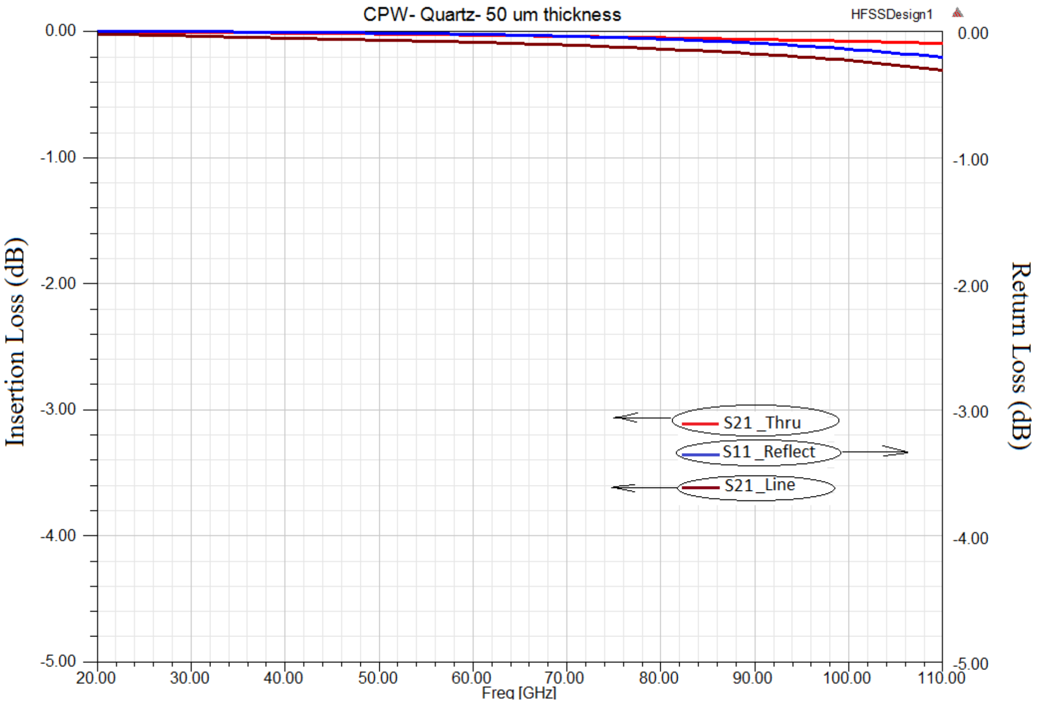

Figure 3.18: The insertion loss of TRL at W-band based CPW / Quartz 50µm thickness.

3.4.2 TRL design at G-band

The previously designed TRL is intended for use with a CPW probe at the LO port at 180GHz for the up converter while the mixer RF port used is via the RWG to micorstrip transition. For this the TRL in this subsection should be based on RWG as well to confirm the measurement results. The TRL at G-band is schematically shown in Figure 3.19 using the antipodal finline transition between a RWG and microstrip line in the form of a fixture connecting the device to the waveguide flanges of a network analyser.

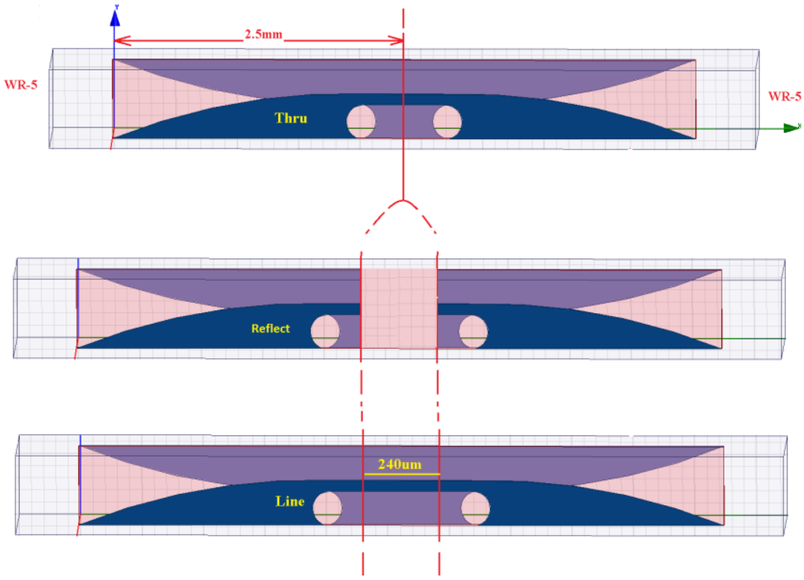

Figure 3.19: TRL at G-band based RWG / Quartz 50µm thickness.

The TRL elements are based on WR-05 where the different length between the Thru and the Line is 240µm, providing 90^{o} shift at 180GHz. The Reflect line is selected to be open circuit to avoid the difficulty in creating a ground connection with the transition’s other side. As a result, the potential performance of both return and insertion losses are shown in Figure 3.20 and Figure 3.21 respectively, where a slight deviation between the thru and the line is observed, which may be resolved by selecting a nonzero-length Thru line.

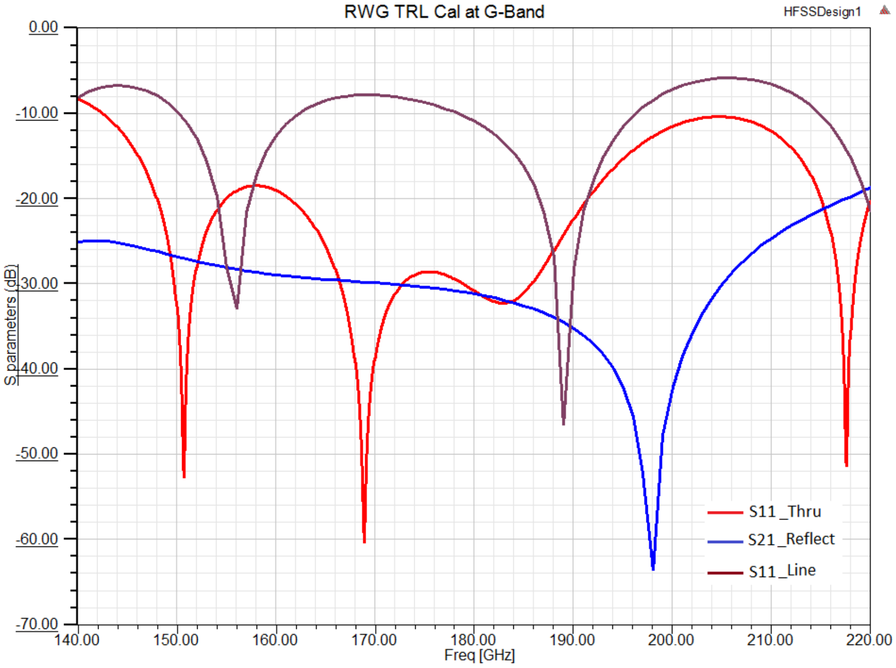

Figure 3.20: The return loss of TRL at G-band based RWG.

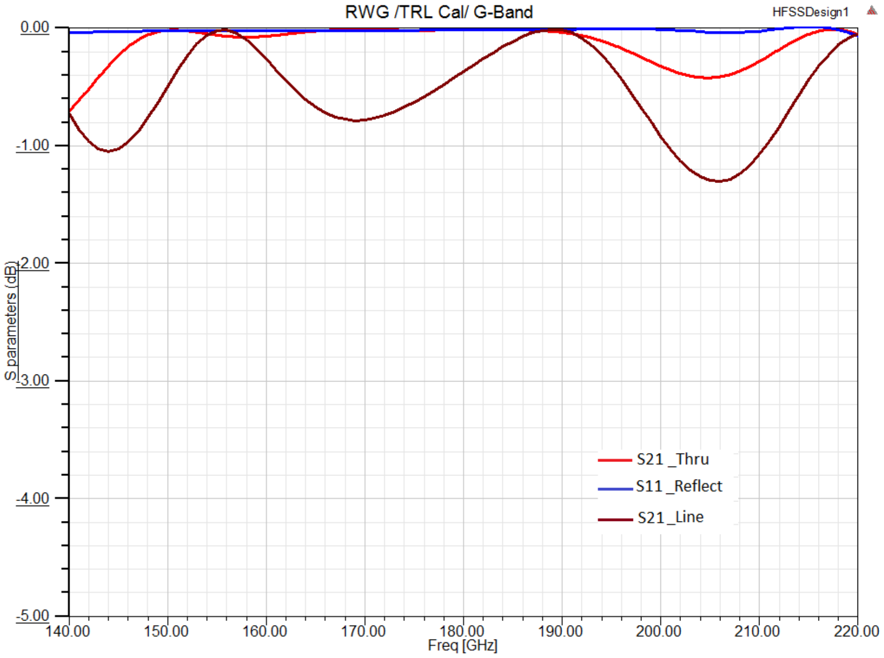

Figure 3.21: The insertion loss of TRL at G-band based RWG.

However, this TRL should be mounted in back to back split blocks, and as these are still the simulated results the measured performance is expected to be slightly different. Based on these reasonable results, now all the main aspects to estimate the complete mixer performance and later measurements are provided. The next chapter will present the design of sub-harmonic mixer operating at the frequencies mentioned earlier and at which these transitions were designed.

3.5 Summary

This chapter aimed to finalise the components required to test the sub-harmonic mixers designed in chapter 5. RWG to microstrip transitions using antipodal finline were considered at two different frequency bands, W-band and G-band, corresponding to LO frequency at 85GHz and RF of 180GHz sub-harmonic mixer. The performance of these transitions was introduced and to validate their performance, E-plane split blocks were designed in a back-to-back configuration. Furthermore, a microstrip to GCPW transition was designed at W-band as an alternative of W-band RWG, giving the flexibility to use a CPW probe instead of using RWG at the measurement stage. For the 110GHz sub-harmonic mixer, on the other hand, a GCPW to GCPW transition was carried out due to this mixer employing a relative small GCPW dimension, which cannot be fitted to the existent CPW probe. For validity with the measurement results in future, this chapter ended by designing a number of TRL calibration standards at W-band and G-band using both GCPW and RWG technology.

Chapter 4 Sub-harmonic Down Conversion RTD Mixers

4.1 Chapter Objective

In the current Chapter, the mathematical equations describing the heterodyne mixing principle are reviewed. Common modes of operation such as fundamental and sub-harmonic, as well as the benefit behind the back-to-back configuration of Schottky diode pair are all discussed. Following this, the chapter presents one of the main goals of the thesis by exploring the design of two-different frequencies (640GHz and 320GHz) of sub-harmonic down conversion mixer based on the fourth harmonic of a LO signal, using both ADS and HFSS software. The focus is to pump these down conversion mixers at especially low LO powers, while at the same time to try to achieve excellent performance.

The various RTD structures used in the current chapter were fabricated at the University of Nottingham during Dr. DP Stenson's PhD program, aimed at oscillator use. They are used in the current thesis to explore their potential use in mixing applications. The growth structure is beyond the current work, alternatively, exploring and discovering the appropriate shape and the nonlinearity that these RTDs should have for mixing is the main goal of this thesis.

Table 4.1 summaries the growth structure of these RTDs. The structure of NU 455 is ant-symmetric, whilst the NU 366 is not due to the presence of the 150nm depletion region (GaAs $5*10^{16}$). This structure was designed as an oscillator/amplifier exploiting the large width of the NDR region, when biased such that the GaAs $5*10^{16}$ is the collector. Although this is not anti-symmetric device, it does give a chance in the simulation to explore two different anti-symmetric structures by mirroring each quadrant in the model as shown in Figure 4.1. This way for a simple structure, we can explore low LO and high LO drive levels for down converters and up converters respectively.

From Table 4.1, the main difference between RTD366 and RTD455 is the position of the nonlinear region within their I-V curve. The RTD455 is closer than RTD366 with respect to the origin, and how this can affect the LO power requirement will be investigated in the current chapter. This may indicate the potential use of a single RTD in place of the dominant Schottky diode pair. This investigation is emerged as the use of the Schottky diode pair in a back-to-back configuration, particularly at high frequencies, comes with two main concerns. Firstly, the I-V characteristics should be identical for these two diodes to exhibit the desired anti-symmetric feature, which requires a high level of controllability during the fabrication. Secondly, the total capacitance is the sum of the two individual capacitances, as the diode pair is connected in parallel, limiting the maximum operating frequency. Furthermore, the two surface based junction are expected to contribute additional noise. Moreover, these two junctions will need more pump power to turn on the diodes at their nonlinearity region, while the availability of LO power at high frequencies is still very low. For this reason, the main aim of this thesis is to find alternative nonlinear elements operating at low amount of LO powers and at high frequencies.

Table 4.1: The growth structure detail of Nottingham devices, named NU366 and NU455[90].

NU-366	**NU-455**
	0.5µm. GaAs ($1*10^{18}$)
0.4µm. GaAs ($2*10^{18}$)	0.1µm. GaAs ($1*10^{17}$)
17Å. GaAs (U.D.)	51Å. GaAs (U.D.)
17Å. AlAs (U.D.)	43Å. $Al_{0.4}Ga_{0.6}As$ (U.D.)
43Å. GaAs (U.D.)	51Å. GaAs (U.D.)
17Å. AlAs (U.D.)	43Å. $Al_{0.4}Ga_{0.6}As$ (U.D.)
17Å. GaAs (U.D.)	51Å. GaAs (U.D.)
1500Å. GaAs ($5*10^{16}$)	0.1µm. GaAs ($1*10^{17}$)
2µm. GaAs ($2*10^{18}$)	2µm. GaAs ($1*10^{18}$)
GaAs (N^+)	GaAs (N^+)

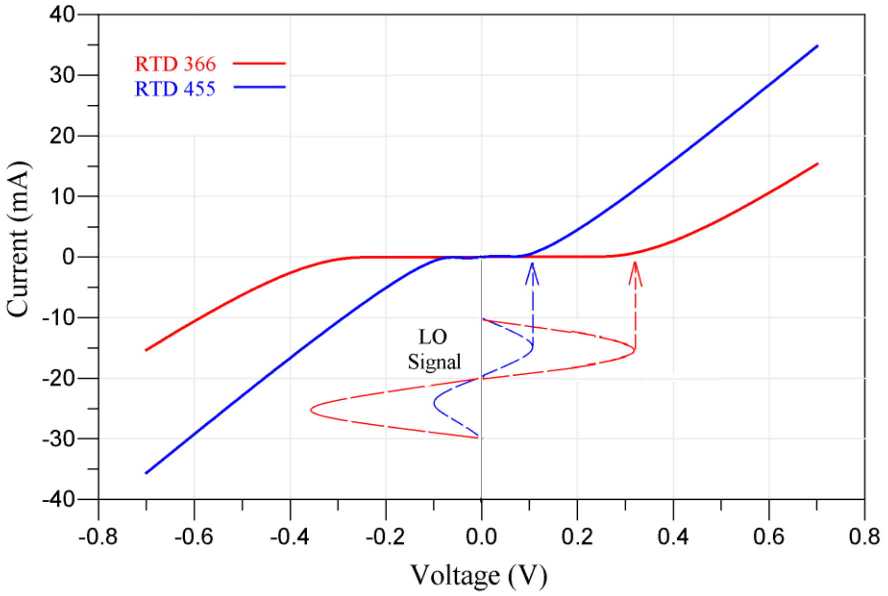

Figure 4.1: Two different RTDs and the potential drive point of the LO signal.

4.2 Introduction

The core element of a mixer is a non-linear junction, where its nonlinearity is responsible for providing the mixing between two input frequencies and producing a set of new output frequencies, whether down-conversion or up-conversion, by respectively taking the difference or the sum of these two main input frequencies and their harmonics. Depending on the preferred application, the mixers can be one of three main types, single ended, single balanced, or double balanced. The advantages and disadvantages of each one are presented in Appendix-I. The performance of mixers is generally evaluated through their Conversion Loss (CL), Noise Figure (NF), Local Oscillator (LO) drive, and isolation between the ports (Appendix-I). Among these, the primary figures of merit are the CL, the LO pump power, and the equivalent noise temperature (T_e) or noise figure. The CL is defined in dB to provide the difference in power level between the desired output signal and the input signal, while the LO power represents the required level at which the optimum performance of a mixer can be demonstrated. Here 0dBm corresponds to 1mW of drive power. The equivalent noise temperature can be presented as $T_e = N_0/Bk$ [96] where N_0 is the output noise expressed in Watts, B is the bandwidth expressed in Hertz, and the k is the Boltzmann constant. The T_e is the equivalent of a so-called white noise source, which represents the all different types of noises in a mixer circuit. Among these, the shot noise and the thermal noise are commonly considered when mixers are characterized. The shot noise is due to the electron flow through the barriers whilst the thermal noise is because of the random thermal motion of the electrons in the device structure. The hot electron noise is also another type of noise that is a function of the diode current leading to an increase in the series resistance[97]. The 1/f noise can also be an issue, because this low frequency noise can be up-converted to much higher frequencies. This noise is a result of traps at the surface capturing and replacing electrons, which can then be up-converted to contribute to the overall noise figure[98]. In this thesis the mixers are characterized with the CL as a function of the LO power level.

Fundamental and sub-harmonic mixers are the broadest classifications where mm and sub-mm wave mixing devices can be operated. In principle, the operating mode depends on the selected harmonic number of the LO signal (usually 2nd or 4th harmonic) for satisfying a certain application requirement. At mm and sub-mm wave frequencies the device parasitics, such as junction capacitance and series resistance, have a marked effect on performance, and LO pump powers are often weak. Fundamental mode means that the intermediate frequency (IF) is only obtained by mixing the fundamental frequency of a radio frequency (RF) signal with that of the LO signal, while the IF signal in sub-harmonic-type operation is produced by taking the difference between the fundamental frequency of a RF signal and where the LO is a sub-harmonic of this, typical a half or quarter of the RF signal.

4.2.1 Fundamental mode based operation

In the ideal case of fundamental mixer operation, once a RF and a LO signal are applied as shown in Figure 4.2, the output IF signals frequencies include both the sum and difference of these different input frequencies. With a low-pass filter, the IF could be written in the down-conversion case as:

$$IF = RF - LO \tag{4.1}$$

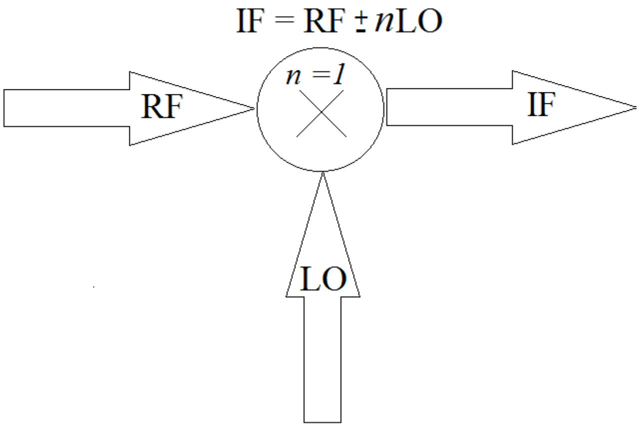

Figure 4.2 : A simple illustration of the fundamental mixer.

On the other side, in the case of up-conversion, the RF at the output port is obtained by mixing the IF and LO at the mixer input port, and then after a high pass filter the RF could be given as:

$$RF = IF + LO \tag{4.2}$$

A nonlinear element has to be involved in such a mixing process. The prospective mixing devices can be diodes, transistors or superconducting junctions. The nonlinear current-voltage characteristics that they possess are exploited to achieve this mixing function. From a conceptual point of view, assuming two different signals applied to a single diode the total voltage across the diode can be written as:

$$V_T = A_T V_{in} \tag{4.3}$$

where the total amplitude (A_T) and the total input voltage (V_{in}) can be represented respectively as:

$$A_T = A_{RF}.A_{LO} \tag{4.4}$$

$$V_{in} = \cos(2\pi_{RF}t) \times \cos(2\pi_{LO}t) \tag{4.5}$$

where A_{RF} and A_{LO} are the amplitude of RF and LO signal respectively.

The total corresponding current of a single Schottky style diode can be expressed as:

$$I_{Ts} = I_S[e^{(V_{Tn})} - 1] \tag{4.6}$$

where I_s and V_{Tn} are the reverse saturation current and the normalised total voltage with respect to the thermal voltage of the diode (i.e., q/ ηkT), where k,q,η and T are the Boltzmann's constant, the electron charge, diode's ideality factor and temperature in Kelvin respectively. The I_{Ts} (s here means a single diode) can be rewritten in the form of a Taylor expansion[99] as:

$$I_{Ts} = I_S[1 + V_{T_n} + \frac{{V_{T_n}}^2}{2!} + \frac{{V_{T_n}}^3}{3!} + \cdots] \tag{4.7}$$

By examining the above equations, it is obvious that a considerable number of frequency components can be provided, not only the sum and difference frequencies are generated within the squared term in Equation 4.7, but twice the frequency of the input frequencies, i.e. 2RF and 2LO are introduced as well. Furthermore, other frequency components such as 3RF, 3LO, (2RF - LO) and (2LO-RF) are embedded through the cubic term of the same equation. In practice since the LO signal is by far the highest amplitude component, its harmonics and mixing products involving these harmonics are the most prominent. As a result, fundamental and sub-harmonic mixing can be performed using a nonlinear element such as a diode. The next section will discuss this in terms of sub-harmonic mode operation.

4.2.2 Sub-harmonic mode operation

On the whole, mixers operated with a sub-harmonic frequency are more widely required at mm wave frequencies than fundamental frequency mixers because of the high cost and complexity of obtaining a local oscillator, even if sub-harmonic mixers show less performance in terms of conversion loss [100]. Apart from the case of fundamental frequency generation, a non-linear element with an anti-symmetric I-V characteristic is necessary to provide efficient sub-harmonic mixing. For a long time, the Schottky diode pair linked in a back-to-back fashion satisfies such a task. Indeed the main benefit behind using the anti-symmetric characteristic of such a combination of diodes is to suppress the mixing at the fundamental frequency; this means that the second harmonic can be generated provided there is enough power at the sub-harmonic[100]. However, the RTD has a single device junction, which when physically symmetric is capable of producing the same anti-symmetric I-V curve, and whose performance in the context of sub-harmonic mixers (n=4) will be investigated in down conversion mixing throughout this chapter, and in up conversion mixing (n=2) in the next chapter. However, to explain the basic principle of sub-harmonic mixing, Figure 4.3 depicts a simple form of a sub-harmonic mixer.

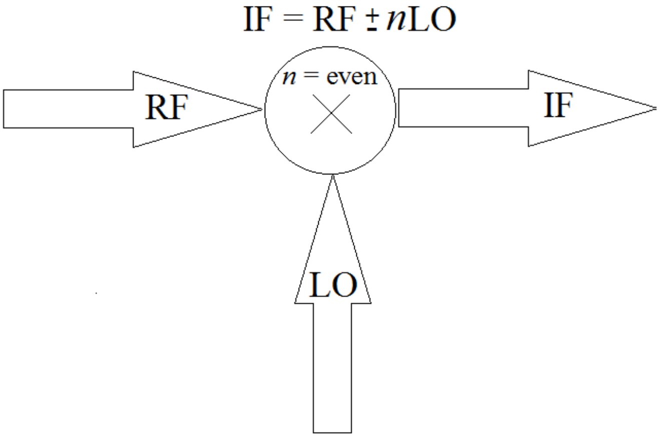

Figure 4.3: A simple illustration of the sub-harmonic mixer.

Once two input frequencies, RF and LO, are applied to a sub-harmonic mixer, the output frequency (IF) can be introduced as:

$$IF = RF \pm nLO \tag{4.8}$$

Where ± indicates the conversion type, down (-) or up (+), while *n* is the mixing order; for instance, by using a sub-harmonic with second order, *n* = 2, and fourth order, *n* = 4, permitting the use of an LO with one-half and one-quarter the frequency respectively that is used with a conventional fundamental mixer (n =1). By increasing the mixing order however, there can be a dramatic decrease in the amplitude of the available LO as can be seen from Equation 4.7 and the conversion efficiency does suffer. Moreover, a large number of intermodulation components are generated, thus a filter at the output of the mixer port is often required. Although a single diode is able to achieve sub-harmonic mixing, an anti-parallel diode pair (APDP), as represented in Figure 4.4, is still a preferred configuration of sub-harmonic mixer circuits due to the intrinsic suppression of fundamental.

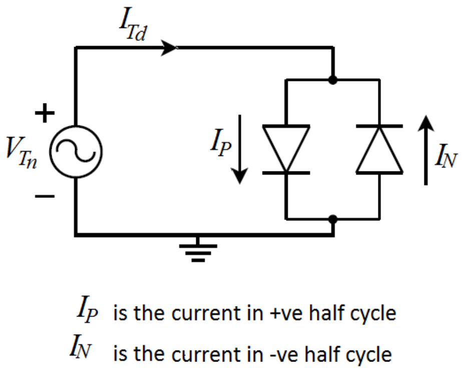

I_P is the current in +ve half cycle
I_N is the current in -ve half cycle

Figure 4.4: A basic configuration of anti-parallel diode pair.

Having two different signals applied to the APDP, the total voltage (V_T) across this configuration is similar to the total voltage of the single diode presented earlier in Equation 4.3; however the total current of these double diodes, I_{Td}, (d here represents the double diodes) will be the sum of two currents presented individually in each half cycle of the input voltage, which can be introduced as:

$$I_{Td} = I_P - I_N \tag{4.9}$$

For which the individual current with the half positive cycle *(I_P)* and the negative one *(I_N)* can be written respectively as:

$$I_P = I_S[e^{(V_{Tn})} - 1] \tag{4.10}$$

$$I_N = I_S[e^{(-V_{Tn})} - 1] \tag{4.11}$$

By adding the two Equations, the I_{Td} can be rewritten in the form of a Taylor expansion[99] as:

$$I_{Td} = I_S[(1 + V_{T_n} + \frac{{V_{T_n}}^2}{2!} + \frac{{V_{T_n}}^3}{3!} + \cdots) - (1 - V_{T_n} + \frac{-{V_{T_n}}^2}{2!} + \frac{-{V_{T_n}}^3}{3!} + \cdots)] \quad (4.12)$$

which can be revised in a simpler form as:

$$I_{Td} = I_S[2(V_{T_n} + \frac{{V_{T_n}}^3}{3!})] \quad (4.13)$$

According to Equation 4.13, a number of frequencies will thus be generated, indicating that the odd sub-harmonic mixing between the input frequencies is available with this APDP configuration in contrast to the even-order products which are clearly prohibited. Furthermore the two main input signals (RF and LO) are still presented at the output port, but these frequencies can be suppressed by employing a filter.

Before moving to the sub-harmonic mixers designs in the next sections, there are some key features that mixers should have to be considered practically at millimeter frequency band and beyond[101]. These features can be summarised as follows:

- The non-linearity portion of the current-voltage characteristic of the diode is required to be adequate since the desired mixing depends on this feature.
- The noise level should be as low as possible at the output port.
- For achieving optimum performance, sufficient impedance matching should be provided at the three different ports of the mixer to maximize the input signals and to reduce the leakage of power.
- A practical amount of LO power is required for pumping the diode. Ideally this should be as low as possible, provided dynamic range and large RF input powers are not a problem.

4.3 RTD sub-harmonic down-conversion mixer design

This section deals with estimating the RTDs' performance as non-linear elements in sub-harmonic down conversion mixing applications, via examining the design of two different sub-harmonic mixers operating at 664GHz and 320GHz. Conceptually, in order to design a proper diode-based mixer, a set of different parts should be distinguished and optimised individually, i.e. by subdividing the structure of the mixer sub-system into the following substructures:

- RF waveguide to planar transition, such as microstrip or coplanar waveguide.
- RF impedance matching network.
- Appropriate non-linear elements such as Schottky diodes, RTDs or others.
- LO impedance matching network.
- RF-LO Filter.
- LO waveguide to planar transition, if LO is at a high frequency.
- IF filter or impedance matching network, and IF amplifier.

The transition types and their design were detailed previously in chapter 3. Their correct functionality was assured and the results are employed here, i.e. the performance of all the sub harmonic mixers presented in this thesis include the transitions losses. The rest of the above mentioned parts will be designed and investigated in this chapter. However, as a key step of the methodology, in order to represent RTDs in a CAD environment and to be able to make a detailed comparison with the counterpart Schottky diode pair, the Symbolically Defined Device (SDD) model provided in the ADS environment is used as no built-in RTD models are currently available. The SDD model only represents the nonlinear resistor (i.e., the thermally assisted tunnelling I-V characteristic) without the associated elements commonly used more elaborate RTD models, such as series inductor, series resistor and parallel capacitor. Adding such elements, possibly through their own SDD representation, is required to more accurately evaluate the potential performance. For verifying the reliability of the SDD model, two different approaches were compared (discussed step by step in Appendix-II). The built-in Schottky model and the author's own SSD model description of a Schottky were used to prove the validity of the SDD model in comparing the Schottky's performance in terms of conversion loss. The comparison between the built-in diode model and the Schottky representation showed <1.5dB difference at the optimum performance for the complete mixer design. Therefore the SSD modelling approach can be considered as a trustworthy tool to estimate the likely performance of the RTD.

The design methodology stages are illustrated in Figure 4.5, where firstly the I-V characteristic of the RTD is modelled using the SDD capability, based on fitting a polynomial to the measured RTD I-V curve using Matlab software. Secondly the sub-harmonic mixer circuit is divided into two impedance matching networks, the RF/IF and the LO, which are individually optimised in Ansys HFSS. Besides these matching networks, two different waveguide to microstrip transitions, using antipodal finline tapers, are designed using HFSS in such a way that the RF and LO signals can be transformed from a waveguide mode to a microstrip mode. The HFSS results of these transitions are exported back to ADS in the form of S-parameters blocks and included in the ADS model to accurately estimate the whole performance of the mixer, including the discontinuity effects.

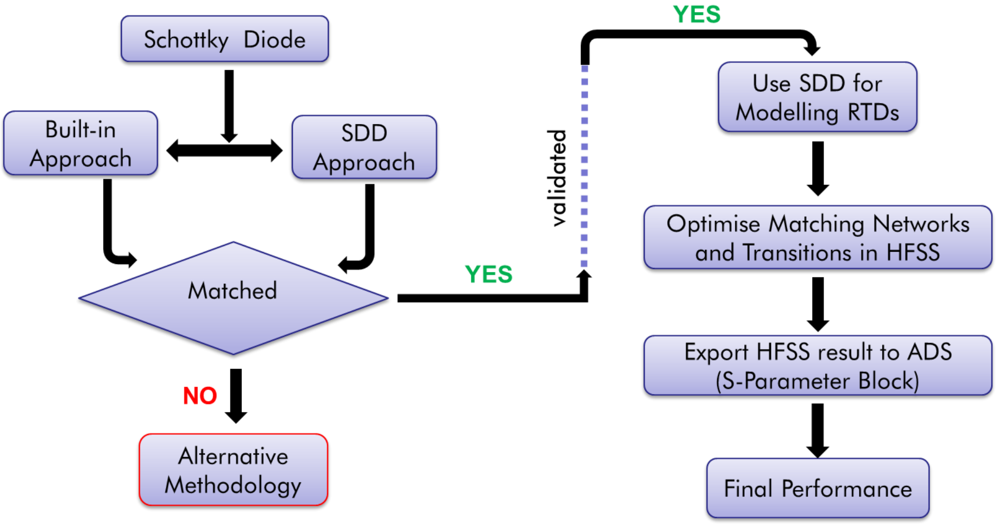

Figure 4.5: The design methodology flow chart.

4.3.1 640GHz 4th Sub-harmonic down conversion mixer

A topology of a sub-harmonic down conversion mixer exploiting the fourth harmonic of the LO signal is shown in Figure 4.6. This sub-harmonic mixer is intended to down convert a high frequency signal of 640GHz to an intermediate frequency signal in the range of 2GHz by mixing the fourth harmonic of a 159.5GHz LO signal. The non-linear elements used are a two single junction RTDs (instead of two-pairs of Schottky diodes), separated by a quarter wave transmission line at the LO frequency. The motivation for the use of a pair of RTDs with the 4th harmonic of the LO signal is to investigate and explore the potential for low LO power requirement, and then compare this to the recent result of a 640GHz 4th sub-harmonic mixer based on two pairs of Schottky diodes[102]. This paper demonstrated a simulated conversion loss of 13.5dB with a LO power of -2.5dB, and this result will serve as a benchmark for the current mixer.

The selected series resistance and junction capacitance are 14Ω and 1.3fF, which are as similar to the typical values for Schottky diodes at this frequency range[102]. Although the Schottky junction structure is different to that of the RTDs, the aim is to evaluate the RTDs in terms of nonlinearity and power requirement when compared to equivalent Schottkies. Note that this 1.3fF capacitor represents the specific capacitance at which the bias voltage is zero, consequently this constant value of the capacitance does not reflect the actual behaviour of the C-V characteristic. To obtain a truly accurate performance the capacitance as a function of the applied voltage should be known (i.e., the measured C-V curve), but no opportunity was found during this PhD program to make this measurement. The focus was on the study of the potential shape of the I-V curves as a function of the physical parameters. However, the nonlinearity region of these RTDs typically shows at a voltage range of 0.1-0.3V, which is close enough to zero bias voltage.

To optimise the circuit, open and short stubs are used at both sides of the RTD pair and impedance matching networks, in the form of transmission lines are empolyed, at the input and the output ports. The main advantage behind providing a short circuit stub of λ/4 at the LO side is to reflect to the RF signal again to the RTD, while having no effect on the LO signal. Likewise, an open stub of λ/2 at the RF side works as a short circuit for LO and open for RF signal, again placing the RTDs at a maximum of the LO signal. In the meantime, in order for the output signal (IF) to be extracted, series and shunt stubs are located on the IF side at λ/4 at RF frequency to filter out the RF and LO.

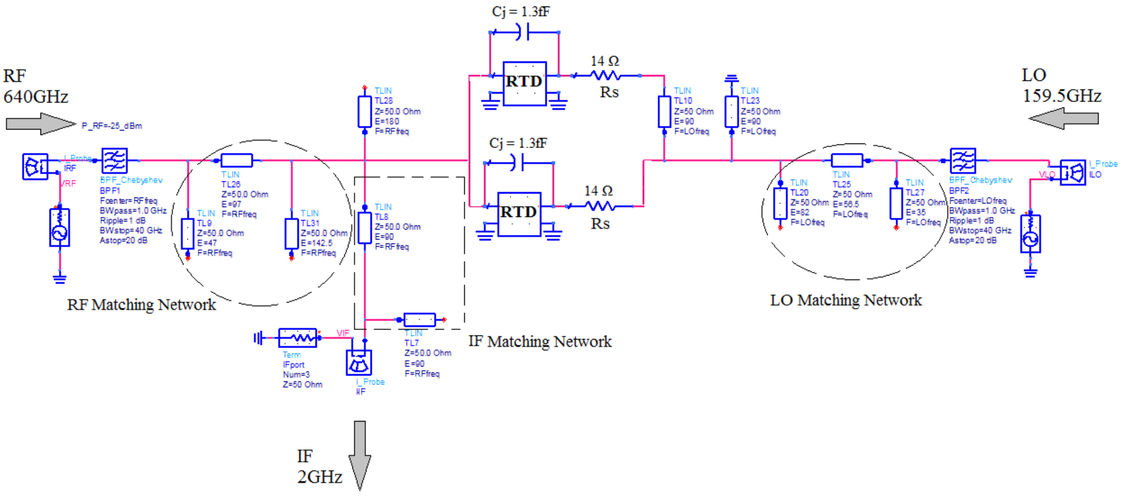

Figure 4.6: The designed topology of a 640GHz mixer circuit.

As mentioned before there are different parameters such as LO drive level, conversion loss (CL), noise temperature, etc., that are used to characterise the performance of a given mixer of which the highest priority is the CL. As a consequence, the performance in terms of CL as a function of LO power (arguably the next most important parameter at these high frequencies) for both RTDs and Schottky two-pair diode is shown in Figure 4.7. The RTDs deliver acceptable levels of CL in range of 17dB compared to the Schottky. The typical CL of a 4th harmonic Schottky mixer at this frequency is in range of 10-12dB with +6dBm, as mentioned in Chapter 1. This initial CL performance is achieved without optimising the mixer, as the focus here is just on the required LO power.

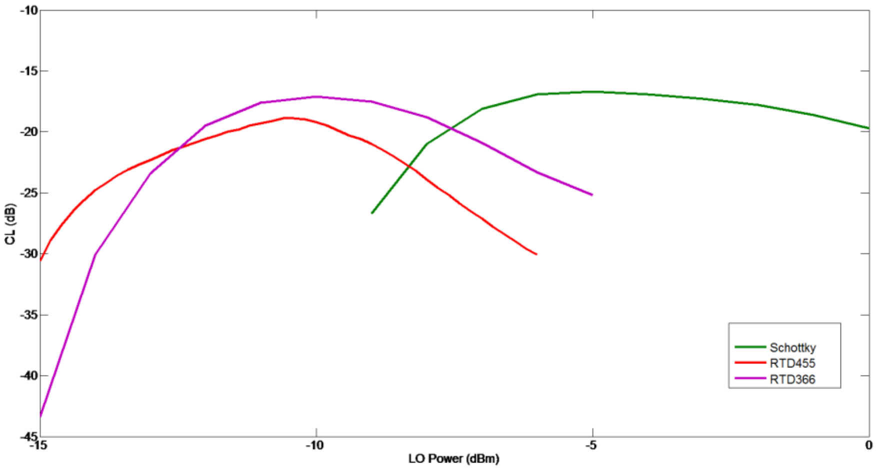

Figure 4.7: The conversion loss performance of the 640GHz mixer.

From the same Figure, there is the prospect that the design based on RTDs requires a very small amount of LO power compared to the Schottky diode version, showing a considerable enhancement in terms of LO power requirements to be less than -10 dBm. Such a feature is a significant advantage in this high frequency region. On the other hand, it should be noted that the simulation of these RTDs are derived from devices operated at a Liquid Nitrogen temperature / 77K. The reason for this is to explore the potential effect of band structure engineering to hopefully adapt the Fermi- Dirac distribution in the emitter to mimic the effect of a reduction in temperature, as discussed in Chapter 2. This cooling is a disadvantage for many applications, but is explored here to gauge the effect on a real room temperature mixer; although 77K is still not super-cooled when compared to SIS and HEB based mixers. However as mentioned earlier, the aim of this study is to explore the potential of tailoring the I-V characteristic to provide efficient mixing at low LO power regardless of the temperature environment. This lies in the fact that RTD growth structure has a very good level of flexibility when compared to other nonlinear elements. This band structure engineering is possible with RTDs but not with Schottkies and, if valid, may also contribute to a lower noise temperature.

4.3.2 320GHz 4th Sub-harmonic down conversion mixer

Based on the previous promising result of the 640GHz mixer, especially using the low LO pumped power, this section will present detailed design steps of a scaled version of 640GHz sub-harmonic down conversion mixer operating at 320GHz, a frequency readily testable at Leeds.

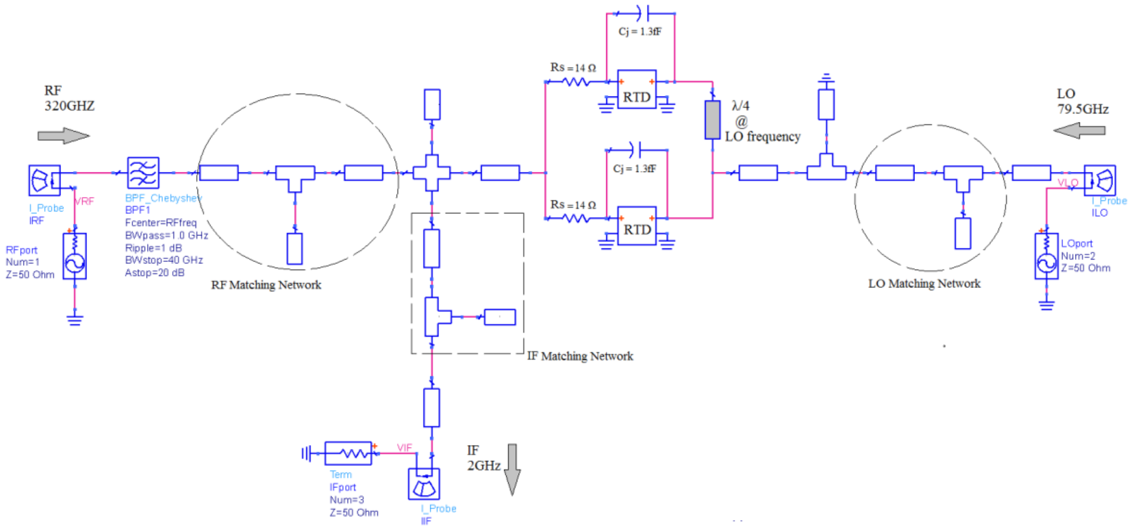

Figure 4.8: The initial configuration of a 320GHz mixer circuit using ADS.

The 320GHz mixer uses the same methodology and its configuration is shown in Figure 4.8. It uses the fourth harmonic of a LO signal at 79.5GHz and again employs a pair of RTDs with slightly different growth structure and based on current-voltage derived from cryogenic temperature measurement, 77K. To obtain a good performance, this configuration will be divided into parts such as RF band pass filter, RF/IF and LO impedance matching networks. These will all be optimised individually and discussed before obtaining the final performance of the mixer.

Firstly the band pass filter at RF port is designed by employing microstrip coupled-lines as shown in Figure 4.9, and optimised using two different software packages, ADS and HFSS. By tuning the width, length and the space between these microstrip lines, the desired performance of the filter can be accomplished. The resulting comparison is shown in Figure 4.10 where the performance is in good agreement at 320GHz (the RF signal). As can be seen from this Figure, there is a small deviation at higher frequencies (i.e., 100GHz and beyond) shown by HFSS. This is due to the EM tool taking the model discontinuities into consideration more accurately compared to ADS.

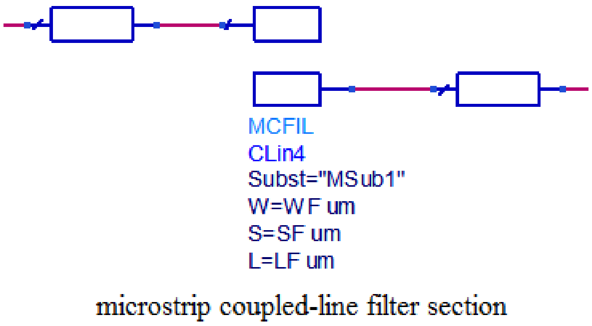

Figure 4.9: The configuration of the band pass filter at 320GHz RF port.

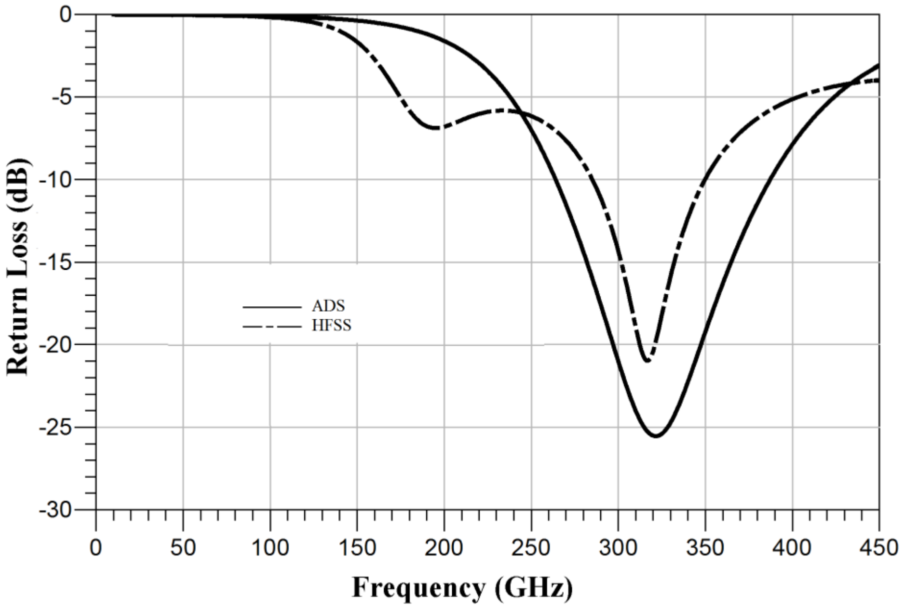

Figure 4.10: The band pass filter performance at 320GHz.

The next step is to optimise the input impedance matching networks both in ADS and HFSS. These are based on different lengths of microstrip transmission lines. These lines have a width of 35µm and a metal thickness of 1µm, while the height of the quartz substrate is 100µm. Such parameters offer a 100Ω characteristic impedance (Zo) which matches well with the output impedance of the waveguide to microstrip transitions (their design detailed in chapter 3). The performance of these impedance matching networks is presented in Figure 4.11 and Figure 4.12 from which a decent performance of these networks is clearly provided at the desired frequencies. Figure 4.11 presents the return loss at the RF input port of the mixer with respect to the RTDs. The incident signal is in a good match with the RTD’s impedance at 320GHz, where the return loss is well below -10dB meaning that at least 90% of the input power can be delivered to the RTDs. Similarly, Figure 4.12 presents the return loss at the input LO port of the mixer with respect to the RTDs. The 79.5GHz LO signal is matched well with the RTD’s impedance where the return loss is also below -10dB.

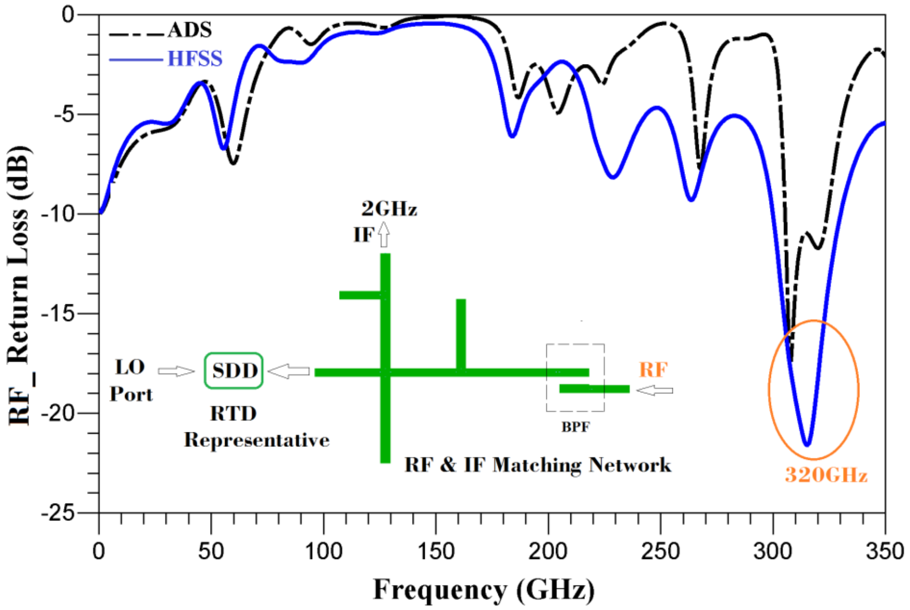

Figure 4.11: RF/IF matching network performance in both ADS and HFSS, at 320GHz.

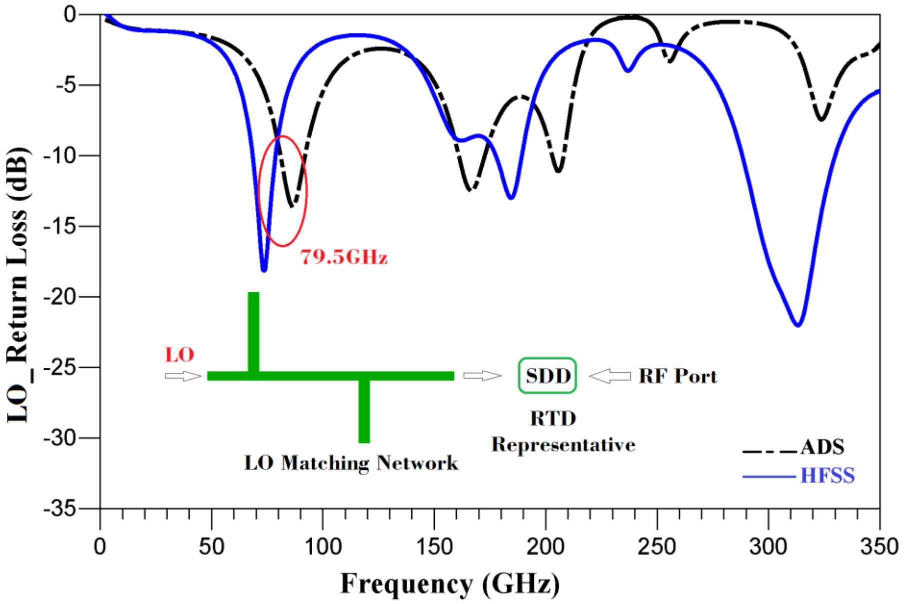

Figure 4.12: LO matching network performance in both ADS and HFSS, at 79.5GHz.

The HFSS results of these previous elements are exported to ADS in the form of S-parameters blocks, shown in Figure 4.13, to accurately evaluate the final performance of the 320GHz mixer.

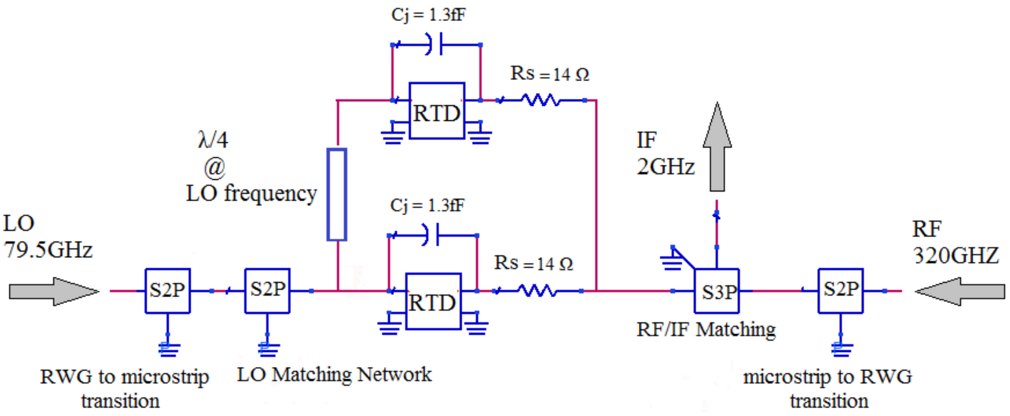

Figure 4.13: The finial configuration of 320GHz sub-harmonic mixer.

Two different RTDs layers, the RTD 366 and RTD 455, are explored in this sub-harmonic mixer circuit as presented in Figure 4.14 and Figure 4.15. These RTDs show improved CL performance (<7dB) compared to the un-optimized 640GHz mixer. The performance of RTD 455 in terms of LO requirements, which is very low in the range of -9.5dBm, when compared to 0Bm of RTD 366, is also a very attractive result, as seen in Table 4.2. The main difference in terms of the low operated LO power between the RTD366 and the RTD455 is the position of the nonlinear region within their I-V curve. This was shown previously in Figure 4.1, where the RTD455 is closer than the RTD366 with respect to the origin.

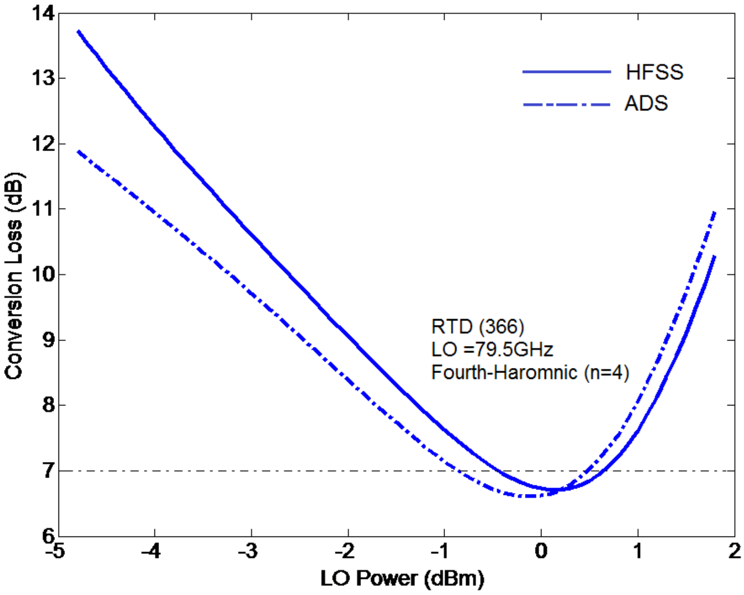

Figure 4.14: The RTD 455 performance at 320GHz.

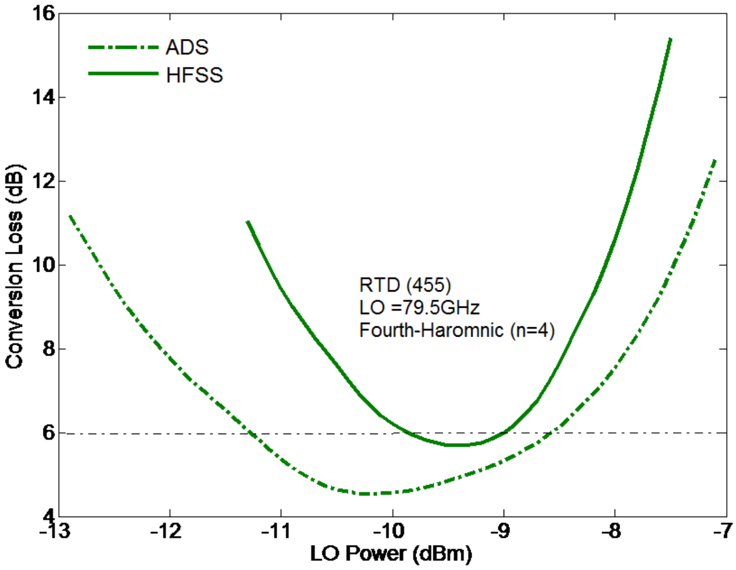

Figure 4.15: The RTD 455 performance at 320GHz.

Table 4.2 compares the RTDs’ result presented in the current work to other published outcomes, based on back-to-back Schottky diodes. The RTD performance in terms of conversion loss is clearly remarkable, especially at sub-millimeter wavelengths and with a low harmonic number and low LO power requirement, which is extremely low when compared to the Schottky diodes. As RTD's layer structure is in the form of a single quantum well sandwiched between two adaptable barriers, such a low drive level is expected since the RTD's knee (i.e., the initial point of the non-linear region) of the I-V curve starts off at 0.15V which is around a quarter of that for a GaAs Schottky voltage (typically 0.7V). Therefore, using a single RTD junction in place of a Schottky diode pair can be considered a very promising alternative.

Table 4.2: Comparison with other published results, based on Schottkies.

Freq. (GHz)	CL (dB) *simulated	Device	LO Signal (GHz)	LO Power (dBm)	Bias	Ref.
182	12.7	Schottky	91	+6.5	±0.4V	[47]
170 - 210	16-12	Schottky	80	+10	1.1mA	[48]
215 - 225	8.2*	Schottky	105	__	none	[49]
310-350	5.7* DSB	Schottky	155	+7	none	[103]
340	7.3* SSB	Schottky	170	+6	none	[54]
320	< 7* SSB	RTD	79.5	0	none	This work
320	< 6* SSB	RTD	79.5	-9.5	none	This work

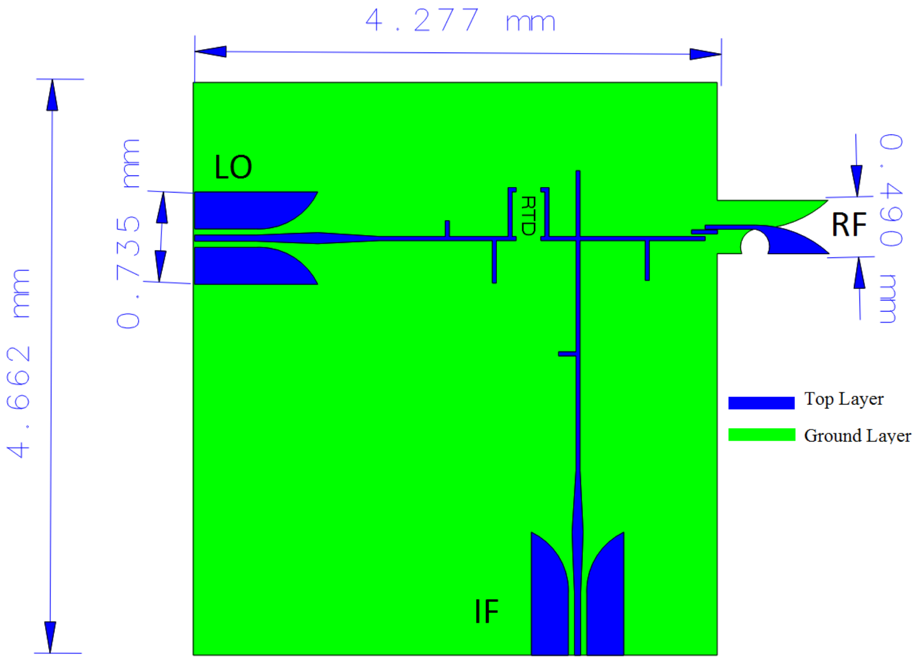

Figure 4.16: 320GHz mixer’s physical mask based on 100µm quartz thickness.

The finial physical mask of this 320GHz mixer is shown in Figure 4.16, and it is already prepared for subsequent fabrication. To proof the concept and efficiently predicate a mixer performance based on RTDs at higher frequencies, a scaled version operating at 18GHz was fabricated and tested at Leeds, which is presented and discussed in section 4.5. The next section will provide a brief overview on fabrication of circuits with chip devices, including wire bonding and flip chip techniques.

4.4 Chip mounting techniques

During the semiconductor fabrication process, a number of chips (e.g. diodes) can be built on a single semiconductor wafer, usually silicon or GaAs. For packaging purposes, these chips are terminated by patterning a metal material (a pad) such that a final connection to an electronic circuit (e.g. a mixer) can be made. In that, the chips are diced out of the wafer and mounted on the circuit using a suitable interconnection technique such as wire bonding or flip chip bonding, which are the two dominant techniques at high frequencies[104]. Wire bonding is the most mature technique employed for assembling the common semiconductor packages up and beyond 100GHz, if the used bond wires are designed properly[105]. As a potential disadvantage the wire length may become longer (more inductive effects) being a crucial factor for high frequency applications. The common used wire materials are silver, aluminium, copper and gold, where the typical diameter of the wire starts at around 10µm and can be extended up to a few hundred µm to satisfy higher power applications[106]. In the wire bonding technique, as shown in Figure 4.17, the chip can be attached using ball bonding or wedge bonding method.

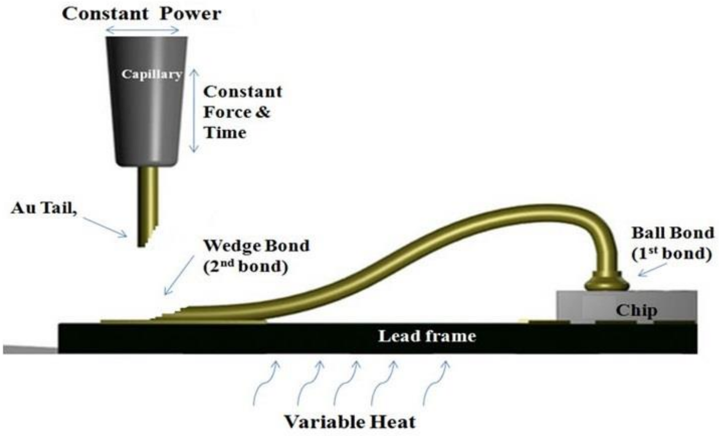

Figure 4.17: A wire bonding arrangement[107].

The ball bonding process normally uses a gold or copper wire to interconnect the two intended materials, while for wedge bonding the wire can be a gold or aluminium wire, where the gold is only required to be heated. The ball bonding is restricted to wires with a small diameter required for interconnection purposes, while the wedge is often used for large diameter wires required in power electronic applications. For both types, the ball and wedge bonding, the wire is bonded at the two intended ends using heat and ultrasonic energy to provide a weld, referred to as a thermosonic bonding process which is employed to increase the wire bond strength and reliability. In ball bonding, there is no need for the wire to be drawn directly as the first bond is in the form of ball, as the name implies, leading to a reduction in processing time. In contrast, in wedge bonding, the wire is drawn in a direct line with respect to the first bond, requiring more time for the alignment tool to complete the process[107].

The alternative interconnection method is the flip chip, where a semiconductor chip is connected to a final circuit using solder bumps. On the top of the wafer these bumps are placed in advance onto the device pads. To attach the chip to the finial circuit, it should be flipped up such that the chip pads are aligned with the circuit pads. Solder reflow takes place to make the interconnection as shown in Figure 4.18, and this is why the flip chip is also known as Direct Chip Attach (DCA) as the chip is attached directly on the circuit[108].

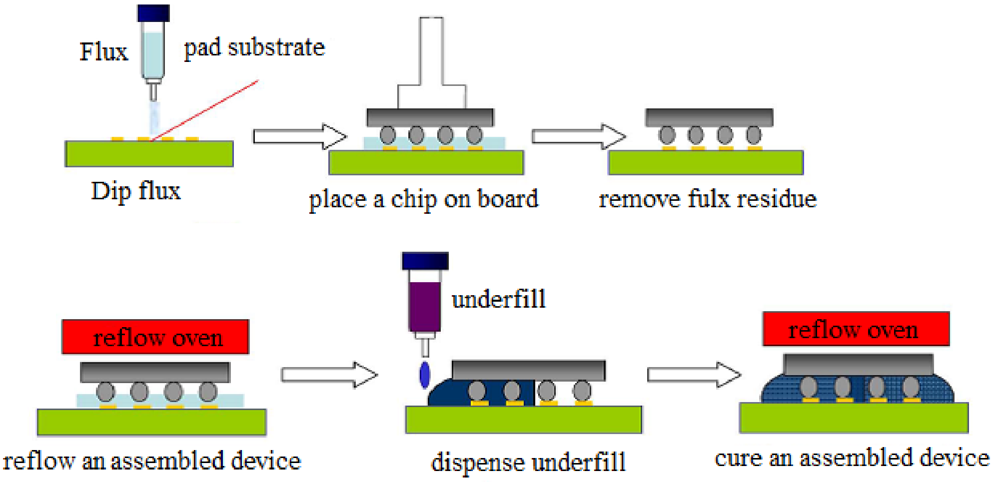

Figure 4.18: The DCA process steps[108].

The area required for the connection is reduced compared to the wire bond technique as the chip input and output are placed on the chip bottom as shown in Figure 4.19. In general the main differences between wire bonding and flip chip are listed in Table 4.

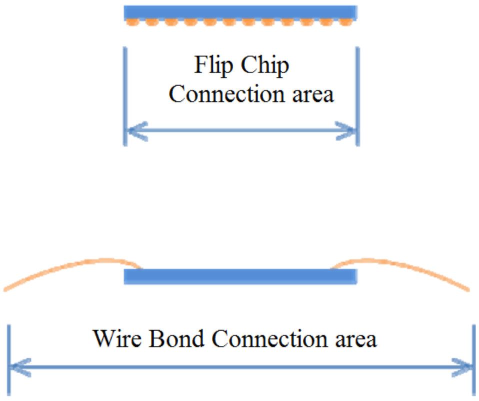

Figure 4.19: The connection area for both Flip Chip and Wire bonding methods[109].

Table 4.3: A comparison between wire bonding and flip chip technique[106].

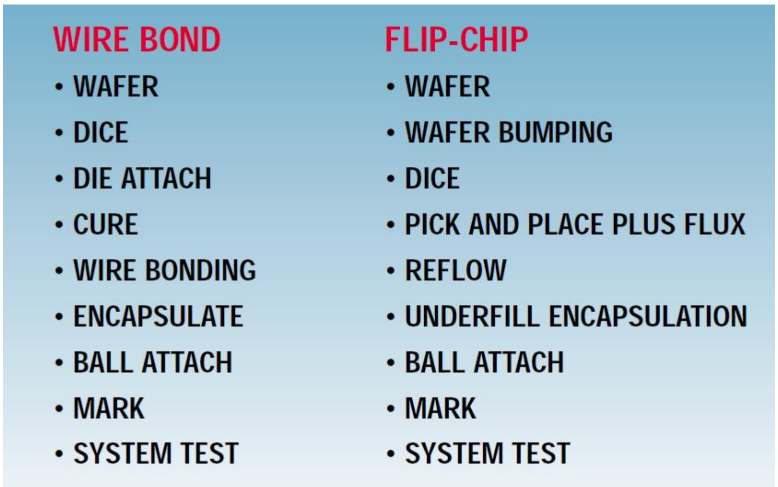

WIRE BOND	FLIP-CHIP
• WAFER	• WAFER
• DICE	• WAFER BUMPING
• DIE ATTACH	• DICE
• CURE	• PICK AND PLACE PLUS FLUX
• WIRE BONDING	• REFLOW
• ENCAPSULATE	• UNDERFILL ENCAPSULATION
• BALL ATTACH	• BALL ATTACH
• MARK	• MARK
• SYSTEM TEST	• SYSTEM TEST

4.5 18GHz 2nd Subharmonic mixer experimental results

This section presents measurement results of an 18GHz sub-harmonic down conversion RTD mixer using the second harmonic of an 8.25GHz LO signal. The purpose of this was to test the principle without the extreme challenge of mount diodes for operating at above 100GHz. The duroid layout of the mixer circuit is shown in Figure 4.20. The mixer circuit is based on GCPW with duroid substrate of 1.3mm thickness, which is the available thinnest substrate at the design time. To firstly validate the circuit design of the mixer before mounting an RTD and for later comparison sake, a back-to-back Schottky diode pair in beam lead form from Philips was mounted, and its DC characteristic was tested as shown in Figure 4.21.

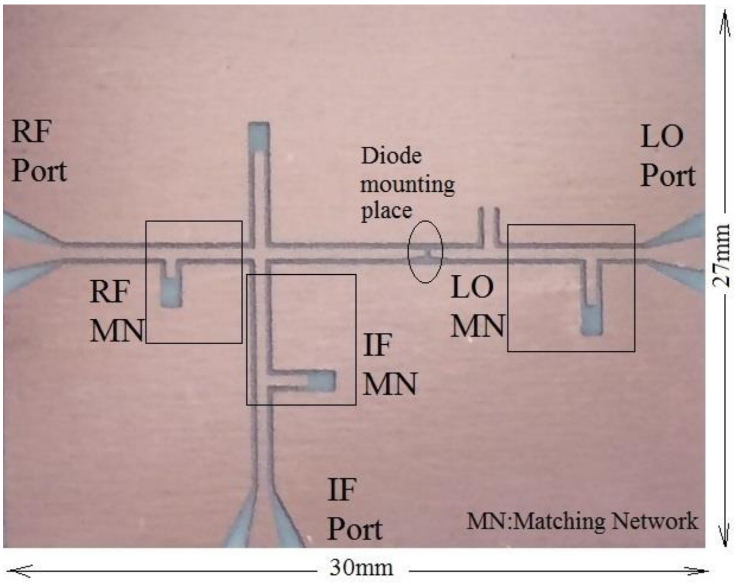

Figure 4.20: The layout of an 18GHz sub-harmonic mixer circuit.

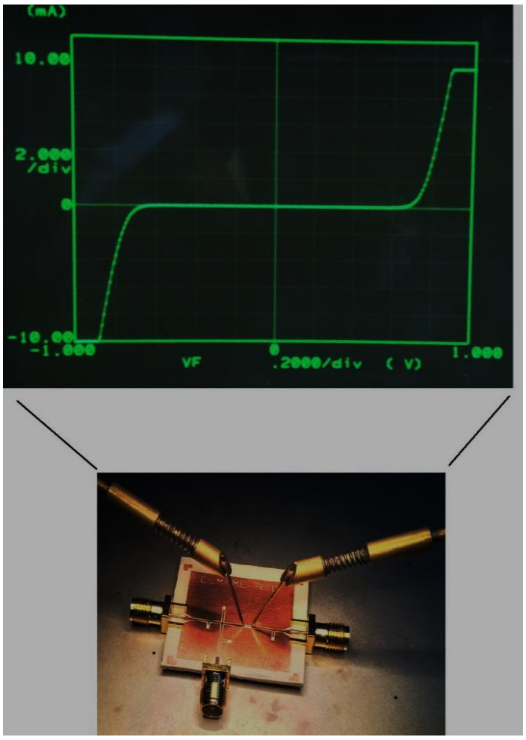

Figure 4.21: Schottky diode pair mounted in the designed mixer circuit, alongside its measured I-V characteristic.

Following this, two input signals (i.e. RF and LO) were applied to the mixer using two Agilent PSG signal generators E8257D, and the output signal (IF) was measured by Agilent PXA Signal Analyser N9030A. The Schottky mixer performance in terms of conversion loss as a function of LO power is shown in Figure 4.22, where the net conversion loss was around 12dB at 7dBm LO power. The total measured conversion loss including the coaxial cables and connector losses was around 21dB at 11dBm LO power. The RF coaxial cable loss was around 8dB at 18GHz and 4.5dB for the LO cable at 8.25GHz, and from the IF mixer port to Signal Analyser was around 1.0 dB. Furthermore the measured mixer shows a good isolation between the LO-to-RF ports in range of the 20 dB, and better than 60dB isolation between the 2LO-to-IF. This is similar to the typical performance for a commercial 2nd sub-harmonic Schottky mixer [1. It is worth noting that the Philips beam lead Schottky diode configuration greatly facilitated the circuit bonding process since the 100µm long beam leads were easy to epoxy to the circuit.

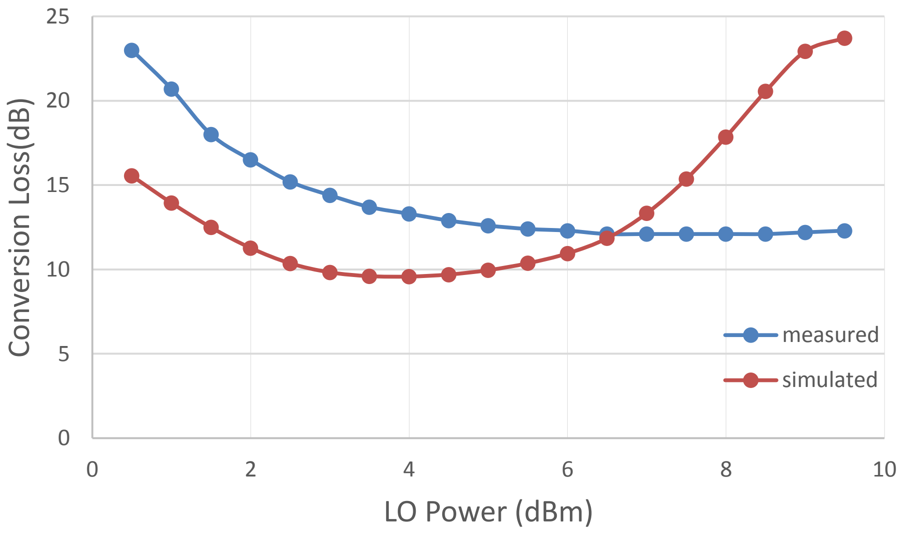

Figure 4.22: The measured vs. the simulated performance of the mixer based on Schottky.

After validating the circuit design using the Schottky diode pair as mentioned above, the next step was to mount some successfully RTDs, fabricated at Leeds, to the mixer circuit. It should be noted that the diodes fabricated at Leeds did not feature any beam leads, which significantly complete the mount process. A number of attempts were carried out but only one RTD was successfully attached to the PCB, unfortunately this RTD was not the optimum nonlinear element for the designed down-conversion mixer circuit. The primary problem with mounting the RTDs was the extremely difficult connection with the small chip contacts and the transmission lines as shown in Figure 4.23. The use of silver loaded epoxy, from EPOTEX (H20E), effect the electrical connection provided problematic for the very small (100µm) contacts, and much more work would be required to understand the unanticipated problem, and some different conducting epoxies from EPOTEX may be more successful.

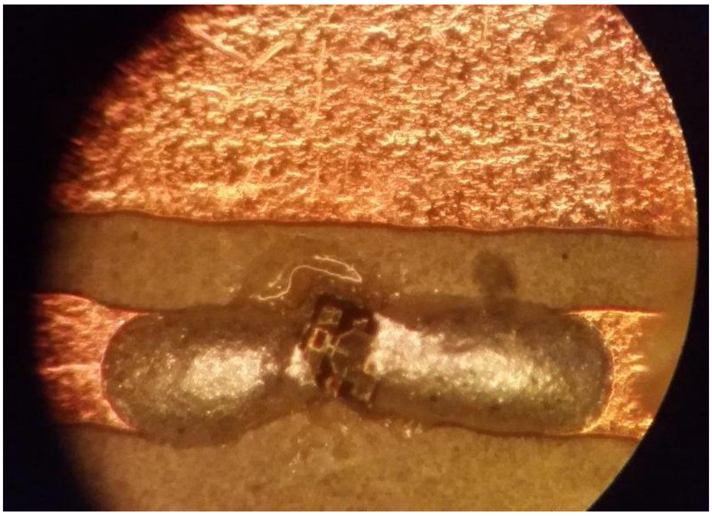

Figure 4.23: An improper connection for the RTD.

This problem was unforeseen in the setting up of the measurement. One of the less good RTD’s was successfully attached, and this was measured as a mixer. Unfortunately the bonding yield of the others devices, together with the processing yield (~50%) meant that although multiple devices were mounted only the least good RTD device was mounted and measured successfully, and there was insufficient time to reprocess more RTDs and circuits. As a consequence, the aim was only to explore the mixing function of the successfully attached RTD, regardless the anticipated, not so good, conversion loss performance. The LO signal was 8.25GHz at 0dBm pumped power, and by changing the RF signal, the measured conversion loss is shown in Figure 4.24. From this figure the best mixing performance was confirmed to occur at 0dBm LO power which confirmed the simulated result. Unfortunately the non-linearity of this devices' I-V characteristic, shown in Figure 4.25, meant that the conversion loss was not as good as the simulation predicted

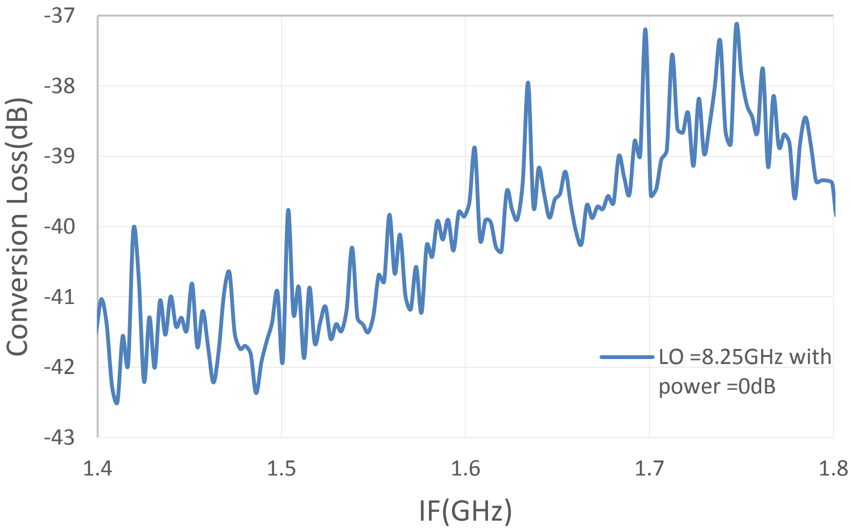

Figure 4.24: The measured performance of the mixer based on RTD.

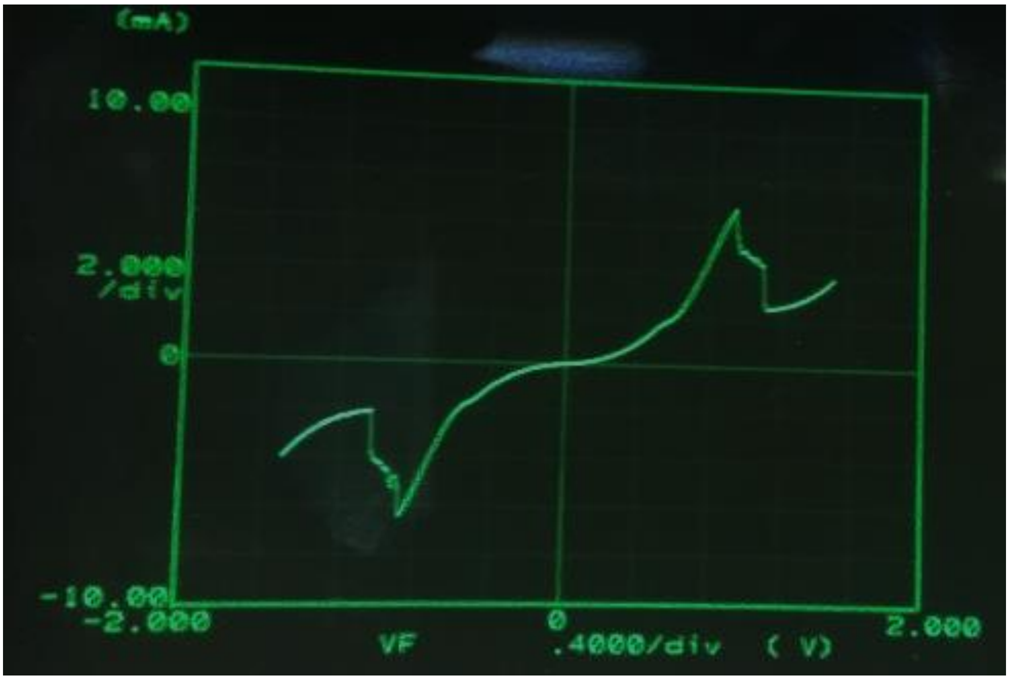

Figure 4.25: The measured I-V characteristic of the attached RTD.

However, based on the results of 320GHz sub-harmonic down conversion mixer, it is a reasonable step to try to find a suitable power source to meet such LO requirements. This will be the main goal of the next chapter, where other RTDs fabricated at the University of Leeds will be explored in this regard.

4.6 Summary

This chapter presented one of the key goals of this thesis, which is the design of sub-harmonic down conversion mixers operating at high harmonic numbers of the LO. Firstly, the mathematical principle of this sort of mixing was described with two different modes of operation, fundamental and sub-harmonic. The benefit behind the use ofthe back-to-back configuration of Schottky diode pair was discussed. Following this, the chapter presented the design and the results of two different topologies of sub-harmonic down conversion mixer (640GHz and 320GHz) based on the fourth harmonic of a LO signal. The 320GHz sub-harmonic mixer showed a very promising performance in terms of both conversion loss and LO power requirement, when compared to other published results based on Schottky diode pair.

Chapter 5 Sub-harmonic Up Conversion RTD Mixers

5.1 Chapter objective

The first part of this chapter is devoted to estimating the conversion loss or the power efficiency, by employing differently sized RTDs in a 3x frequency multiplier. This part also investigates the output power harmonics of the RTDs using polynomial-type approach in MATLAB, and then compares their results to a Schottky diode pair in a back-to-back configuration. The second part of this chapter presents the design of two different sub-harmonic up-conversion mixers incorporating a single RTD, with the second harmonic of a pumped LO signal, extensively using both ADS and HFSS software. The aim in this chapter is to explore the maximum power which is associated with good conversion efficiencies and a tolerance of high pump powers, leading to highest output power.

The RTDs used in this chapter were fabricated at the University of Leeds by the group led by Dr.DP Steenson. Table 5.1 illustrates the growth structure of these RTDs for three different layers that were fabricated, named L938, L939 and L940. Each layer produced five different sizes of device as shown in Table 5.2.

Table 5.1: The growth structure detail of Leeds devices, named L938, L939 and L940[110].

	L938 - L940			L939		
Description	Thickness (nm)	Material	Doping (cm^{-3})	Thickness (nm)	Material	Doping (cm^{-3})
Top n+ Contact	500	GaAs	2×10^{18}	500	GaAs	2×10^{18}
Graded n Layer	100	GaAs	2×10^{16}	100	GaAs	2×10^{16}
Spacer Layer	10	GaAs	Undoped	10	GaAs	Undoped
Barrier	5	$Al_{0.4}Ga_{0.6}As$	Undoped	1.7	AlAs	Undoped
Quantum Well	5	GaAs	Undoped	5	GaAs	Undoped
Barrier	5	$Al_{0.4}Ga_{0.6}As$	Undoped	1.7	AlAs	Undoped
Spacer Layer	10	GaAs	Undoped	10	GaAs	Undoped
Graded n Layer	100	GaAs	2×10^{16}	100	GaAs	2×10^{16}
Bottom n+ Contact	500	GaAs	2×10^{18}	500	GaAs	2×10^{18}
Buffer Layer	100	GaAs	Undoped	100	GaAs	Undoped
Substrate	500,000	GaAs	SI/UD	500,000	GaAs	SI/UD

Table 5.2: The size of Leeds devices, named L938, L939 and L940.

Diode	D1	D2	D3	D4	D5
Area	30µm^2	60µm^2	110µm^2	225µm^2	450µm^2

The corresponding measured I-V Characteristics of these RTDs are shown in Figure 5.1 through Figure 5.3. The author used them in the current thesis to explore their potential use in up mixing applications, by designing a multiplier and different sub-harmonic up conversion mixers at two different high frequency bands, and making a comparison with a back-to-back pair of Schottky diodes (the junction area is 20µm^2), whose I-V characteristic is shown in Figure 5.4 where its equivalent circuit is also illustrated. The control of the growth structure of these RTDs is beyond the scope of the current work, alternatively, exploring and discovering the appropriate shape and the nonlinearity these RTDs should have for such an application is the main goal of this thesis.

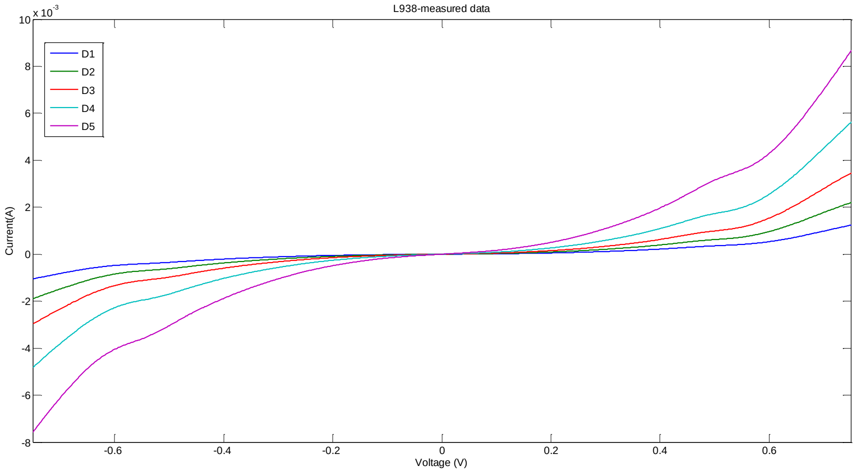

Figure 5.1: The I-V Characteristics of RTDs-L938.

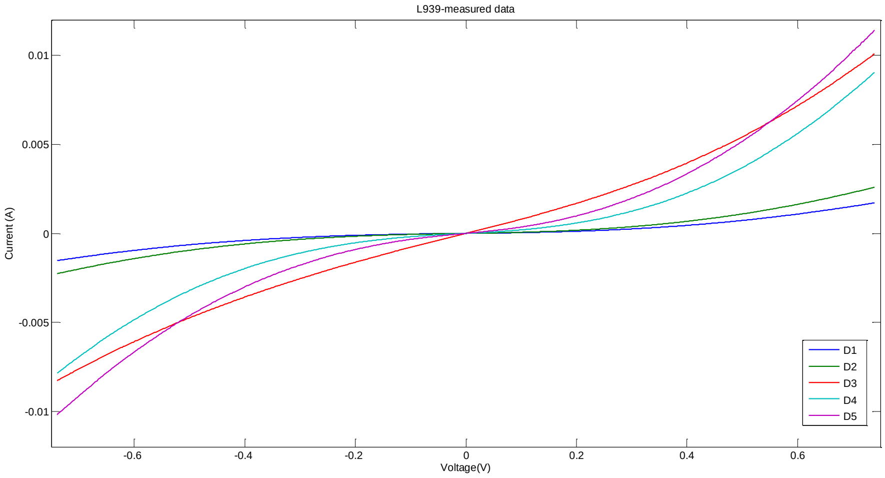

Figure 5.2: The I-V Characteristics of RTDs-L939.

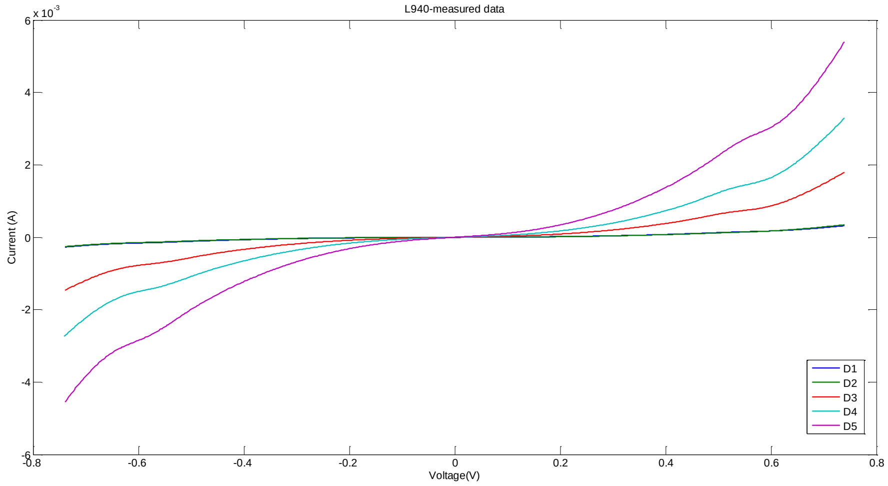

Figure 5.3: The I-V Characteristics of RTDs-L940.

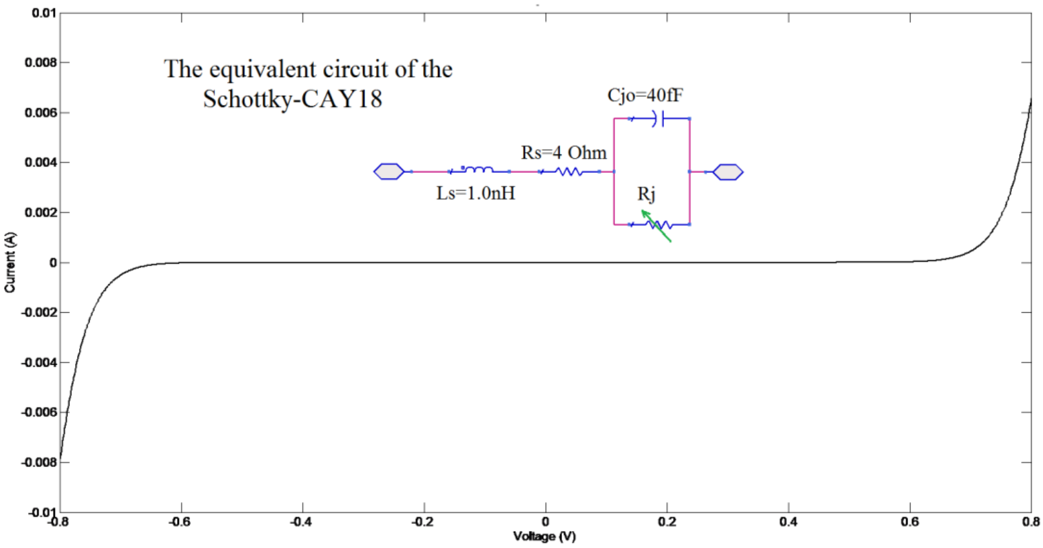

Figure 5.4: The I-V Characteristic of Schottky diode pair.

5.2 Frequency tripler design

The lack of power amplifiers at the higher frequencies gives a chance for multipliers to be considered as alternative power sources to support other high frequency applications.

In this section the potential use of RTDs as multipliers, particularly as Triplers, is explored by selecting a 210GHz operating frequency, which is frequently used for terrestrial communications.

As essential requirements, non-linear elements such as Schottkies or RTDs have to be carefully presented with its own circuit, where the embedding impedances can be matched properly. It is consequently a realistic step to begin with a configuration without having optimisation elements such as filters or impedance matching networks in such a way that a decent comparison between Schottky pair and a single RTD can be accurately accomplished. Based on this, a configuration of the tripler circuit is depicted in Figure 5.5. The circuit consists of two ports named F_{in} with 70GHz and F_{out} with 210GHz for presenting input and output signals respectively, nonlinear element (i.e., a single RTD or a Schottky Pair) and a power source at the input port as well as a passive element like a resistor at the output side.

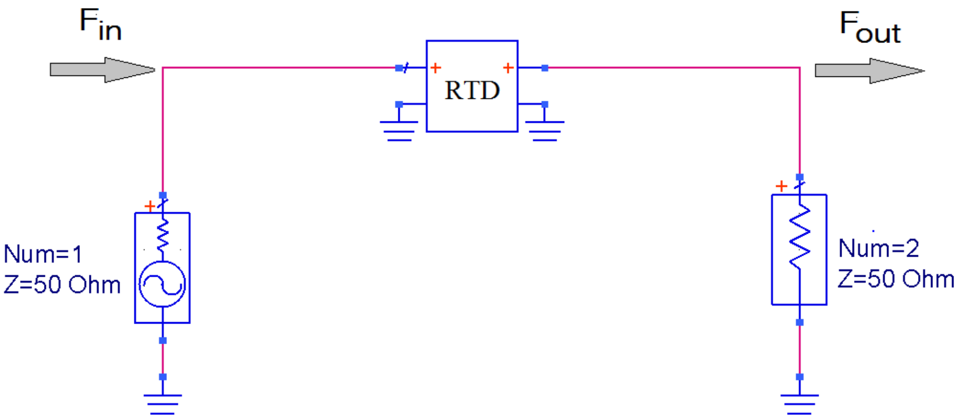

Figure 5.5: A basic un-optimized 210GHz tripler frequency circuit.

By running the harmonic simulation in ADS, the expected frequency conversion performance of these different RTDs and the Schottky diode pair is presented in Figures 5.6 to Figure 5.8. It can be seen from these Figures that the poorest conversion loss is shown with the RTD L939 while the RTD L938 and RTD L940 are slightly improved over the Schottky diode. Such deterioration in terms of RTD L939's performance lies in the fact that this RTD has a different growth structure compared to RTD L938 and RTD L940. The reason behind this is that the RTD L939 was designed to have a much higher current density with thinner barriers, and deliberately incorporate it in down-conversion mixing circuits, that use a small amount of power to work well. This is however not ideal for multipliers or up-converter circuits which require more pump power than down conversion mixing ones. Furthermore, when comparing the Schottky diode to the RTD L938 and RTD L940 it can be observed that the performance of these RTDs, especially these with smaller junction area is improved at high input power, reflecting the power high handling capability.

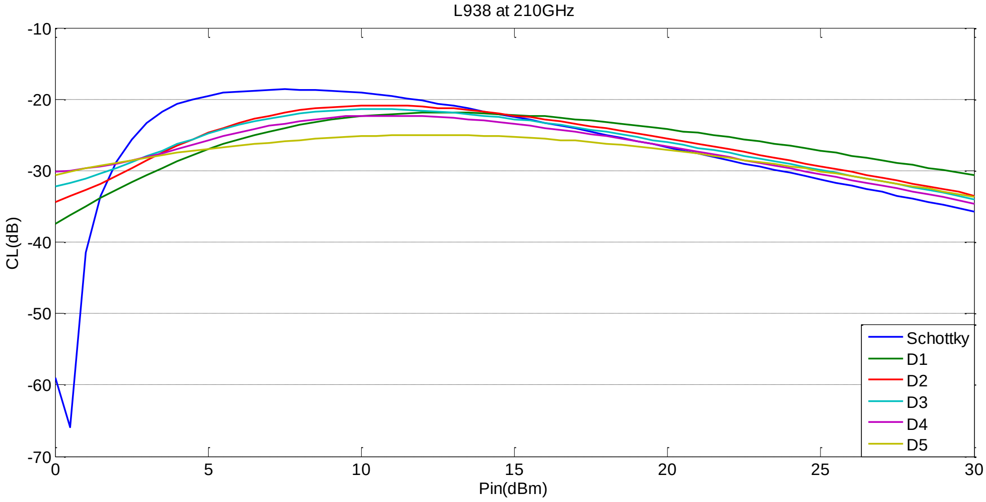

Figure 5.6: CL of RTDs-L938 and Schottky pair.

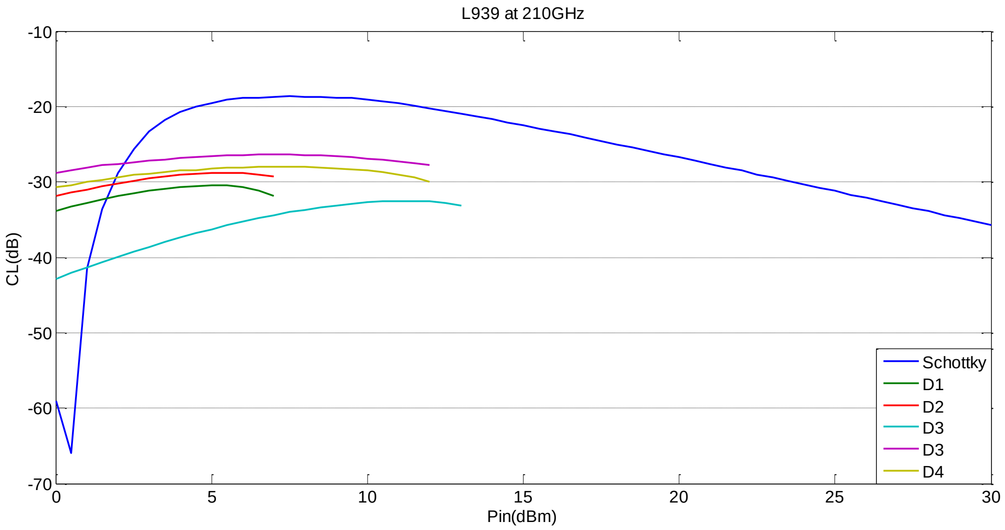

Figure 5.7: CL of RTDs-L939 and Schottky pair.

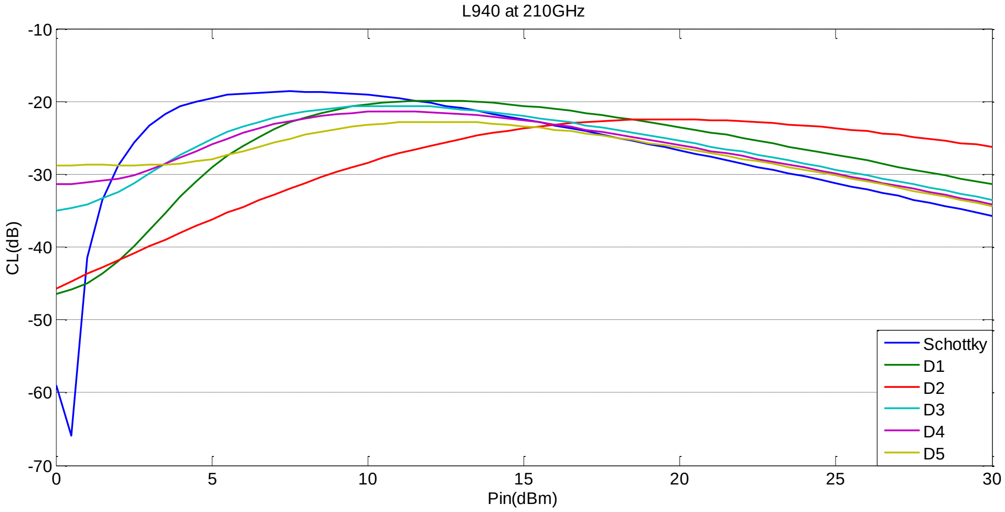

Figure 5.8: CL of RTDs-L940 and Schottky pair.

In principle, the power conversion efficiency of the nonlinear element mainly depends on the nonlinearity within their I-V curve, i.e. number and power of the harmonics. Based on this concept and the initial result presented above, there is still a need to conduct further investigation by looking at the number and amplitude of the potential harmonics of RTDs and comparing then with a Schottky diode pair. In other words, there is a need to explore how the shape of the I-V characteristic affects the conversion efficiency, with the aim of leading to some better layer structures, and this is the main concern of the next section.

5.3 RTD harmonic investigation

In the current section the performance of RTDs as odd harmonic multipliers is estimated using a polynomial approach in MATLAB. The polynomial equation here represents the output current of a given RTD as a function of the input voltage (i.e. the measured I-V curve of a RTD). The MATLAB m-file is provided in Appendix–IV. For example, the polynomial equation that can represent the I-V characteristic of RTD is:

$$\mathrm{I} = (0.0023954 * \mathrm{V}.^{5}) + (0.00050729 * \mathrm{V}.^{4}) + (0.00080934 * \mathrm{V}.^{3}) - (0.00010408 * \mathrm{V}.^{2}) + (0.00029871 * \mathrm{V}) + (3.628\mathrm{e} - 006); \qquad (5.1)$$

In this case the input voltage (V) can be simply presented as a LO pump signal, i.e. $\mathrm{A}\cos(2\pi_{LO}t)$, and by changing the amplitude of this signal (A), it will be easier and more straightforward to look at output harmonics which will indicate how strong nonlinearities provided by the I-V characteristics of these RTDs are. Consequently, the applications of these RTDs could be conveniently distinguished in terms of down or up converting mixing signals. Another potential outcome for this, the structure of these RTDs (i.e. I-V characteristics) could be modified to favour a certain application requirement. In this sense, a number of RTDs with different sizes are employed, alongside a commercial Schottky diode pair for comparison purposes. The selected junction area for Schottky is 20µm^2, RTD-L938 is 30µm^2, RTD-L939 is 60µm^2, and RTD-L940 is 225µm^2.

Firstly by taking a look at the fitted I-V characteristics of a number of measured RTDs and a commercial Schottky diode pair shown previously in Figure 5.1 to Figure 5.4, it is obvious that both the RTDs and the Schottky pair have anti-symmetric I-V characteristics, which means that the even harmonics are naturally suppressed. The focus here is on the harmonics' amplitude, not on the operating frequency or the capacitance (junction area) and for simplicity the input frequency is selected to be 100Hz (i.e. the input frequency = 0.1 of the sampling frequency). The reason behind using this low frequency is to avoid the effect of the parasitic elements, such as the series resistance and the parallel capacitance, at high frequencies, consequently the focus is entirely on the nonlinear resistance (I-V characteristic).

The emphasis will be only on the amplitude of the odd harmonics generated as a function of pumped signal amplitude. Figure 5.9 through Figure 5.14 show how the shape of the I-V curves can affect the potential output harmonics (conversion efficiency). Figure 5.9 shows the potential output harmonics at 0.2V where the 1st harmonic of the RTD-L939 has the highest amplitude compared to the Schottky and the other RTDs, but in contrast the 3rd harmonic of the Schottky is the highest.

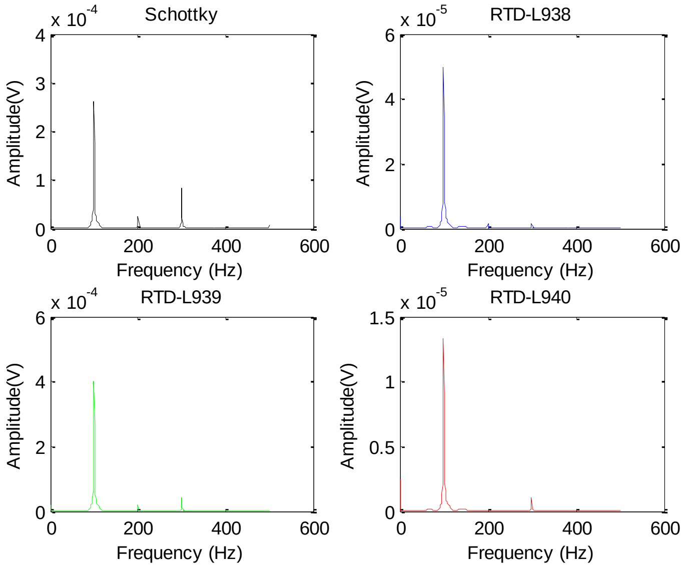

Figure 5.9: RTDs and Schottky pair spectrum at 0.2V of pumped signal.

Figure 5.10 shows the potential output harmonics at 0.4V where the 1st harmonic of the RTD-L939 is still the highest among the Schottky and the other RTDs, whilst the 3rd harmonic of both RTD-L939 and the Schottky is on the same order. Also the same Figure shows the 5th harmonic is only generated by Schottky up to this voltage range.

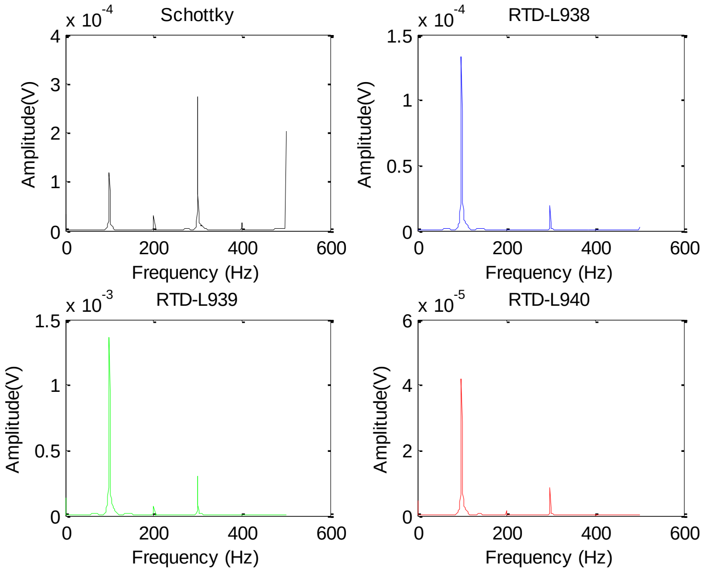

Figure 5.10: RTDs and Schottky pair spectrum at 0.4V of pumped signal.

Figure 5.11 shows the potential output harmonics at 0.6V where the amplitudes for both the 1st and the 3rd harmonic of the RTD-L939 are the highest compared to the Schottky and the other RTDs, and also the 3rd harmonic of all the RTDs is higher than the Schottky. The same Figure also shows the 5th harmonic is still only generated by the Schottky.

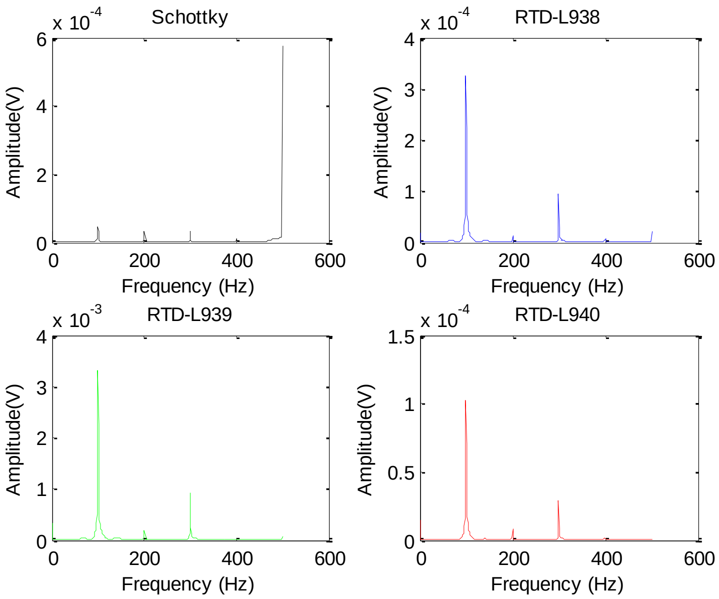

Figure 5.11: RTDs and Schottky pair spectrum at 0.6V of pumped signal.

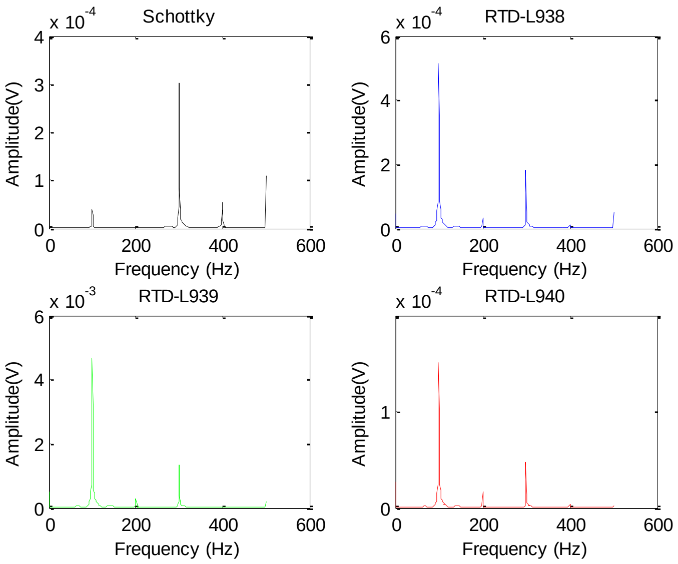

Figure 5.12: RTDs and Schottky pair spectrum at 0.7V of pumped signal.

Figure 5.12 shows the potential output harmonics at 0.7V where the 1st and the 3rd harmonic of the RTD-L939 are the highest amplitude compared to the Schottky and the other RTDs. The same Figure also shows the 5th harmonic is generated by the Schottky and the RTD-L938 at which the Schottky is still the highest.

Figure 5.13 shows the potential output harmonics at 0.75V where the 1st harmonic of the RTD-L939 is still the highest amplitude compared to the Schottky and the other RTDs, but the 3rd and the 5th harmonic of Schottky are the highest compared to all the RTDs. This is expected as the typical Schottkies operate within this voltage range (≥0.7V).

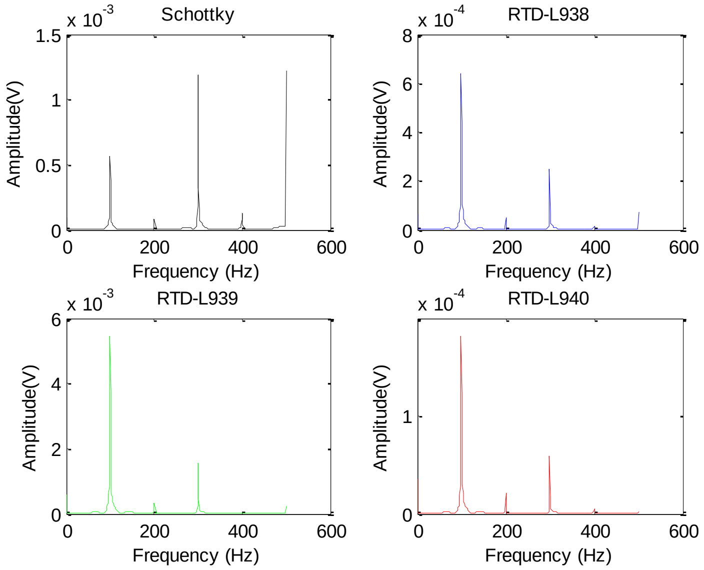

Figure 5.13: RTDs and Schottky pair spectrum at 0.75V of pumped signal.

Figure 5.14 shows the potential output harmonics at 0.8V where the 1st harmonic of the RTD-L939 is again the highest compared to the Schottky and the other RTDs, but the 3rd and the 5th harmonic of Schottky are still the highest compared to all the RTDs.

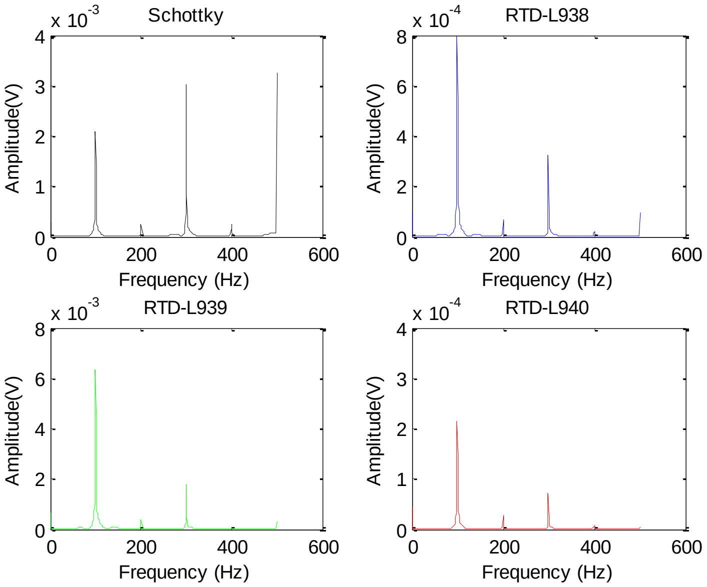

Figure 5.14: RTDs and Schottky pair spectrum at 0.8V of pumped signal.

To conclude then, it can be observed from the preceding Figures that the RTD’s harmonics are lower in comparison to the Schottky diode, except the 3rd harmonic of the RTD-L939 which is occasionally higher before 0.7V. However, when the pumped signal amplitude is ≥ 0.7V the Schottky’s harmonics clearly dominate, as the typical nonlinearity region of Schottkies lies in this voltage range. Referring to the RTDs I-V characteristics shown previously, both the RTD L938 and RTD L940 have a different growth structure compared to RTD L939, therefore they need more driving power than RTD L939 in order for the nonlinearity to be adequate. Based on these estimated results, one can conclude that the RTD L939 could be a favoured option in a down conversion mixing case, while both the RTD L938 and RTD L940 are more suitable for up-conversion mixing applications. In the meantime, the Schottky diode shows higher harmonic power output than the RTDs, and this reflects that the selected Schottky diode (CAY18) has a strong nonlinearity region within its I-V curve. For this, these RTDs with such a growth structure cannot be compared with this Schottky diode and new RTDs with appropriate I-V curves should be produced to confirm the current results. One of the main reasons for wishing to investigate this was the initial expectation that the RTD layers may have better properties compared with the surface junction based Schottkies. Furthermore multiplier series connected RTD layers can easily be produced and thus these again could be driven harder than Schottky based devices. This study therefore was just an initial investigation using the layer structures which are already available rather than bespoke new layers.

It is expected that odd harmonics are only generated with such anti-symmetric I-V characteristics; thus, the applications of these RTDs based frequency conversion are limited in the form of a tripler, quintuple and so on. As a consequence of this investigation, the emphasis in the next section will instead be on using these RTDs in a sub-harmonic up conversion mixer.

5.4 RTD sub-harmonic up-conversion mixer design

As mentioned previously, there is still a limited availability of amplifiers at the mm-wave frequencies, particularly for short range mm-wave communication systems. A high output power up conversion mixers may offer an alternative in this regard. This current section therefore aims to evaluate the RTDs' performance in terms of up-converting signal applications by designing two different sub-harmonic mixers operating at mm-wave frequencies, 110GHz and 180GHz, using two different technologies, grounded coplanar waveguide (GCPW) and microstrip. Again the 110GHz version is simply a scaled down version which should be easier to measure.

However, in order for these RTD simulations to be at a good level of reliability, a comparison with a Schottky diode pair is again preferable. Such a comparison with published results of Schottky diode pair[54] is presented in Appendix IV, which shows promising performance for a single RTD compared to a Schottky diode pair.

5.4.1 180 GHz 2nd Sub-harmonic upconverter mixer

This subsection presents a 180 GHz sub-harmonic upconverter mixer employing a single RTD with the second harmonic of a pumped LO signal. The mixer shown in Figure 5.15 is operated at 85 GHz LO signal with pump power of 10 dBm and 10GHz IF with a set value of power.

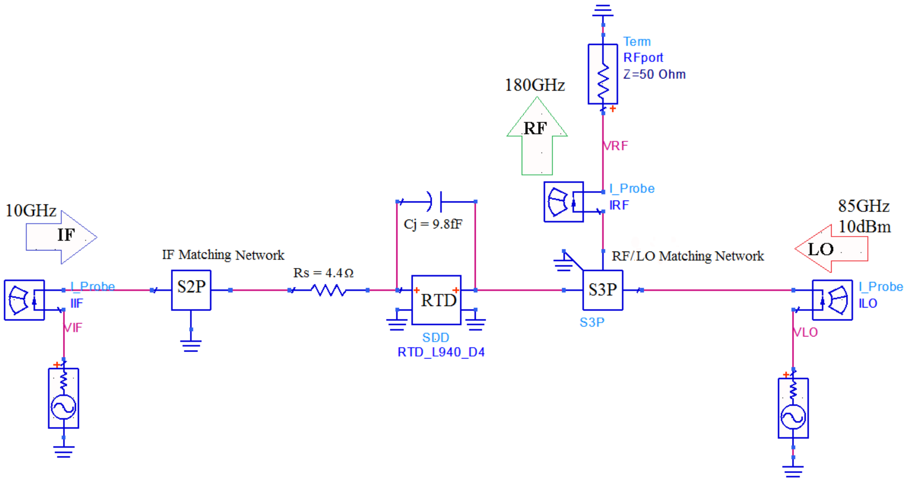

Figure 5.15: A 180GHz sub-harmonically upconverter mixer topology.

The initial estimated output power performance of this circuit, based on two different transimision lines, GCPW and Microstrip, is presented in Figure 5.16. A 3dBm improvement in terms of output power is clearly provided once microstrip lines (O/P power = -6.5dBm) are used instead of GCPW (O/P power = -9.5dBm). From the same

Figure it can also be observed that the optimum input power of the GCPW was 7dBm while it is 12dBm in the case of microstrip. This can be explained as GCPW is not capable of handling more input power when compared to microstrip. Such a higher loss, thus low power capability of GCPW, may be due to the propagation of additional modes such as slot mode and microstrip mode. The former mode can be defined by electrical fields induced from the side ground or the so-called reference plane to the signal trace, while the microstrip mode is exhibited when the fields are distributed from the side grounds to the underground plane.

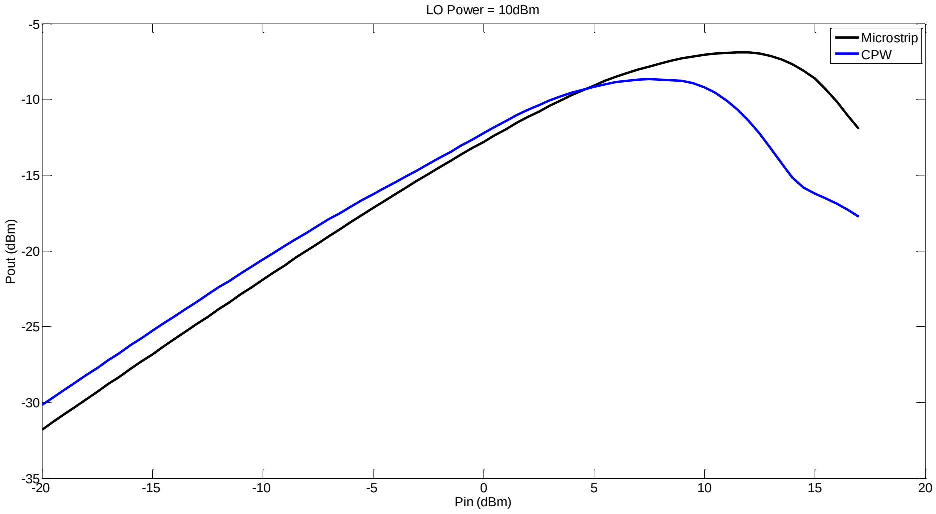

Figure 5.16: Pout at different values of input power at 10dBm LO.

It should be noted that discontinuities are not included at this stage, which are expected to diminish the performance as it will be notable throughout the following subsections. However, in order for this simulated performance to be closer to the realistic result, various discontinuities should be considered in this design. There are already microstrip discontinuities such as tees, crosses and others provided in ADS environment while such an advantage is not available for CPW as no CPW discontinuities are supplied in ADS.

It could be more precise if such discontinuities are designed with 3D EM software such as HFSS. However, as pointed out earlier, there is still a lack of RTD-built in model in a commerical software, and the Symbolically Defined Device (SDD) tool provided in ADS is used to include the I-V characteristic of RTDs in this mixer circuit.

Additionally, it should be mentioned that junction capacitances and series resistances are still largely unknown for these current RTDs, but a step to extract RTDs' impedances is taken into consideration in the next phase. Based on this, junction capacitance with value of 9.8fF and 4.4Ohm of series resistance are selected, again to be similar to a Schottky diode at this frequency range.

The effects of the discontinuities, designed in HFSS, are presented in Figure 5.17, which shows a 3dB decrease in terms of the desired output power at 180GHz compared to ADS without discontinuities. The blue curves are the conversion losses, which more useful to define the 1dB compression point where the optimum output power can be determined. For example the output power is -6.5dBm with the ADS (black solid line) while it is around -9.5dBm with the HFSS (balck dished line), both at 4dBm of the 1dB input power. A further decussion of the 1dB compression point will be presented soon when it is time to estimate the final performance for this mixer.

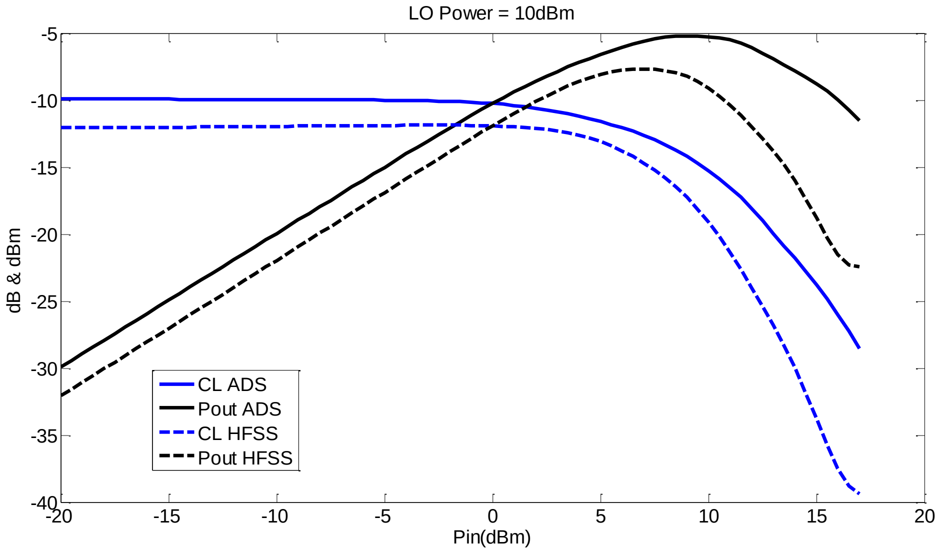

Figure 5.17: The initial CL and Pout performances at 180GHz as a function of input power, Pin.

From this initial result, it could be worthwhile to present a line-for-line comparison, to distinguish the effect of discontinuities in both ADS and HFSS. Subsequently, Figure 5.18 shows only how the IF matching network can be configured (dimensions) in both ADS and HFSS, while its performance is presented in Figure 5.19.

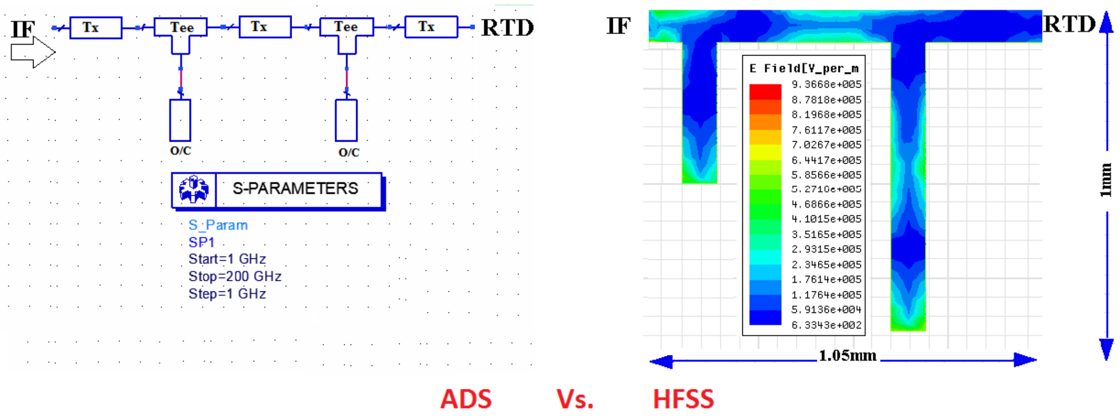

Figure 5.18: IF Side matching network configuration in ADS (left) vs. HFSS (right).

Figure 5.19 presents the return loss at the IF input port of the mixer with respect to the nonlinear device, i.e. the RTD. The 10GHz incident signal is in a good match with the RTD's impedance, where the return loss is below -12dB, meaning that more than 90% of the input power is provided to the RTD. There is also a good match at around 160GHz which is not anticipated, but this has no effect on the performance as it is distant from the intended input single (i.e., 10GHz), and it can also be improved by further optimization.

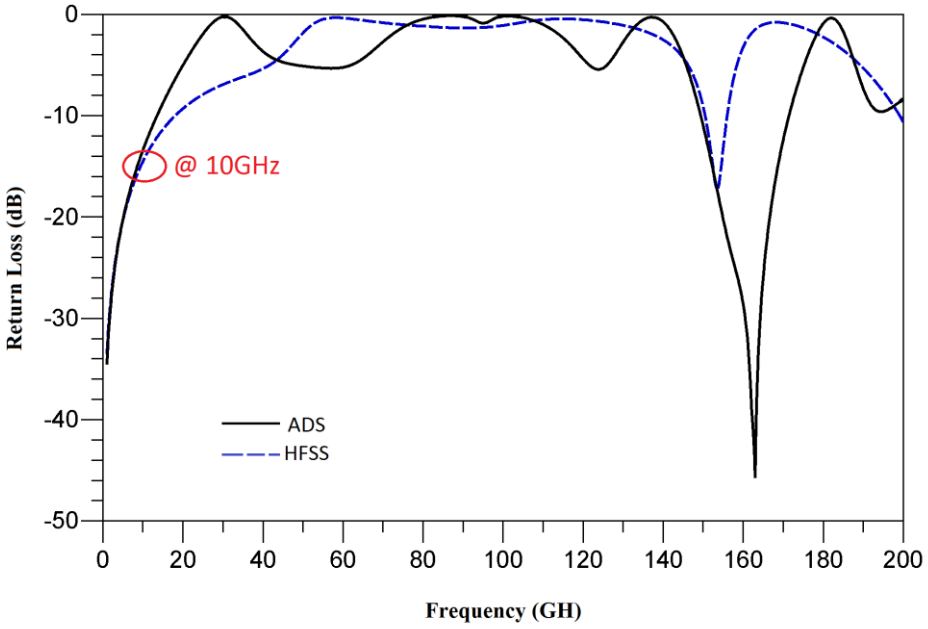

Figure 5.19: Return Loss at 10GHz IF Side.

Similarly, the LO/RF impedance matching network layout in both ADS and HFSS is shown in Figure 5.20, alongside its performance in Figure 5.21.

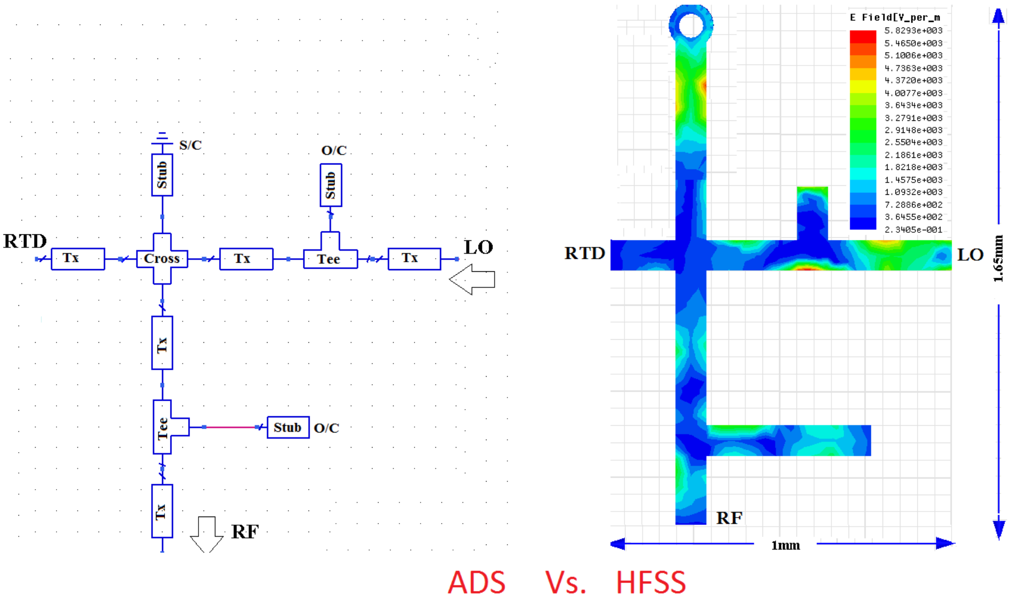

Figure 5.20: LO and RF Side matching network configuration in ADS (left) vs. HFSS (right).

Figure 5.21 shows the return loss at the 2nd input port of the mixer (the LO port) in respect of the RTD. The 85GHz LO signal shows a good match with the RTD’s impedance, where the return loss is below -15dB.

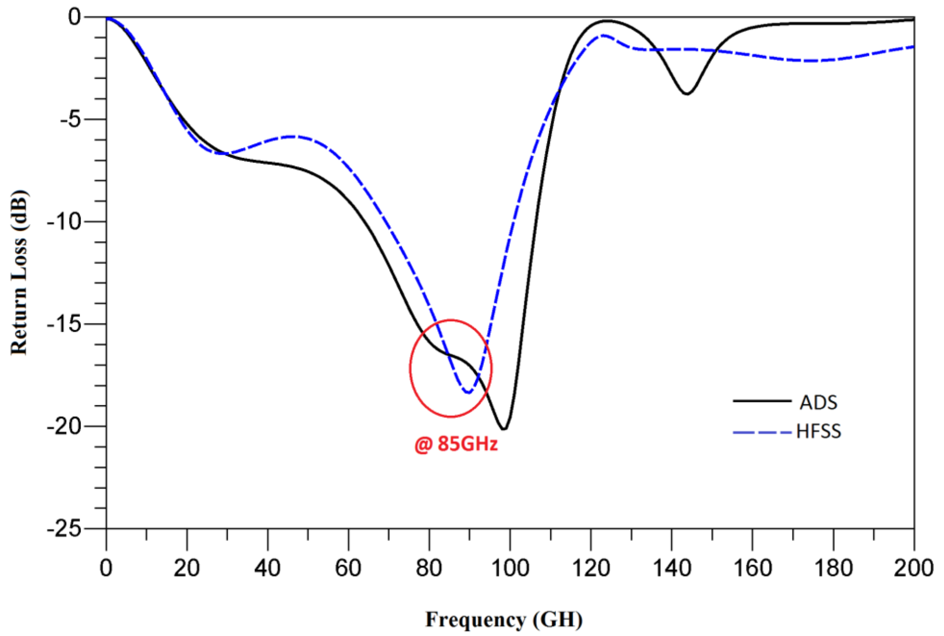

Figure 5.21: Return Loss at 85GHz LO Side.

From these Figures, a good level of agreement between ADS and HFSS is provided, even if there is a slightly different performance when the frequency is increased. This is expected due to HFSS being based on a 3D FEM solver, meaning that some factors such as conductors losses, dielectric losses, radiation losses (i.e. boundary conditions set up) and others have to be taken into account during the simulation, which are less well modelled in ADS.

Figure 5.22 shows the performance in terms of CL(dB) and P_{out} (dBm) as a function of P_{in} (i.e, IF power) at 10dBm of 85GHz LO signal. The Figure shows a slight difference in performance due to the transition effects seen by the HFSS result when compared to the ADS result. Figure 5.23 presents the P_{out} performance at the 180GHz mixer as a function of the 85GHz LO power, where a good performance with these low LO powers is offered. The 180GHz mixer's physical mask is shown in Figure 5.24.

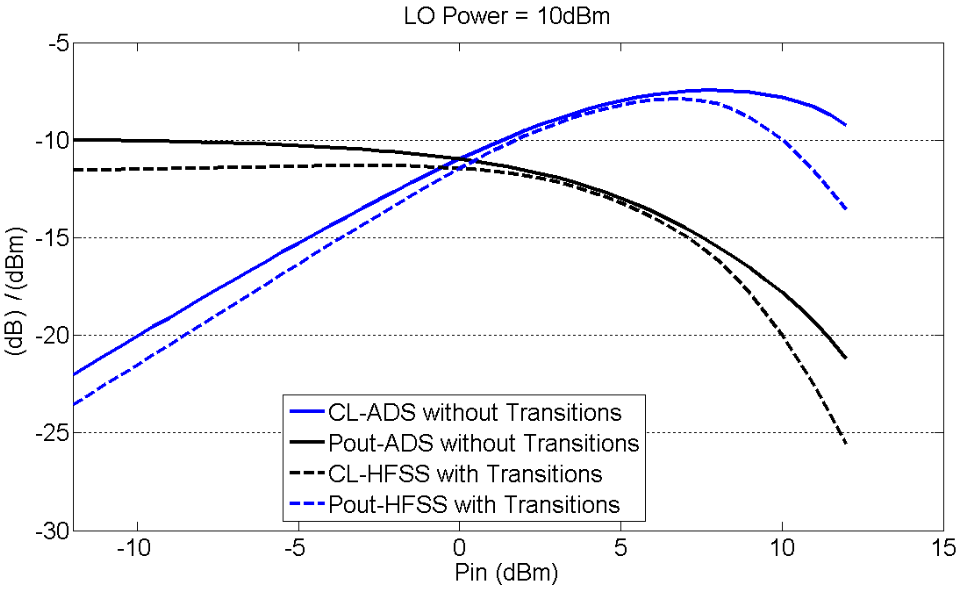

Figure 5.22: Mixer performance with and without transitions.

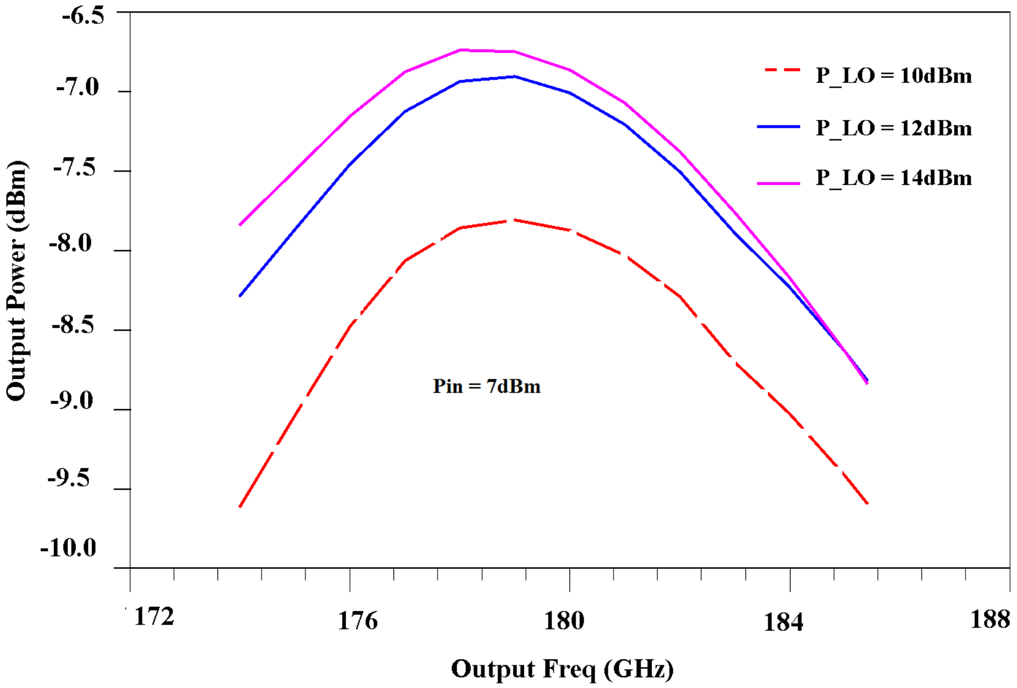

Figure 5.23: Pout performance as a function of LO power, at Pin =7dBm.

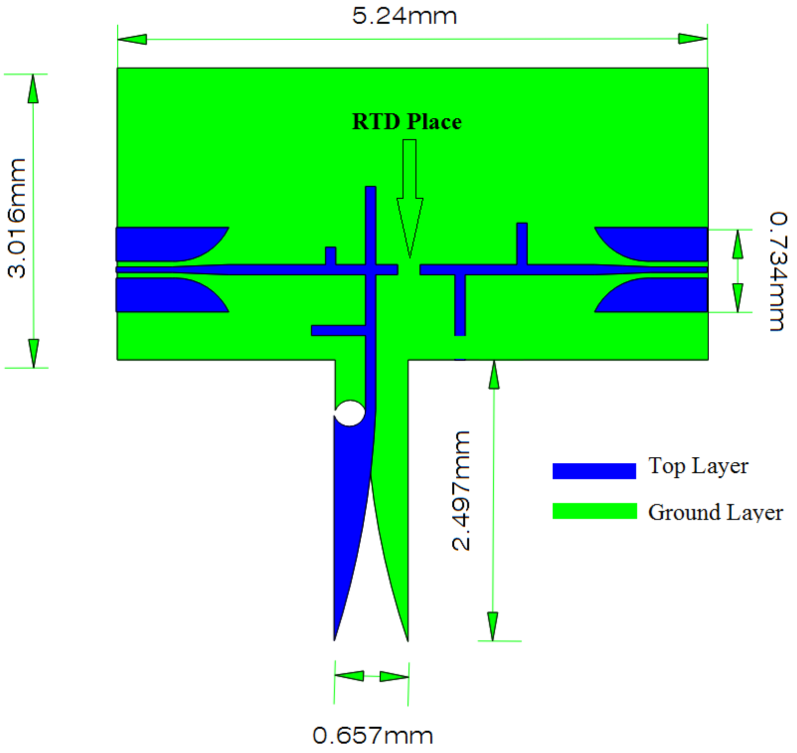

Figure 5.24: The180GHz mixer’s physical mask using 50µm quartz thickness.

However, the power handling capability of a given mixer, operated under high power conditions, can be basically characterised by two parameters, one-dB compression point (1dB) and third-order intermodulation products (IP3). The 1dB can be calculated or measured by applying a single tone at the mixer RF input port and observing the output performance as a function of the input power level. The 1dB point is indicated by where the conversion loss drops by 1dB from the linear region due to further increases in terms of the input power. The two-tone IP3 can be distinguished once two similar amplitude signals with a certain spacing in frequency are applied to the input port. When mixing with an LO signal, the two-tone IP3 becomes close enough to the desired output signal and consequently may be difficult to remove or be filtered. The issue related to IP3 lies in the fact that IP3 amplitude grows three times faster with respect to the input power. As a consequence both the desired output signal and two-tone IP3 are at the same level at a certain point in terms of the input power, making it difficult to separate the desired output signal. This can be theoretically determined by extrapolation because in the actual situation the output mixer performance is compressed before the IP3 matches the anticipated level of the output signal. The 1dB compression point and the IP3 point indicate the maximum useable powers that can be applied and thus, together with the noise floor or minimum detectible signal, determine the dynamic range.

The LO power is selected to be 10 dBm for the 180GHz mixer to estimate the corresponding intermodulation products as shown in Figure 5.25. The upper part of this Figure shows the resultant output power is in the range of -7dBm (1-dB O/P) at 1.5dBm of the 1-dB input power (1-dB I/P). The lower part of this Figure shows the intercept point of the two-tone IP3 where the IP3-input (IIP3) is at 11.5dBm while the IP3-output

(OIP3) is at 0dBm. This is a respectful result compared to a state of the art Shcottky diode pair. More details are given in Appendix-IV where the RTDs showed an adequate suppression level and power handling capability.

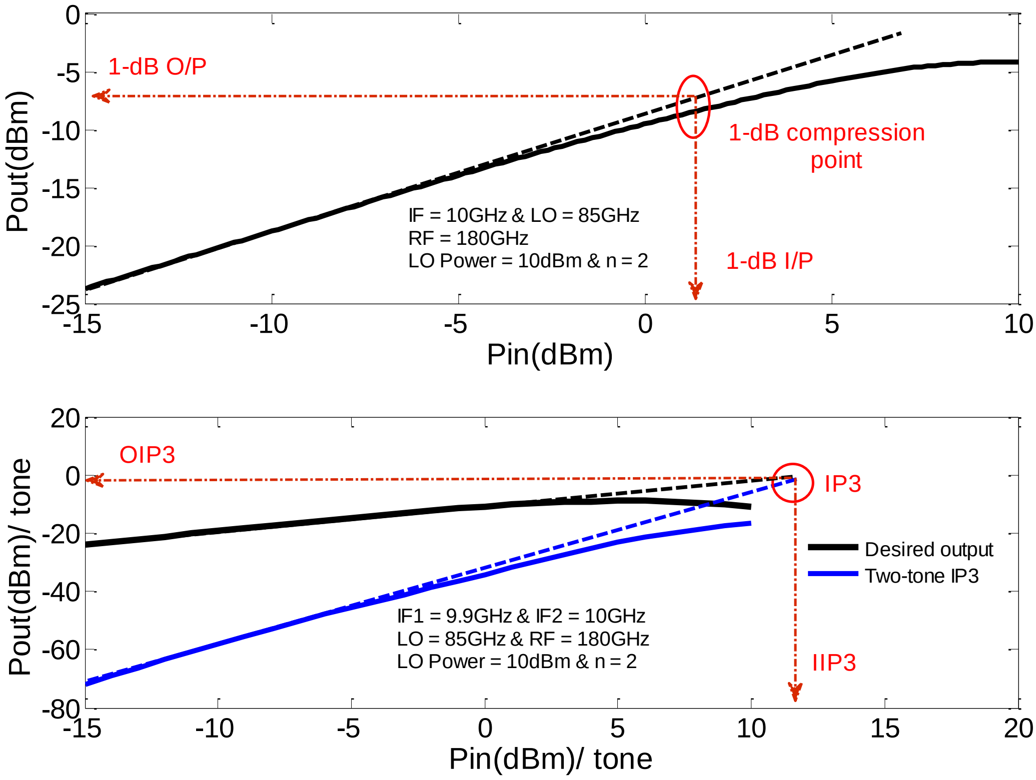

Figure 5.25: Output power as a function of input power for the 180GHz mixer.

Furthermore, in order to distinguish the effects of selected values of junction capacitance and series resistance on the P_{out} performance, a different value of junction capacitance and series resistance are employed as shown in Figure 5.26 and Figure 5.27. These Figures still show acceptable performances, and this is a good indication if the current selected values of junction capacitance (9.8fF) and series resistance (4.4Ohm) are not the same as the actual ones. Correspondingly, a full design of a 110GHz 2X sub-harmonic upconverter mixer, using GCPW technology is presented in the following section at which the performance of CPW can be compared to microstrip.

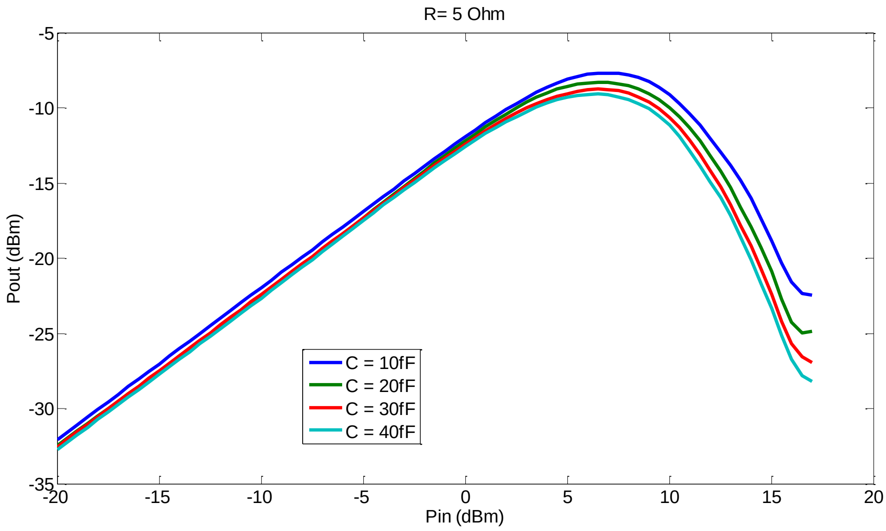

Figure 5.26: Junction capacitance effect on Pout at 5 Ohm series resistance.

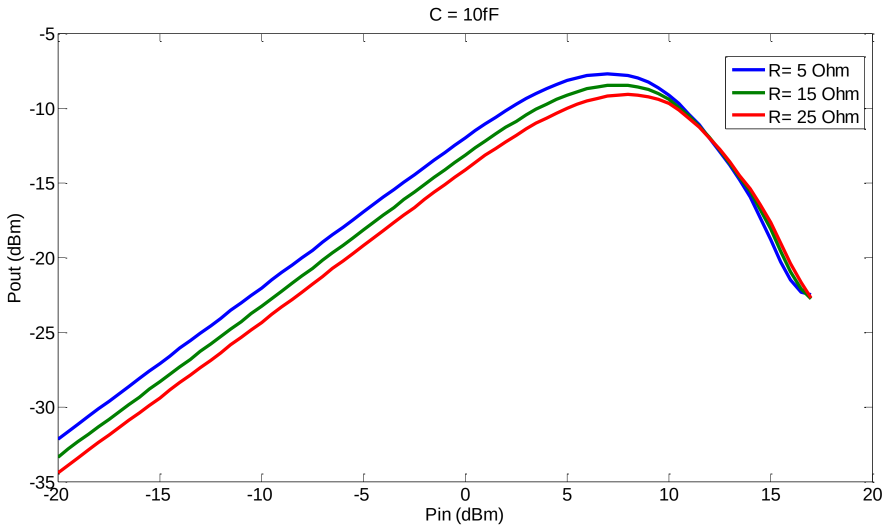

Figure 5.27: Series resistance effect on Pout at 10fF junction capacitance.

5.4.2 110 GHz 2nd Sub-harmonic upconverter mixer

The aforementioned 180GHz sub-harmonic mixer showed a good suppression level and power handling capability when compared to a Schottky diode pair (more details in Appendix-IV). This in turn can provide an opportunity for an RTD based up-conversion mixer to be a potential candidate for common use at mm-frequencies, instead of using power amplifiers or in place of fundamental LO pumped sources. For more investigation, this section explores a 2nd sub-harmonic up-converter mixer operating at 110GHz and using CPW instead of microstrip. The CPW can be wafer probed and the accessible wafer probes are limited to 110GHz here at the University of Leeds. Figure 5.28 shows the 110GHz mixer circuit which employs 20GHz and 45GHz as IF and LO input frequencies respectively, while the output RF signal is 110GHz based on the second harmonic of the LO signal. Additionally, a LO power source with 16dBm is selected to pump the single RTD while IF power has a set of values. As mentioned before, CPW elements such as tees, crosses and air bridges are not provided in the ADS package, leading to the design of these elements in HFSS for providing more precise result with respect to the performance in reality.

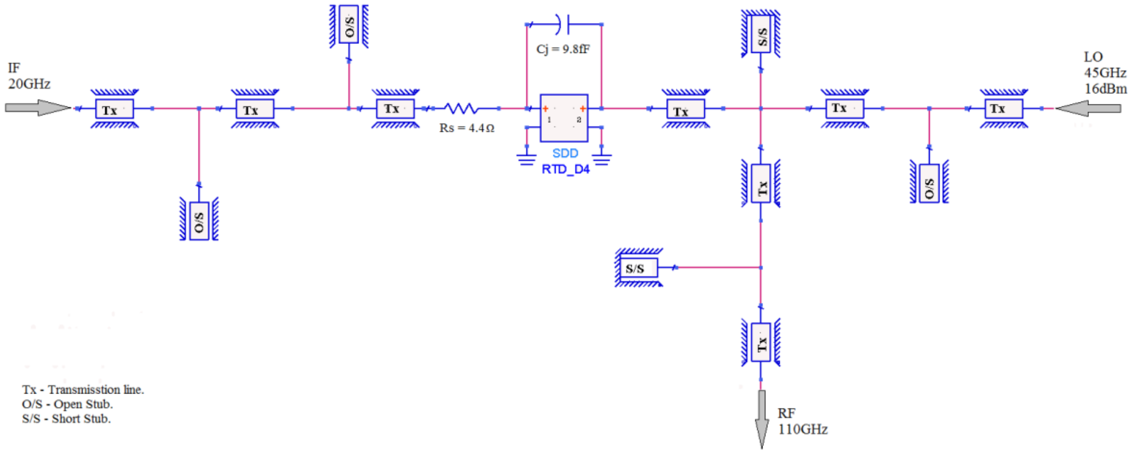

Figure 5.28: A 110GHz mixer topology without discontinuities in ADS.

Figure 5.29 depicts only the configuration of the IF impedance matching network in both ADS and HFSS, while Figure 5.30 presents the impedance matching performance in terms of the return loss at the 20GHz IF input port with respect to the RTD. A good match is found with the RTD's impedance at the desired frequency (20GHz), where the return loss is just below -10dB. Although there is good agreement between the ADS and HFSS, there is a resonant frequency at around 100GHz provided by the HFSS, resulting, it is thought from the lack of accuracy for modelling the air-bridges in the HFSS.

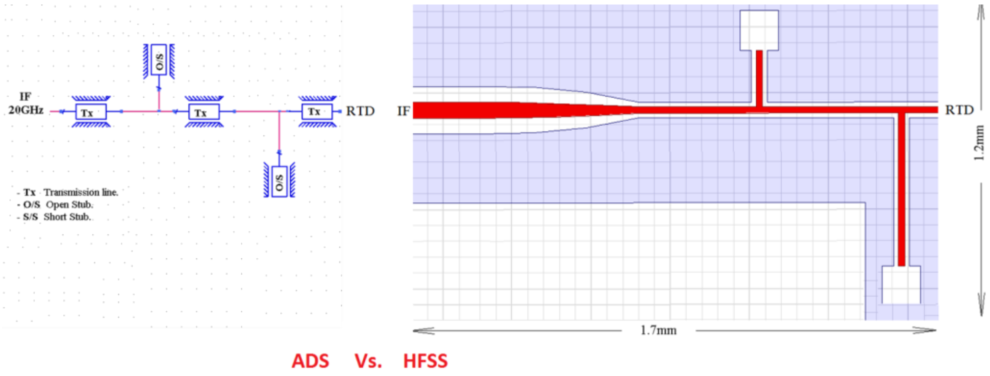

Figure 5.29: IF Side matching network configuration, ADS Vs. HFSS.

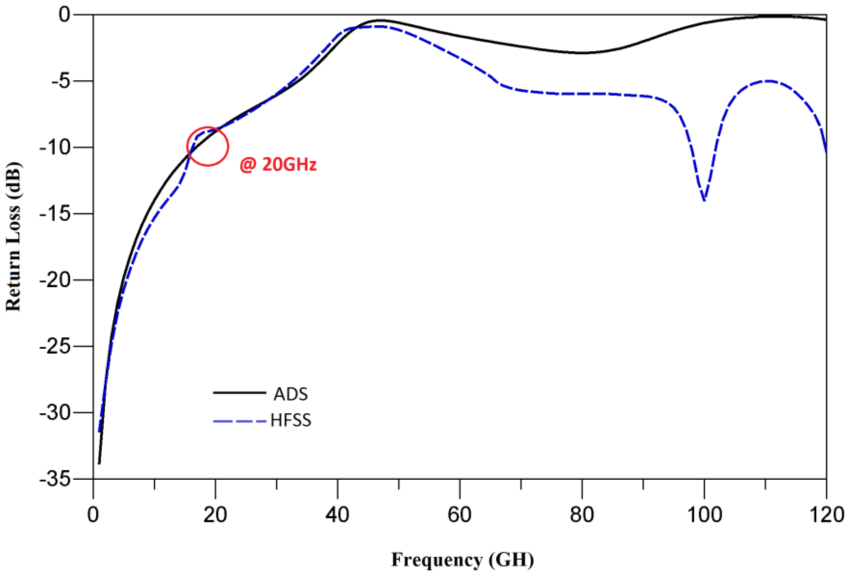

Figure 5.30: Return Loss at IF Side, 20GHz.

Likewise, the LO/RF matching network layout is shown in Figure 5.31 while the corresponding return loss performance is presented in Figure 5.32, where a good agreement between ADS and HFSS results can be seen. This Figure shows that the return loss is below -15dB, particularly at the desired frequency of 45GHz. Again, the HFSS result shows some fluctuations or resonances over the whole frequency band. This can be interpreted as additional losses to other modes involved such as slot and microstrip modes, pointed out in the previous subsection. This could also be due to the lack of accuracy during the modelling of air bridges, which are used such that the voltage has to be equally divided between the two ground sides surrounding the signal line.

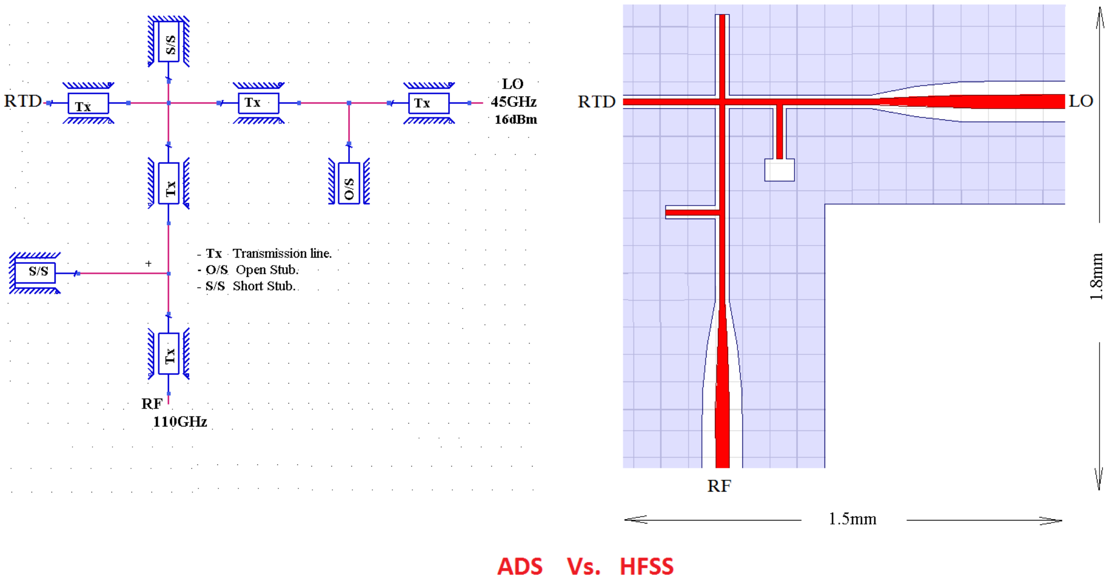

Figure 5.31: LO/RF Side matching network configuration, ADS Vs. HFSS.

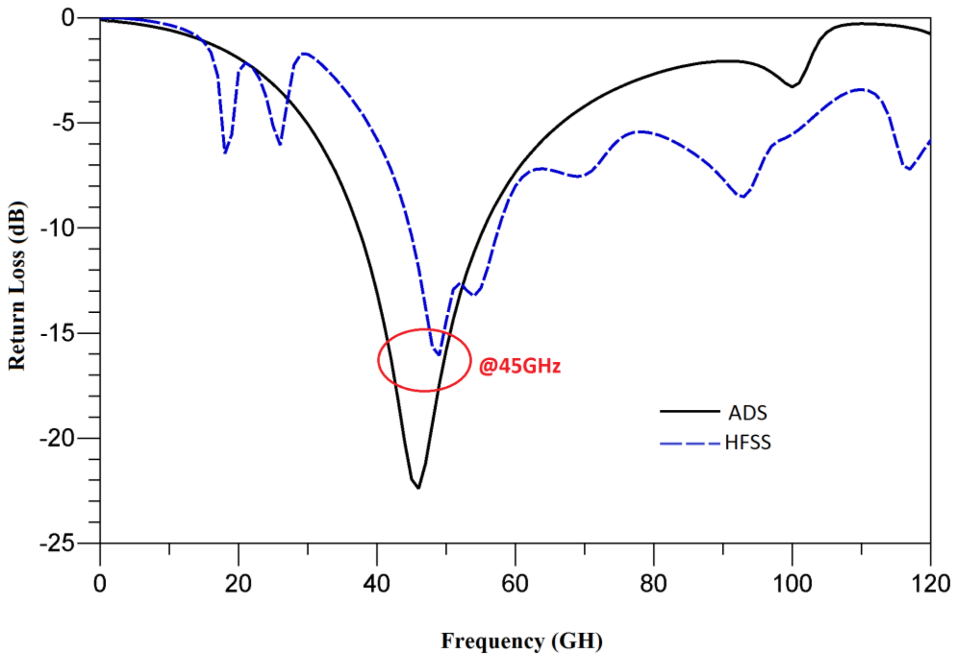

Figure 5.32: Return Loss at LO Side, 45GHz.

Alternatively, the performance in terms of conversion loss can be estimated as shown in Figure 5.33 where two different sized RTDs are used. It can be clearly seen from this Figure that not only an output power in range of -5dBm is achievable, but a reasonable level of conversion loss is achievable as well, which is around 10dB.

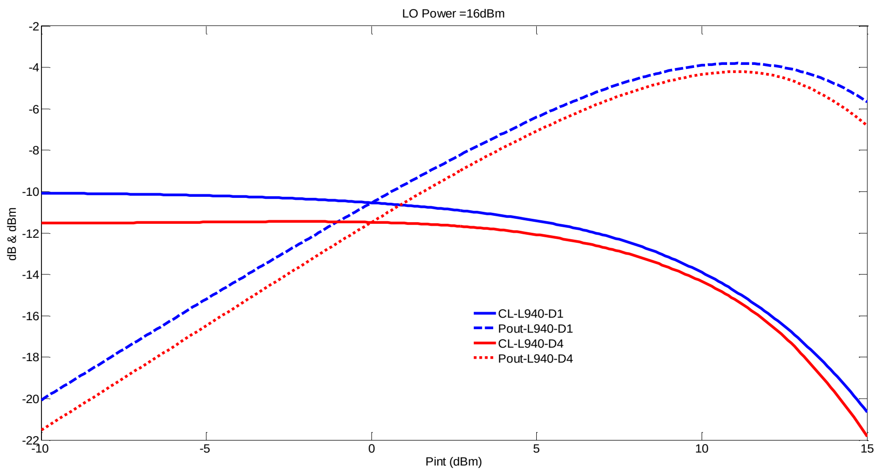

Figure 5.33: CL and Pout performance as a function of Pin.

The corresponding intermodulation products can be expected as shown in Figure 5.34, where the output power is around -0.5dBm at the 1-dB compression point of 6dBm. Beyond this compression point and up to 10dBm input power, an output power of ≥ 0dBm can be achieved since the suppression of the IP3 is around 20dBc up to this 10dBm input power. Regarding the fabrication of this mixer, the physical mask has been completed as presented in Figure 5.35, and the final circuit awaits to be fabricated in cleanroom environment.

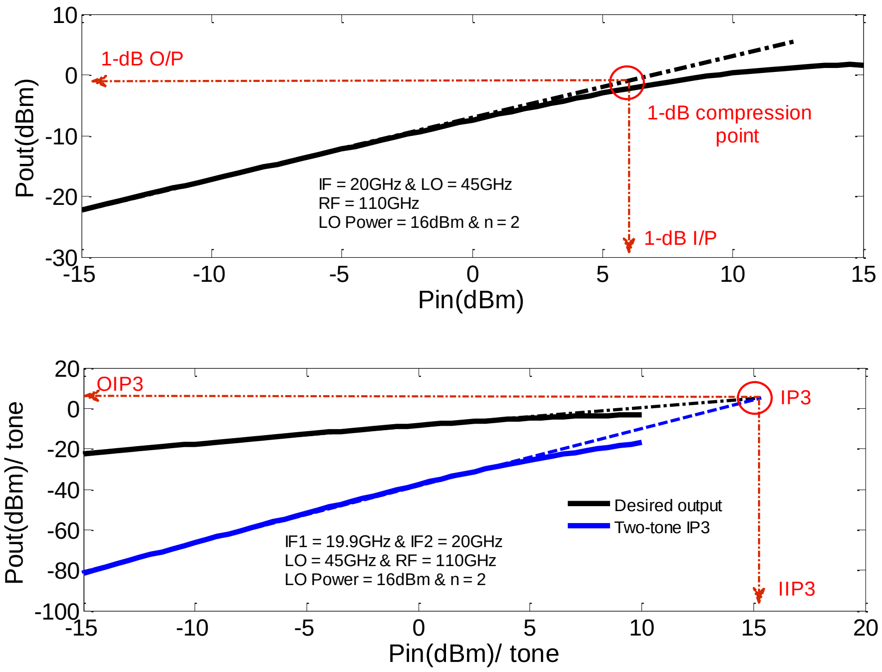

Figure 5.34: Output power as a function of input power at 110GHz.

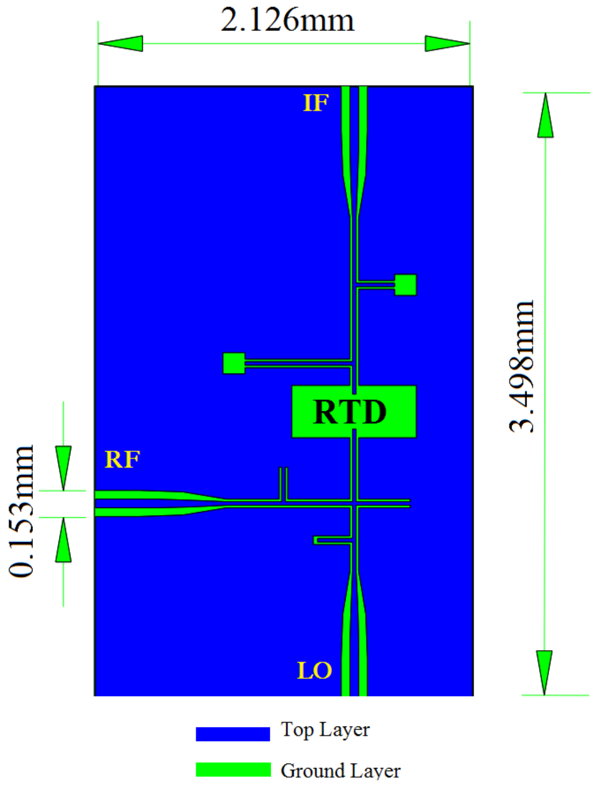

Figure 5.35: The110GHz mixer’s physical mask based on 100µm GaAs thickness.

In conclusion, Table 5.3 summarises the important results of the current different designs (110GHz and 180GHz), comparing a single RTD junction against a pair of back to back Schottkies. At higher frequencies, the RTDs are obviously capable of providing adequate output powers indicating that the maximum power handling of the single RTD is competitive when compared with the Schottky pair. This can be explained as the RTD offers the ability to engineer the I-V characteristics to much greater degree than the Schottky diodes; consequently using a single RTD junction in place of a Schottky diode pair could be an effective substitute. Furthermore, these different designs demonstrate better than 20dB port to port isolation, and more information is given in APPENDIX-IV.

Table 5.3: Comparison with other published results.

Frequency	Topology	Device	Output Power	Reference

(GHz)			(dBm)	
273	2xSHM	2 Schottky diodes	-17	[111]
110	Doubler	4 Schottky diodes	0	[112]
110	2xSHM	2 Schottky diodes	-6	[113]
110	2xSHM	Single RTD	-0.5	Current work
110	2xSHM	2 Schottky diodes	-6	Current work
180	2xSHM	Single RTD	-7	Current work
180	2xSHM	2 Schottky diodes	-11	Current work

5.5 Summary

The chapter presented another key aspect of this thesis by exploring the RTDs in up-converting mixers at different high frequencies. Firstly, the chapter explored the potential of using RTDs in a frequency multiplier (3x triple) using polynomial-type approach in MATLAB. The prospect of using a single RTD in place of Schottky diode pair was investigated in this chapter as well, where two different sub-harmonic pumped (n=2) up-conversion mixers featuring single quantum barrier junctions were designed and evaluated using the symbolically defined device capability in ADS and transmission line optimisation using HFSS. The performance in terms of efficiency and maximum output power compared with optimised Schottky diode based designs was found to be competitive. The aim was to explore high drive level mixers and conversion efficiencies. The performance is explored via one design operating at 180 GHz and providing -7dBm of output power while the second operates at 110GHz exhibiting an output power of -0.5dBm.

Chapter 6 Conclusions and Future Work

6.1 Conclusions

The potential applications of Resonant Tunnelling Diodes (RTDs) in the millimetre and sub-millimetre wavelength region were explored throughout this thesis, and concluded as follows:

In chapter 1, the main objective was to summarize the published results of back-to-back Schottky diodes mixers in terms of conversion loss and local oscillator power requirements, which served as a benchmark and comparison for the RTDs presented in this thesis, as both anti-parallel Schottky diode pairs and single junction RTDs exhibit similar anti-symmetric I-V characteristics. The typical conversion loss performance of Schottky diode based mixers was found to be around 8dB below about 500GHz and 10-12dB above, while the pumped LO power is typically on the order of 6 dBm.

In chapter 2, the effects of temperature on the carrier distribution, and consequently I-V's, of the RTDs was reviewed. The electrons at low temperature (77K) require a small bias to be aligned with the ground resonant state inside the well, resulting in a sharp nonlinear region in the I-V curve. The resultant current density is higher compared to the 300K case, where the nonlinear region is relatively smooth and more spread out. Consequently the current density is lower, reflecting the lower number of electrons available for tunnelling. This chapter also showed how the RTD's layer structure can be adjusted individually to produce a particular I-V characteristic for a certain application such as up or down mixing. It can be concluded that the current density increases (high transmission probabilities) through the use of thinner barriers and as the ground state resonant energy inside a thinner well is higher compared to a wider well due to the confinement being reduced, this results in the NDR occurring at higher applied bias. It also provides a wider FWHM in the transmission probability, leading to a significantly higher current density. Furthermore, the peak-to-valley current ratio (PVCR) is increased, corresponding to the separation among the quantised energy levels inside this thinner well increasing. These factors can be utilized to engineer a particular I-V characteristic to suit the application.

In chapter 3, the aim was to finalise the components required to eventually test the sub-harmonic mixers. A set of transitions using antipodal finline were designed at different frequency bands. The performance of these transitions was introduced and to validate their performance, E-plane split blocks were designed in a back-to-back configuration. For validity with the measurement results in future, this chapter ended by designing a number of TRL calibration standards at different frequency bands using both GCPW and RWG realisation, which is required to properly evaluate each part of the design.

Chapter 4 and chapter 5 presented the main goals and outcomes of the thesis, which were the design of different topologies of sub-harmonic mixers both in down and up mixing applications. The investigation in chapter 4 was to pump the down conversion mixers at much lower than typical LO powers using RTDs. The aim in the chapter 5 was to extend the maximum pump power, which implies good conversion efficiencies and a tolerance of high pump powers, leading to highest output power, again using RTDs. In chapter 4, the design and the potential results of two sub-harmonic down conversion mixers, operating at 640GHz and 320GHz, based on high harmonic numbers for the LO (n=4) were completed. The 320GHz sub-harmonic mixer showed very promising performance in terms of both conversion loss and LO power requirement, when compared to other published results based on Schottky diode pair. The conversion loss was below 6dB at a very low LO power of -9.5dBm. The future work would be to validate this experimentally. In chapter 5, the potential of using RTDs in a frequency triple, using polynomial-type approach in MATLAB was initially studied. From this, it can be concluded that the RTD's harmonics were lower compared to the Schottky diode, except the 3rd harmonic of the RTD which was occasionally higher when the applied voltage was below 0.7V. However, when the signal amplitude was ≥ 0.7V, the Schottky's harmonics clearly dominated, which is expected as the typical nonlinearity region of Schottkies lies in this voltage range. One of the main reasons for investigating this up-conversion was the initial expectation that the RTD layers may have better properties (tolerant to higher powers), compared with the surface junction based Schottkies. Furthermore multiplier series connected RTD layers can easily be produced and thus these again could be driven harder than Schottky based devices. This study therefore was just an initial investigation using the layer structures which are already available rather than bespoke new layers, and unfortunately this did not prove favourable in support of the use of RTDs in this application. The prospect of using a single RTD for up conversion mixing purposes at mm wavelengths was investigated in this chapter as well, where two different sub-harmonic pumped (n=2) up-conversion mixers featuring single quantum barrier junctions were designed and evaluated using the symbolically defined device capability in ADS and the transmission line optimisation using HFSS. The performance in terms of efficiency and maximum output power were compared with optimised Schottky diodes based designs. In this approach, the aim was to explore high drive level mixers and conversion efficiencies. The performance is explored via one design operating at 180 GHz and providing -7dBm of output power using 10dBm of a LO power, while the second mixer operates at 110GHz exhibiting an output power of -0.5dBm using 16dBm of a LO power.

6.2 Future work

Based on the current simulated results, the priority of the next phase should be given to fabrication and measurement of these mixer designs and to make a comparison, and confirm the current promising simulated results, as the eventual aim of the thesis is to realize a similar design with an operating frequency of 640GHz for meteorological studies. The second potential avenue of work is to produce new RTDs with different I-V characteristics to confirm the possibility of the current RTDs as frequency tripler’s, because the selected Schottky diode (used for comparison purposes in this study) has a strong nonlinearity region provided within its I-V curve, and for this, the current RTDs with such a growth structure cannot be compared with this Schottky diode. The penultimate measurement would be to confirm the up-conversion results. Finally, the noise of these RTDs should be investigated, and compared with other solid state devices.

APPENDIX-I

MIXER CONFIGURATION TYPES

This Appendix provides a brief review of the most common types of mixers, where their use in a specific application can be determined by their function as well as the nonlinear elements used, such as diodes and transistors. Mixers can be divided into different types as: single-ended, single-balanced, double-balanced, sub-harmonic up conversion, sub-harmonic down conversion, up-conversion image rejection, down-conversion image rejection and so on. The three main types are single ended, single balanced, and double balanced, which are a function of the desired application and the restriction of the fabrication processes. The performance of mixers is broadly evaluated using the following terms[99]:

- Conversion loss: The ratio expressed in dB to provide the level of the desired output signal to the input one.
- Noise Figure: The ratio which determines the Signal to Noise Ratio (SNR) to SNR at the input and the output, respectively.
- LO drive: The level of the Local Oscillator (LO) power at which the optimum performance of a given mixer can be obtained.
- Isolation: The leakage of power from one port to another, i.e. RF into IF, LO into IF or LO into RF port.
- Third-order Input and output Intercept Point (IIP3 and OIP3): As soon as the output power of both undesired intermodulation products, and the desired signal is equal, the input power is referred to as IIP3 and the output power is referred to

as OIP3, which both are crossed at a point called third-order intermodulation products (IP3).

– Single-Ended Mixer (SEM)

A basic and most common topology is shown in Figure I.1a, which comprises a single diode and filters at the three different ports. Balance (isolation) is relatively complicated with this type, but once the three different ports (RF, LO and IF) are well separated a good isolation can be provided using suitable filters. In addition to their simple configuration, single-diode based mixers are capable of exhibiting a decent conversion loss, compared to other topologies shown in Figure I.1. Unlike other configurations, single-diode mixers use a low local oscillator power, since only a single junction is employed as a nonlinear element. Their simplicity is also favored at millimeter wave frequencies. There are nevertheless some drawbacks of this type of mixer, which is a relatively sensitive to terminations and has not enough ability to adequately suppress the unwanted components, i.e., spurious signals[99].

– Single-Balanced Mixer (SBM)

The common block of a single-balanced based mixer is depicted in Figure I.2b. The typical conversion loss that can be provided by this configuration is higher compared to the mixer based on a single diode. Typically, more Local Oscillator power is also required since two diodes are used in such a mixer. However, better isolation between the three ports is provided, and also the suppression for the RF or LO signal is good in such a topology [99].

– Double- Balanced Mixer (DBM)

A simple diagram of a double-balanced mixer is illustrated in Figure I.3c. This mixer has some benefits in terms of port-to-port isolation and the rejection of spurious signals. Low conversion loss could be obtained with this mixer. A high LO drive, in addition, is required with this topology as more nonlinear devices are used[99].

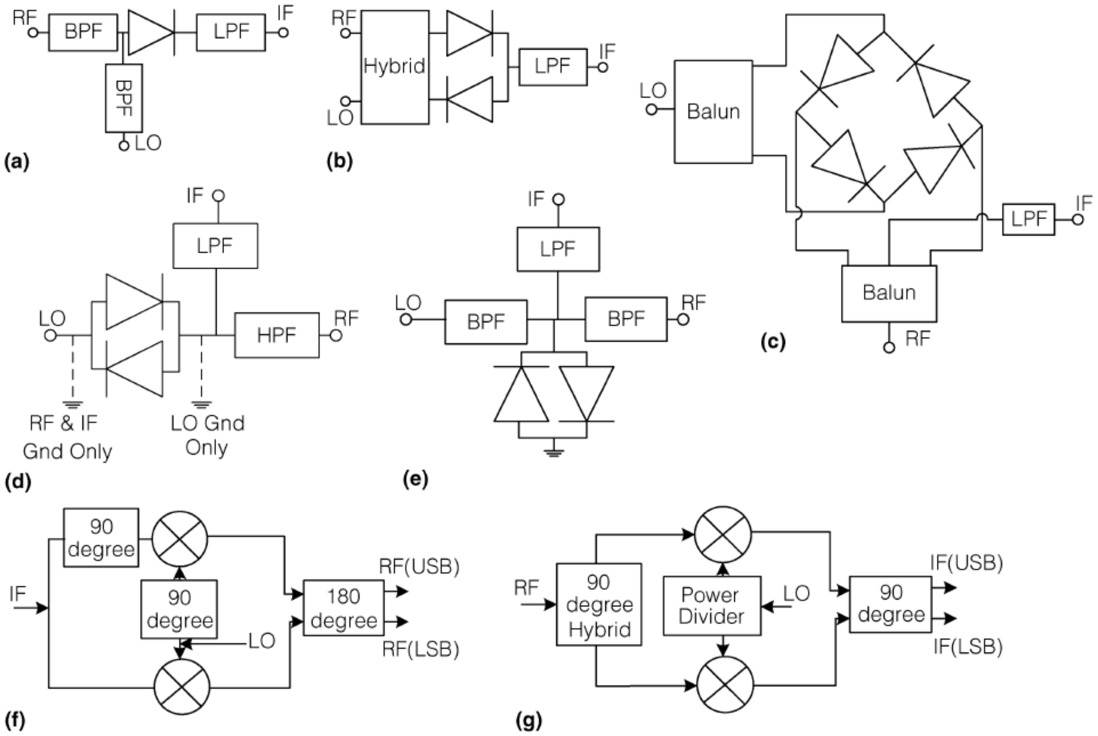

Figure I.1: A simple block for a set of millimeter wave mixers: (a) single-ended (b) single- balanced (c) double-balanced, (d) sub-harmonic up conversion, (e) sub-harmonic down conversion, (f) up-conversion image rejection, (g) down-conversion image rejection. (LPF: Low Pass Filter, LSB: Lower Sideband and USB: Upper Sideband.)[114].

APPENDIX-II

SYMBOLICALLY-DEFINED DEVICE RELIABILITY

The key purpose of this appendix is to confirm the reliability of the Symbolically Defined Device (SDD) model, prior to evaluating the potential use of RTDs in mixing applications. For this, two different models are compared, namely the built-in Schottky model and a user defined SDD model description of a Schottky. These are used to prove the validity of the SDD model in describing the Schottky's performance in terms of conversion loss. The comparison between the built-in diode model and the Schottky representation showed < 1.5 dB difference at the optimum performance for the complete mixer design. Therefore the SDD modelling approach can be considered as a trustworthy tool to estimate the likely performance of an RTD.

For the built-in Schottky model, the design is approached with a primary configuration of a Schottky based mixer circuit as depicted in Figure II.1. The mixer is constructed with three ports, namely 18GHz of RF and 8.85GHz of LO as input signals and 300MHz of IF as an output signal (i.e., down conversion mixing using second sub-harmonic of LO signal). Additionally, a pair of commercial diodes (CAY-18 from Philips) were used in the simulation, whose equivalent circuit is illustrated in Figure II.2. Three current probes were also placed at the three different ports while a resistor was used to terminate the IF side. Moreover, the power for both input signals was provided by two power sources located at the RF and LO port. The used RF power is -20dBm while the LO power has a set of values such that the LO influence on the conversion loss can be distinguished.

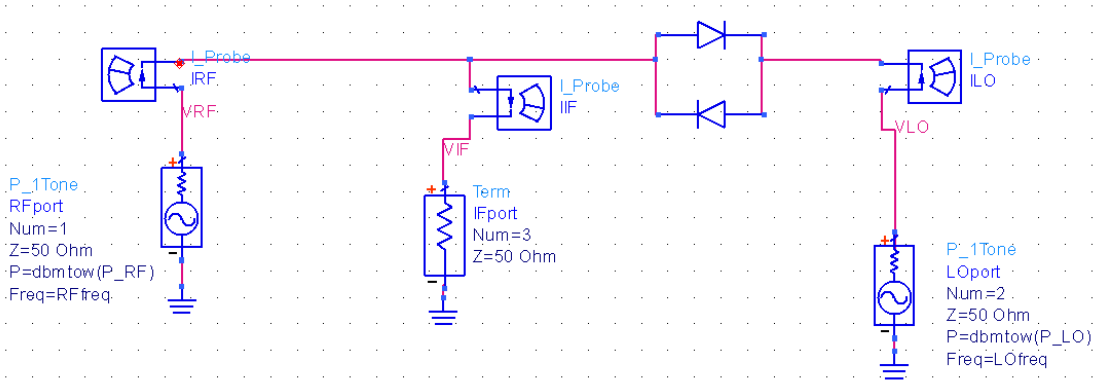

Figure II.1: The initial configuration of the mixer circuit.

Running the harmonic balance simulator in Agilent ADS, the initial performance can be estimated as 22dB conversion loss at LO power in the range of 3-5dBm. This initial result is relatively high, i.e. a reasonable result should be below 10dB in this frequency range. It should be noted that there are no external elements added to optimise the circuit, such as transmission line stubs or filters. This initial conversion loss will therefore serve as a guide towards the next design steps.

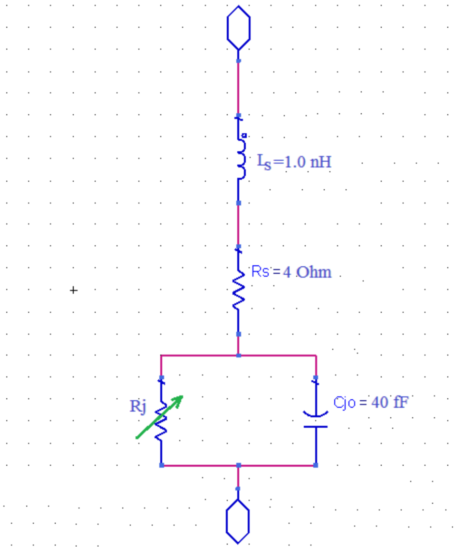

Figure II.2: The equivalent circuit of Schottky diode.

The figure of merit of the mixer performance is the conversion loss (CL) as a function of LO power. In order to reduce the CL obtained in the previous stage and to improve the signal match, different transmission line stubs are added to both sides of the diode pair and IF ports as shown in Figure II.3. Providing a short circuit stub of λ/2 at the RF frequency to the LO side presents a reflection path to the RF signal to be applied again to the diode pair with no effect on the LO signal. Likewise, an open stub of λ/4 at the LO frequency to the RF side will work as a short circuit for the LO and open for RF signal. Also, two series stubs are located adjacent to the diode pair to maximise the reflected RF and LO signals at the diode pair. These additional stubs helped achieve a reasonable performance in terms of CL around 8.2 dB at 4 dBm of LO power.

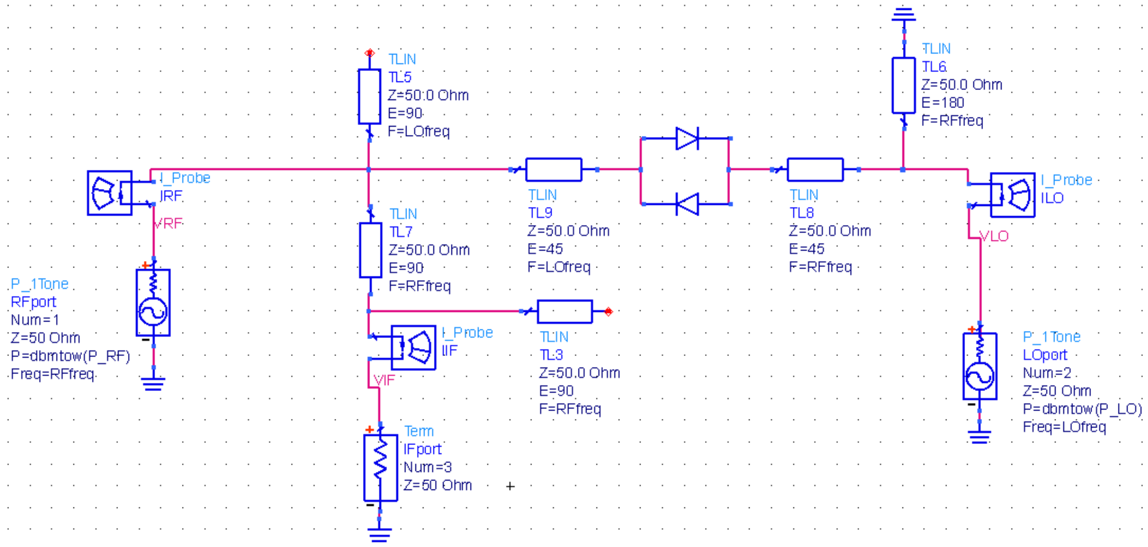

Figure II.3: The intermediate mixer circuit involved a set of stubs.

As an attempt to minimise the leakage of other signals to the RF port, pass-band filter (PBF) is introduced at the RF side as show in Figure II.4. As a result, the best CL is 4.8dB at 3dBm of LO power as depicted in Figure II.5. It should be noted that the simulation during this stage is using ideal transmission lines since the main aim of this part of the study is to only estimate Schottky diode pair performance using two different approaches under similar conditions.

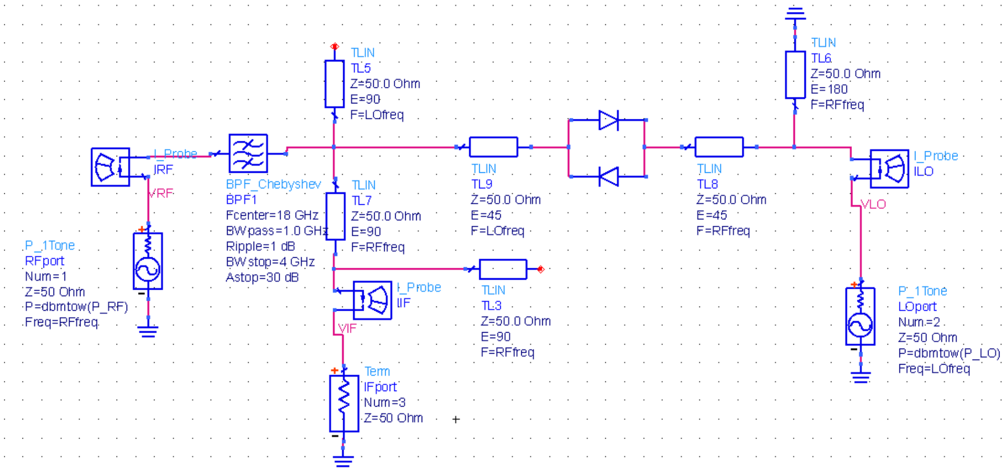

Figure II.4: The Final topology of the mixer circuit using built-in model.

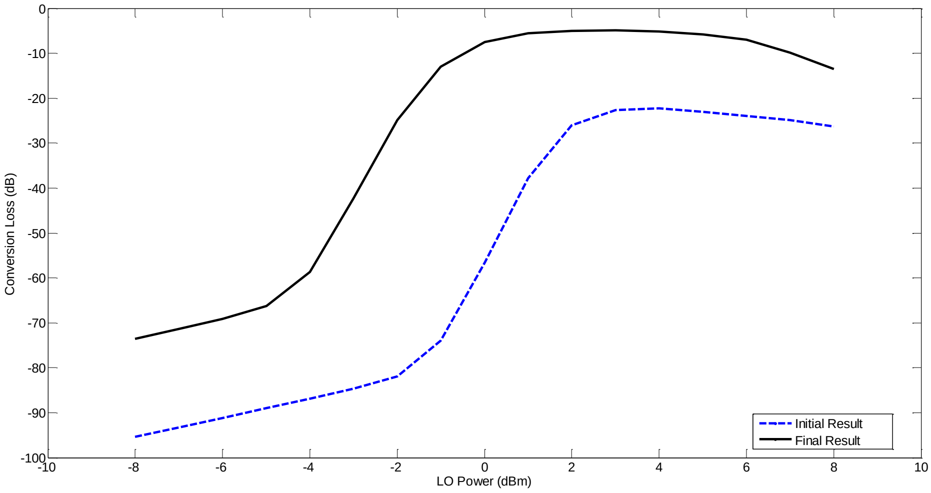

Figure II.5: The initial and final conversion loss at 18GHz.

To begin with the SDD representation, the Schottky diode pair, in the same mixer topology used earlier, i.e. similar to the Figure II.1, will be re-simulated using the SDD model. It is based on a polynomial equation, extracted by fitting a measured I-V curve using the Matlab package. Figure II.6 shows the I-V characteristic of Schottky diode pair using two different methods, built-in model and SDD, where a good agreement is clearly provided.

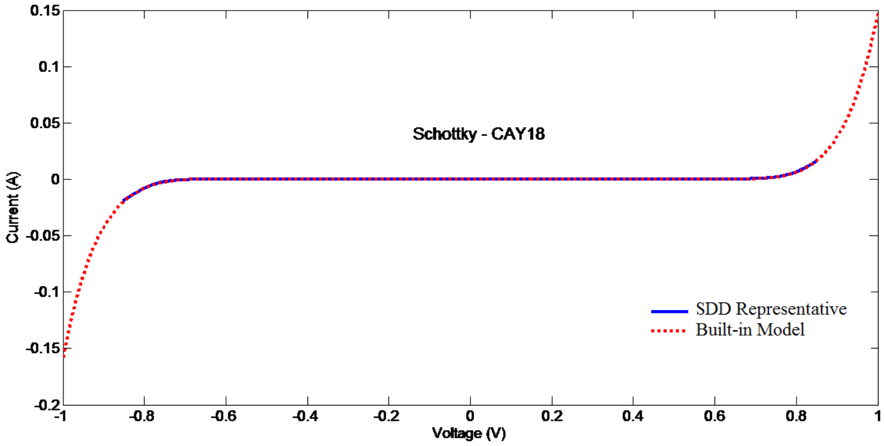

Figure II.6: Measured and fitted I-V curve of Schottky CAY-18.

The result for the conversion loss using the two different approaches at a set of different LO powers is illustrated in Figure II.7. From this Figure, it can be seen that there is a small deviation in the range of 0-4dBm LO power, but the obtained CL was just a dB higher than that of the built-in model. It is consequently obvious that this modeling method is capable of providing the explicit performance of a given RTD.

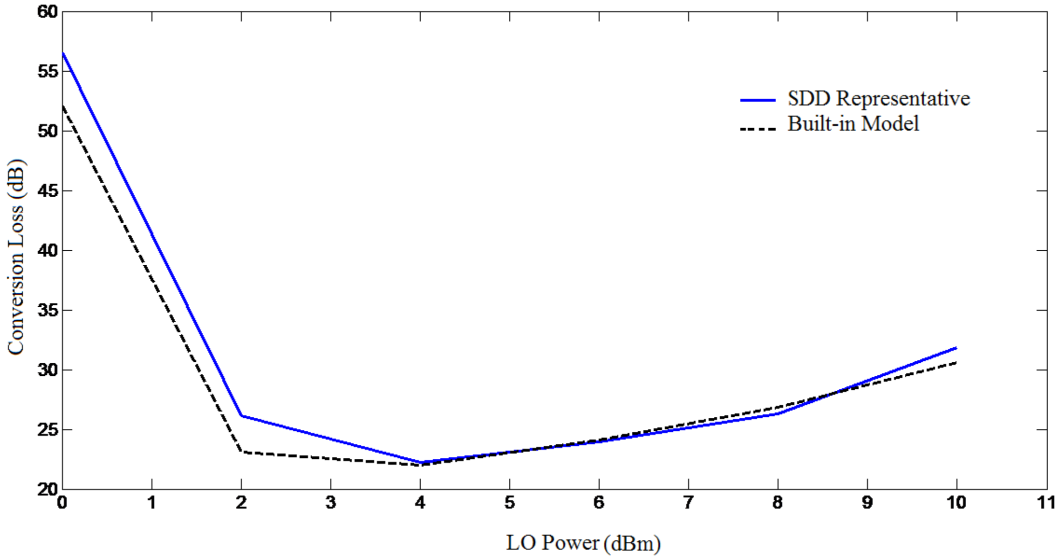

Figure II.7: The conversion loss using two different approaches.

APPENDIX-III

INITIAL DESIGNS OF SUB-HARMONIC UP-CONVERTER MIXER

This part aims to explore the initial performance of RTDs used in up-mixing applications. In order for the RTD mixer to be investigated, a comparison with Schottky diode pair is preferable at this stage. A comparison with a recently published result for a Schottky diode pair at 270GHz is presented here. The ultimate goal of this part (chapter 5) is to explore the approach by designing two different sub-harmonic mixers operating at 110GHz and 180GHz using two different technologies, i.e. coplanar waveguide and microstrip.

- An initial Design of a 210GHz Mixer

A sub-harmonic up conversion mixer circuit is presented in Figure III.1, which has an input frequency of IF at 10GHz and LO pump signal at 100GHz, while the output signal (RF) is based on the second harmonic of the LO signal, i.e. RF equals 210GHz. For comparison purposes the mixer circuit is deliberately made simple at this stage, except a band-pass filter (BPF) is provided at the input side.

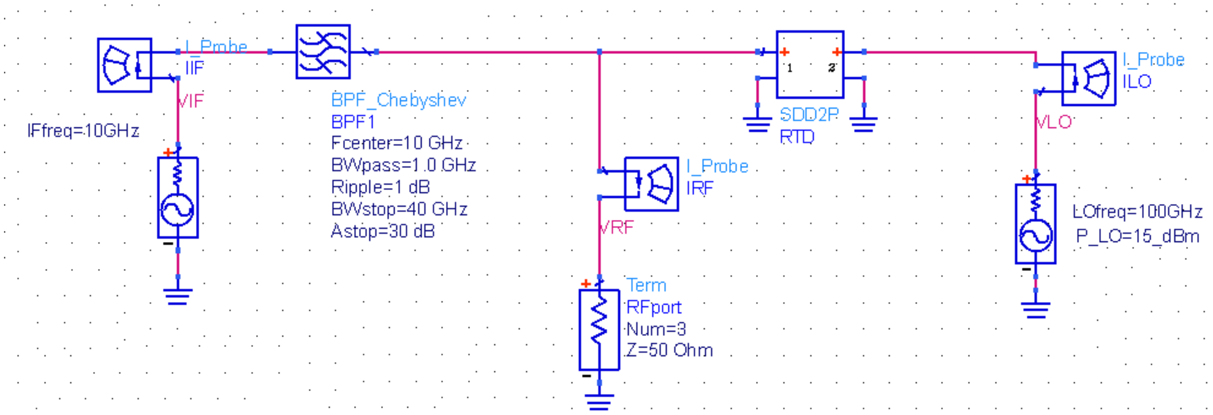

Figure III.1: 210GHz 2x up-converter mixer circuit.

Although there are no matching networks or transmission line stubs employed yet since the purpose is only comparison, Figure III.2 shows that the L940-D2 is capable of providing a reasonable performance in terms of conversion loss, when compared to the Schottky diode pair shown in Figure III.3. At the same time, it should be mentioned that the non-linear element losses (i.e. parasitic elements) are embedded in the form of a parallel capacitor, series resistor and series inductor, and are not taken into consideration in this simulated result.From these figures, the power efficiency of a single RTD (L940-D2) is higher than a Schottky pair. As a consequence of this initial estimation of the RTDs performance, a set of different configurations of sub-harmonic up-converter mixer will be presented in the following section.

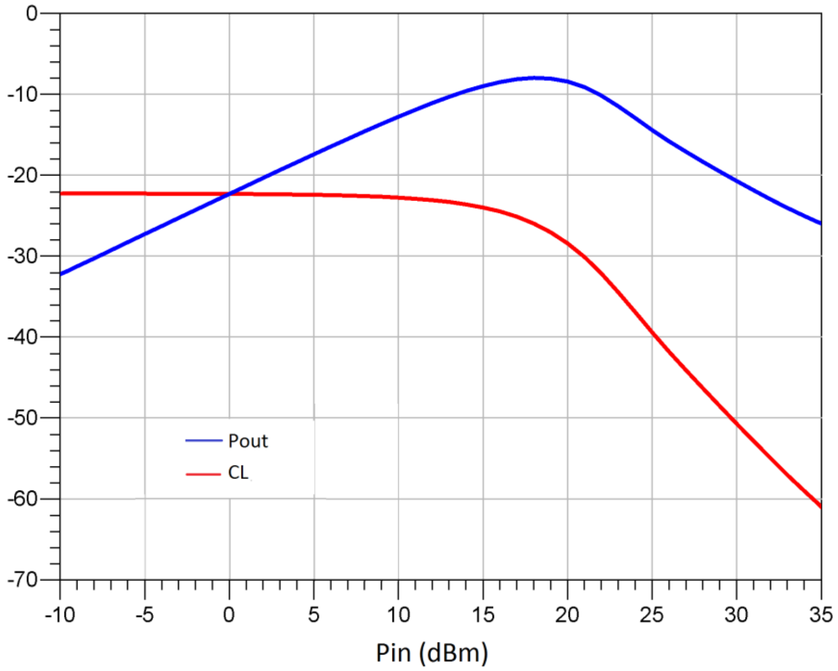

Figure III.2: L940-D2 CL at 15dBm LO power.

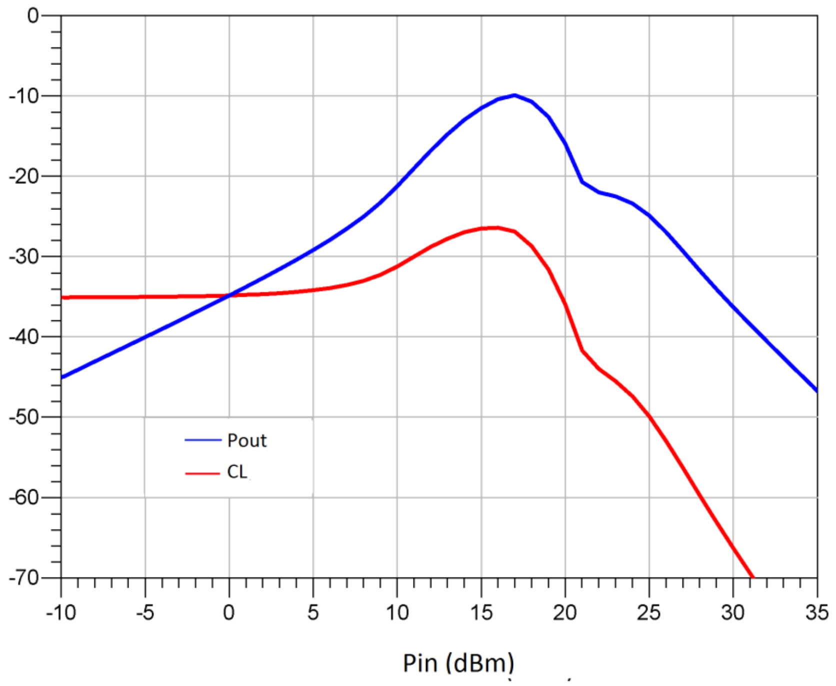

Figure III.3: Schottky CL at 15dBm LO power.

- 273GHz 2X Sub-harmonic up-converter Mixer

In this section more investigation of these RTDs in up converter mixer circuits is explored by making a simple comparison with a recent paper presented by Rui Li[111]. Li used IF and LO signals at 135GHz and 69GHz respectively in a 273GHz 2nd sub-harmonic up converter mixer circuit based on a Schottky anti-parallel diode pair (APDP), where its main parameters are shown in Table III.1. The achieved conversion loss by Li was 17.7dB at 270GHz when 6.5dBm and 0dBm of LO and IF power signals are applied.

Table III.1: Main parameters of APDP

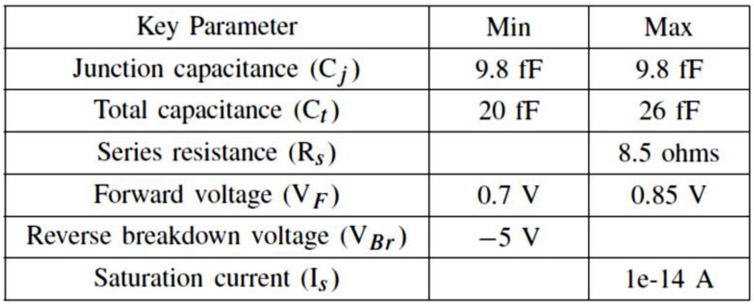

Key Parameter	Min	Max
Junction capacitance (C_j)	9.8 fF	9.8 fF
Total capacitance (C_t)	20 fF	26 fF
Series resistance (R_s)		8.5 ohms
Forward voltage (V_F)	0.7 V	0.85 V
Reverse breakdown voltage (V_{Br})	−5 V	
Saturation current (I_s)		1e-14 A

In order for incident power to be efficiently handled, proper impedance matching networks should be provided at the three different ports of a mixer circuit. Such a matching network can simply be presented by using a set of transmission line. For this, the proposed configuration of the sub-harmonic up-converter mixer in this current work is shown in Figure III.4, which differs from Rui Li mixer in that it benefits from open and short stubs at both sides of the SDD (nonlinear element representation of RTD in ADS environment) instead of using a duplexer.

As mentioned previously, the great feature behind providing a short circuit stub of λ/2 at the IF frequency to the LO side is to present a reflection path to the IF signal to be applied again to the RTD, and this will not affect the LO signal since the LO frequency is half of the IF signal. Likewise, an open stub of λ/4 at the LO frequency to the IF side works as a short circuit to the LO while providing an open circuit to the IF signal since the IF frequency is double the LO signal. In the same way, the RF output signal can be extracted by adding series and shunt stubs at the RF side of λ/4 at IF frequency.

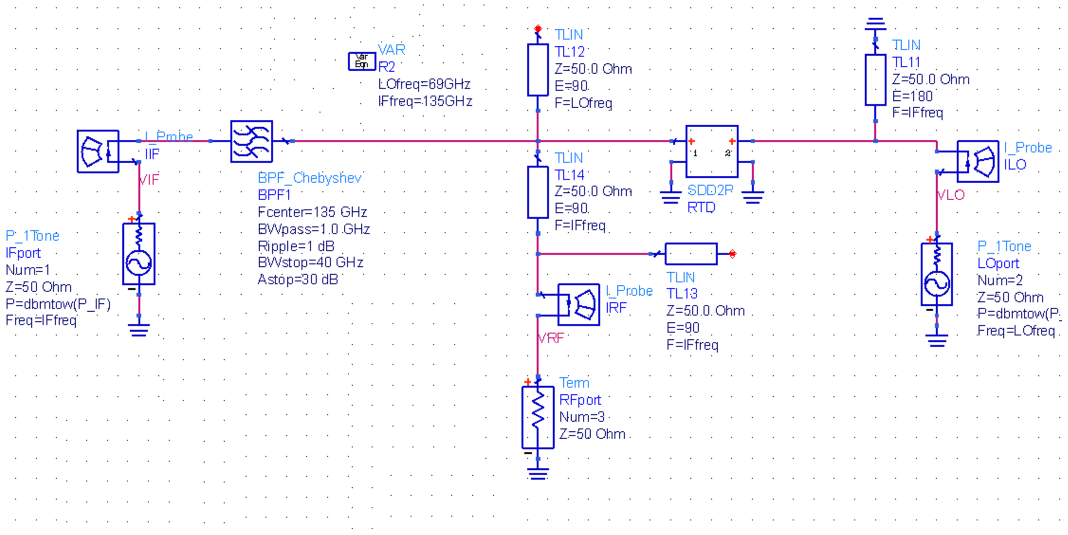

Figure III.4: 273GHz 2X up-converter mixer circuit.

The estimated conversion loss of different RTDs as a function of LO power is shown in Figure III.5 and Figure III.6. From these Figures, it is obvious that the RTDs have a reasonable performance, and this consequently leads to a comparison with the Schottky pair using the same mentioned parameters, shown in Table III.1. The result of this comparison is presented in Figure III.7 and Figure III.8 where the desired efficiency is obtainable with around 15dBm for both the IF and LO powers using a single RTD while the efficiency is slightly lower in the APDP case. However, it should be noted that Li's result was based on measurements while the current result is still simulated in which non-linear element losses and discontinuities, such as tees and crosses, are not accounted for as well as using ideal transmission lines. As a consequence the design presented in chapter 5 takes such differences (losses) into consideration. The output frequencies are at 180GHz and 110GHz with two different technologies, microstrip and grounded coplanar waveguide (GCPW), and using 3D EM tool such HFSS Software so that simulated results can be compared to the measured.

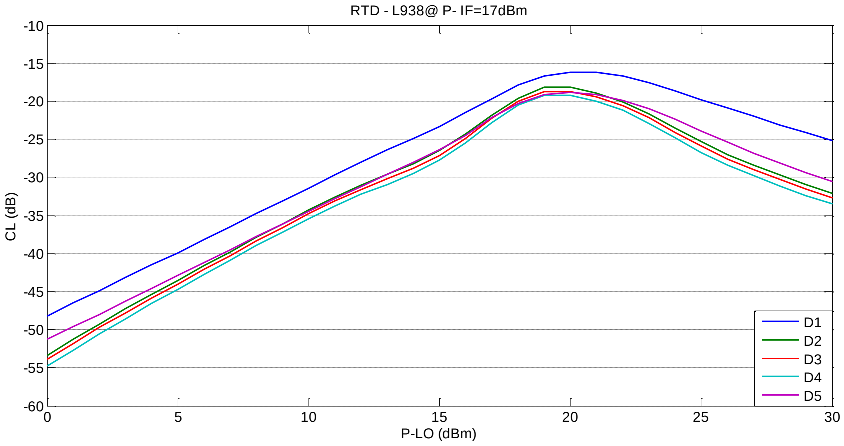

Figure III.5: CL of different size RTDs-L938.

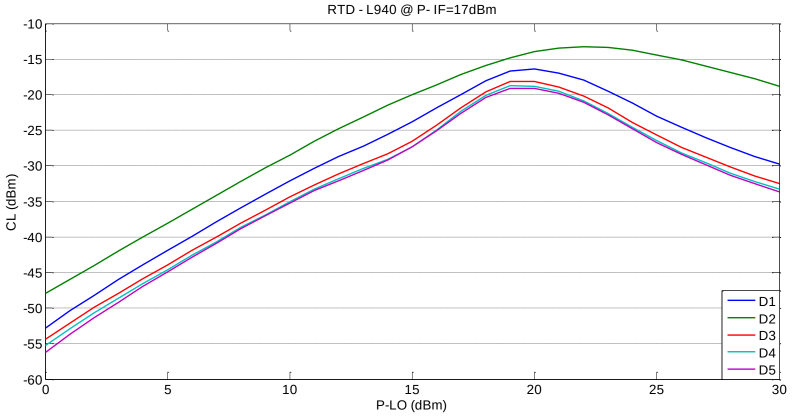

Figure III.6: CL of different size RTDs-L940.

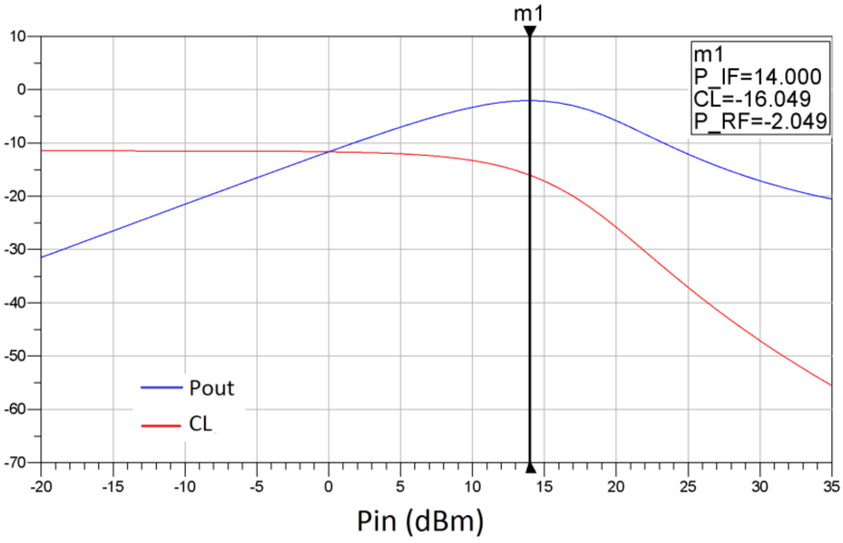

Figure III.7: L940-D2 CL at 15dBm LO power.

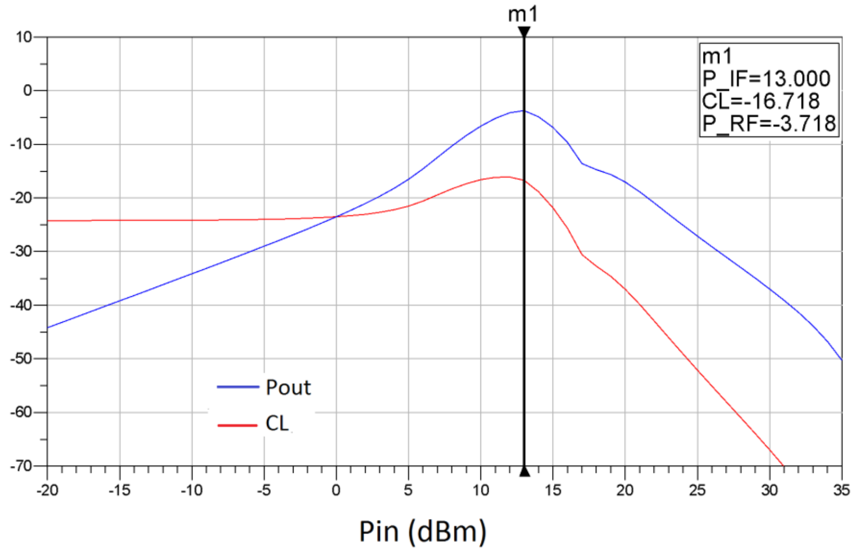

Figure III.8: Schottky CL at 15dBm LO power.

APPENDIX-IV

POWER HANDLING CAPABILITY

This part explores the power handling capability of the RTDs when compared to the Schottky diode pair at two different frequencies, using microstrip line and CPW technologies. For a given mixer, the power handling capability can be characterised by two parameters, one-dB compression point (1dB) and third-order intermodulation products (IP3). The 1dB can be calculated or measured by applying a single tone at the mixer input port and observing the output performance as a function of the input power level. The 1dB point indicates the point at which the conversion loss drops by 1dB from the linear region due to further increase in terms of the input power. Alternatively, the two-tone IP3 can be distinguished once two similar amplitude signals with a given frequency spacing are applied to the input port. After mixing with the LO signal, these two-tone IP3 become close enough to the desired output signal and consequently may be difficult to be properly removed. The issue related to IP3 lies in the fact that its amplitude grows three times faster with respect to increasing input power. As a consequence both the desired output signal and two-tone IP3 are at the same level at a certain point in terms of input power, and this can be theoretically determined by extrapolating the trends. In the actual situation the output mixer performance is compressed before the IP3 matches the anticipated level of the output signal.

-110GHz and 180GHz up-converter mixers results and discussions:

The conversion loss of the 110GHz RTD mixer is 8.1dB at 1dB input and output powers of 5.5dBm and -2.6dBm respectively as shown in Figure IV.1, while the two-tone IP3, with a two-IF input frequency of 20GHz and 19.9GHz, are above 15dBm and 8dBm of

IIP3 and OIP3 respectively as shown on the same Figure. The suppression of IP3 mainly depends on the input power, and this can be explained as the IP3 suppression is 41dB and 2L0 suppression is 25dBc at input power of -6dBm (10dBm below the 1dB input power retaining the output performance in the linear region) as shown In Figure IV.2. The IP3 level below the desired output signal is -20dBc and 2L0 suppression is 37.5dBc at input power of +5.5dBm (1dB input power at which intermodulation products is being growing) as shown in Figure IV.3. However, the power leakage between the mixer ports is above 22dB as shown in Figure IV.4.

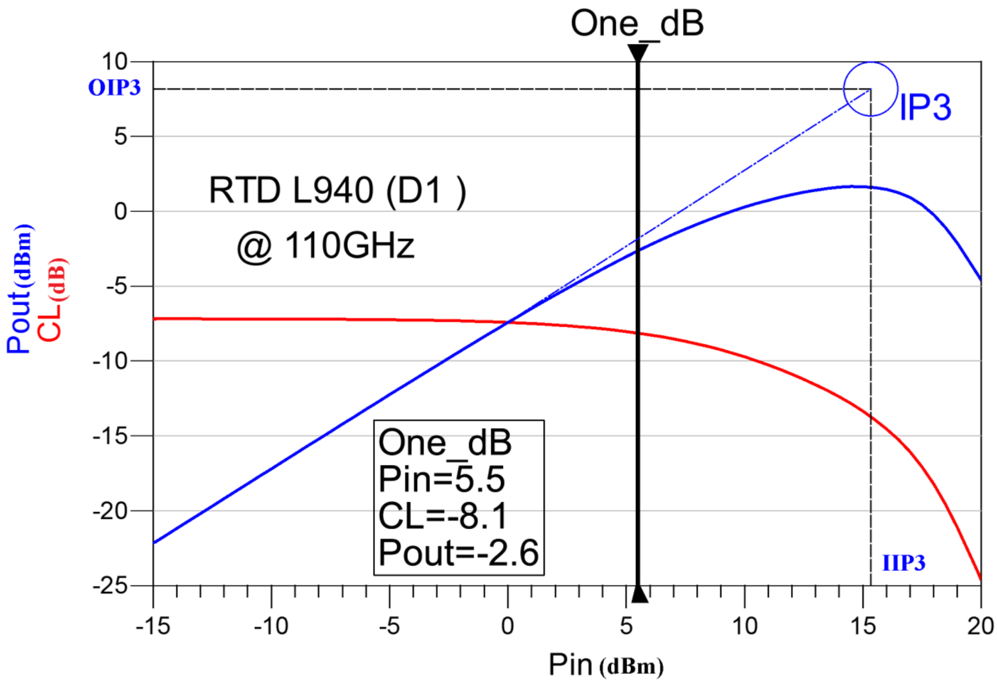

Figure IV.1: RTD output power as a function of input power.

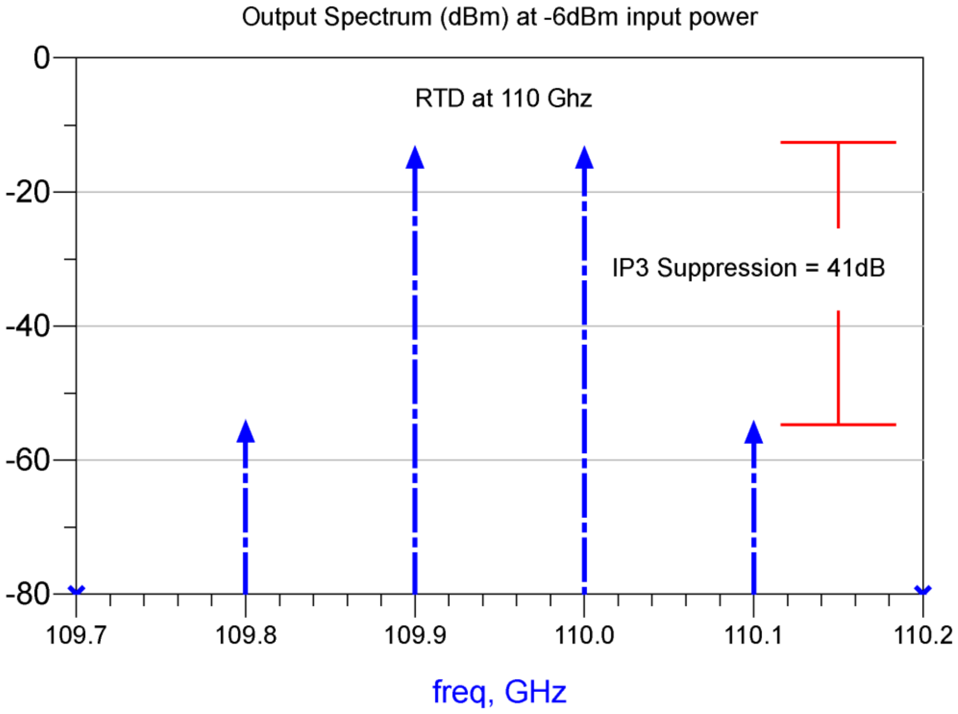

Figure IV.2: IP3 suppression at -6dBm of RTD 110GHz mixer.

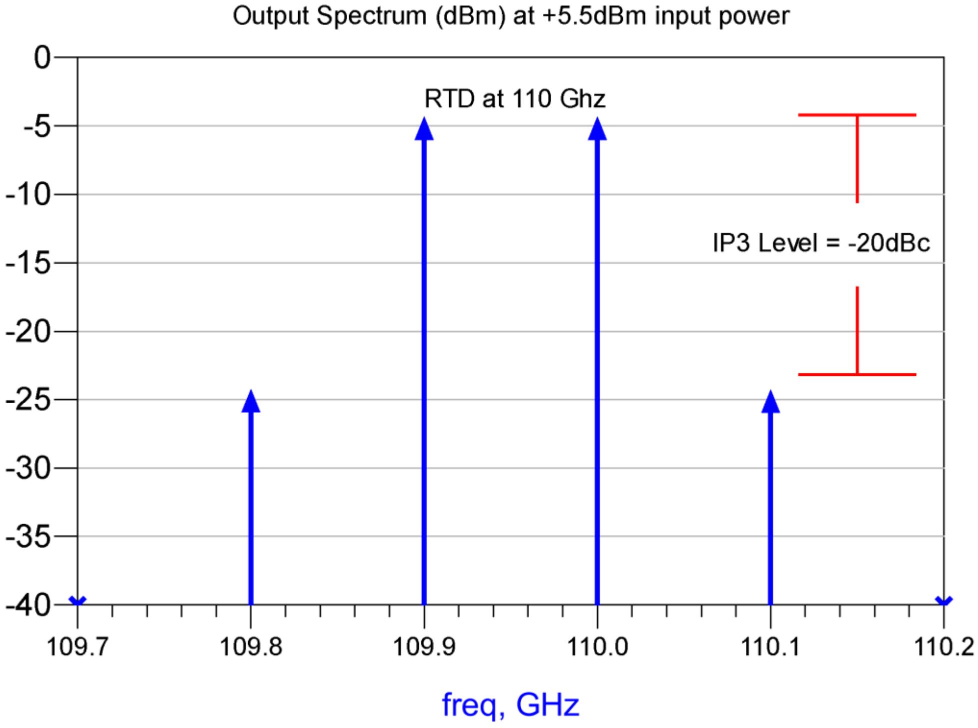

Figure IV.3: IP3 suppression at +5.5dBm of RTD 110GHz mixer.

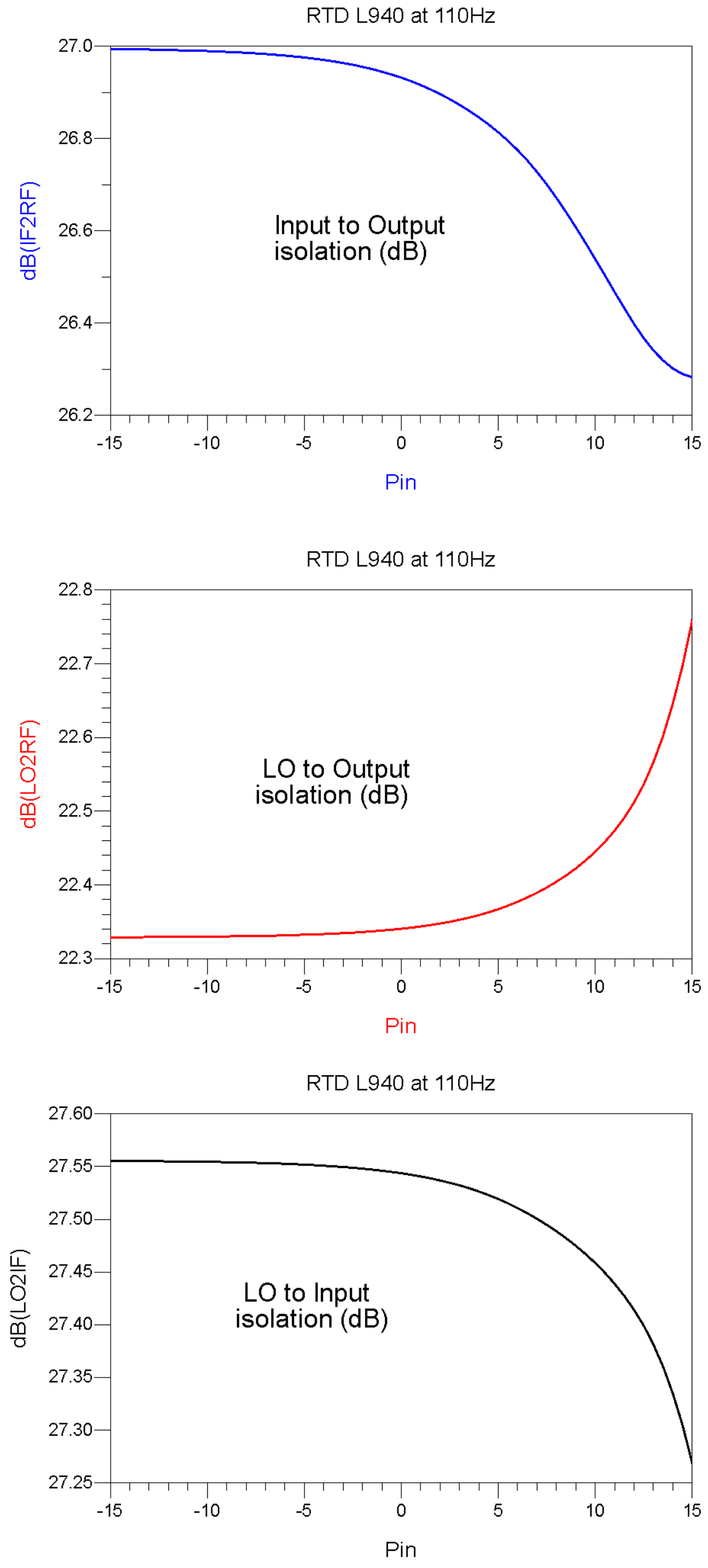

Figure IV.4: Power leakage between the RTD mixer ports.

In order to explore the potential of this RTD in up-conversion mixing application, the rest of this appendix will provide a line-with-line comparison (Figures and Table at the end) with a state of the art Schottky diode, namely DBES105a, which is a commercially available Schottky diode pair used extensively in the literature in a similar situation.

The conversion loss performance of the 110GHz Schottky mixer is 8.3dB at 1dB input power of 1.6dBm and 1dB output power of -6.7dBm as presented in Figure IV.5, while the IIP3 and OIP3 are 11.3dBm and 3.5dBm respectively. According to these results, the power handling capability of RTD is more efficient than the Schottky diode pair. Likewise, for 180GHz mixer the RTD shows a good performance as can be seen form Figure IV.7 when compared to the Schottky results presented in Figure IV.6. As a conclusion, Table IV.1 summarises the important results of both RTD and Schottky diode pair.

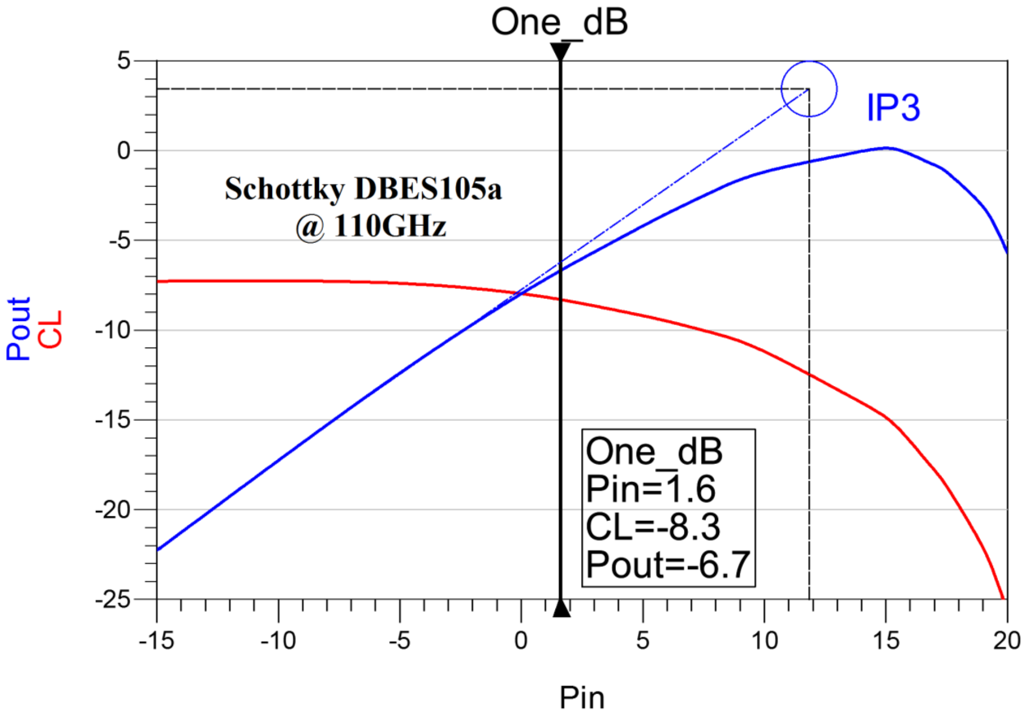

Figure IV.5: Schottky mixer output power at 110GHz as a function of input power.

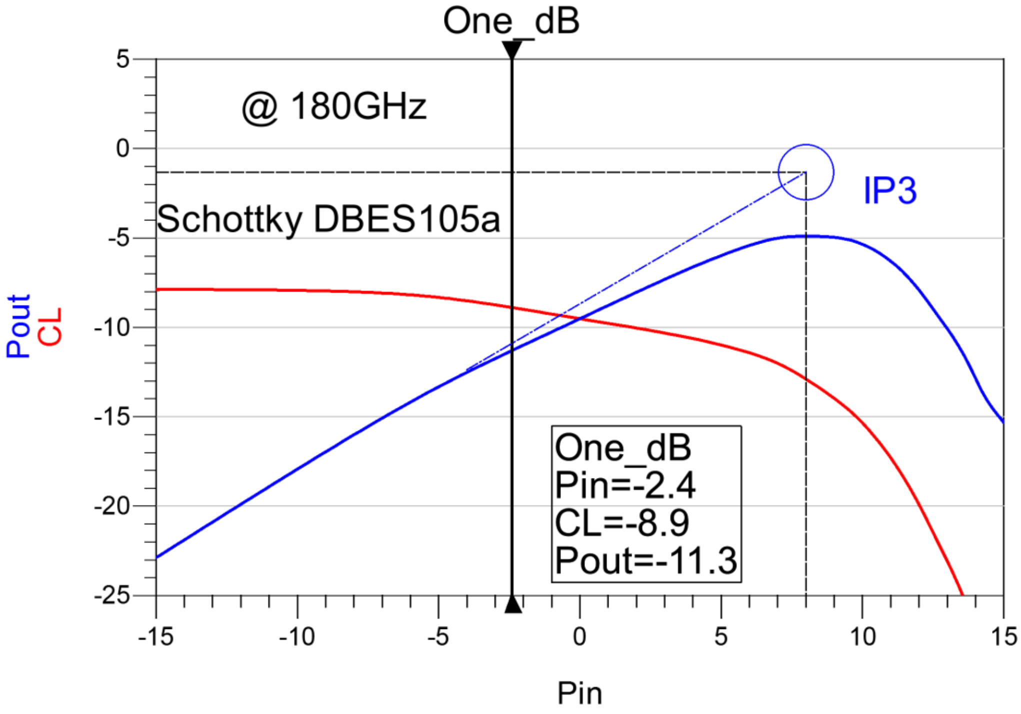

Figure IV.6: Schottky mixer output power at 180GHz as a function of input power.

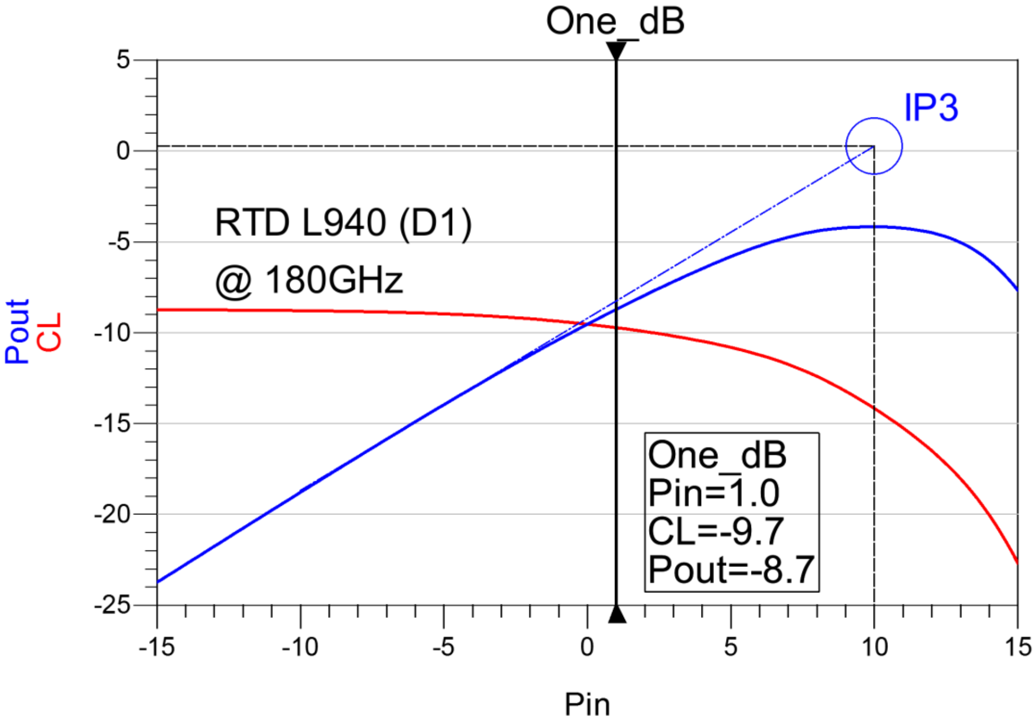

Figure IV.7: RTD mixer output power at 180GHz as a function of input power.

Table IV.1. RTD vs. Schottky pair performance.

Parameter	**Frequency (GHz)**	**Schottky-DBES105a**	**RTD-L940**
CL at 1-dB point	110	8.3	8.1
	180	8.9	9.7
1-dB Input Power	110	1.6	5.5
	180	-2.4	1.5
1-dB Output Power	110	-6.7	-2.6
	180	-11.3	-7
IIP3 (dBm)	110	11.8	15.4
	180	8	11.5
OIP (dBm)	110	3.5	8
	180	-1.5	0
IP3 Suppression (dBc)	110	24	20
	180	0.5	5.5
2*LO Suppression (dBc)	110	53.1	37.7
	180	39.4	42.1
IF to RF Isolation (dB)	110	27	26.8
	180	19.2	23.3
LO to RF Isolation (dB)	110	25.1	22.3
	180	26	26
LO to IF Isolation (dB)	110	29.1	27.5
	180	15	21
LO Power (dBm)	110	16-18	16-18
	180	10-12	10-12

- **Matlab Code**

```matlab
% This code presents the output harmonics of a RTD's Current characteristic at a given input voltage
A = input('what is the input voltage amplitude (A) : ');
Fs=1000;                          % the Sample frequency
Fin =0.1*Fs;                      % Input frequency
Ts = 1/Fs;                        % the Sample time
L = 1000;                         % the signal Length
t = (0:L-1)*Ts;                   % time vector in the x-axis
V = A*cos(2*pi*Fin*t);            % the input voltage
%The following polynomial equation represents the measured I-V characteristic of RTD-L938 D1
I1= (0.0023954*V.^5) + (0.00050729*V.^4) + (0.00080934*V.^3) - (0.00010408*V.^2) + (0.00029871*V) +(3.628e-006);
%The following polynomial equation represents the measured I-V characteristic of RTD-L939 D2
I2=(- 0.00838021*V.^5) +(0.00042806*V.^4) + (0.021795*V.^3) + (0.00089562*V.^2) + (0.0019824*V) -(8.216e-006);
%The following polynomial equation represents the measured I-V characteristic of RTD-L940 D4
I3=(8.2047e-005*V.^5) + (0.00015271*V.^4) + (0.00054161*V.^3) + (-6.088e-006*V.^2) + (7.0443e-005*V) +(1.2587e-006);
%The following polynomial equation represents the measured I-V characteristic of Schottky
CAY18 = (0.28313*V.^7) - (0.014338*V.^6) - (0.23751*V.^5) + (0.0098893*V.^4) + (0.055769*V.^3) - (0.0016267*V.^2) -( 0.0031419*V) + (3.6633e-005);
% the following step is to convert from the time domain to frequency domain for the Schottky (named CAY18)
NFFT = 2^nextpow2(L); % Next power of 2 from the signal Length
CAY18 = fft(CAY18,NFFT)/L;
f = Fs/2*linspace(0,1,NFFT/2+1);
% the following plot only for the single-sided amplitude spectrum.
subplot(2,2,1)
plot(f,2*abs(CAY18(1:NFFT/2+1)),'k');
title('Schottky')
ylabel('Amplitude(V)')
% the following is to convert the current of the RTD-L938 (named I1) to frequency domain
NFFT = 2^nextpow2(L);
I1 = fft(I1,NFFT)/L;
f = Fs/2*linspace(0,1,NFFT/2+1);
% the Plot only for the single-sided amplitude spectrum.
```

```
subplot(2,2,2)
plot(f,2*abs(I1(1:NFFT/2+1)),'b');
title('RTD-L938')
ylabel('Amplitude(V)')% The end
%the following is to convert the current of the RTD-L939 (named I2) to
frequency domain
NFFT = 2^nextpow2(L);
I2 = fft(I2,NFFT)/L;
f = Fs/2*linspace(0,1,NFFT/2+1);
% the Plot only for the single-sided amplitude spectrum.
subplot(2,2,3)
plot(f,2*abs(I2(1:NFFT/2+1)),'g');
title('RTD-L939')
xlabel('Frequency (Hz)')
ylabel('Amplitude(V)')
% the following is to convert the current of the RTD-L940 (named I3)
to frequency domain
NFFT = 2^nextpow2(L);
I3 = fft(I3,NFFT)/L;
f = Fs/2*linspace(0,1,NFFT/2+1);
% the Plot only for the single-sided amplitude spectrum.
subplot(2,2,4)
plot(f,2*abs(I3(1:NFFT/2+1)),'r');
title('RTD-L940')
xlabel('Frequency (Hz)')
ylabel('Amplitude(V)')
% The end of the code
```

APPENDIX-V

SOLIDWORKS DETAILS

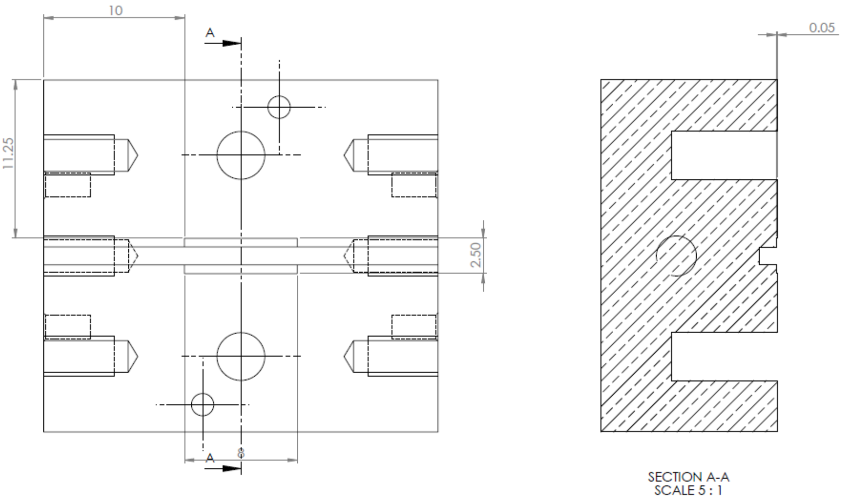

Figure V.1: The left split-block used for W-band transition based on 50µm substrate quartz thickness.

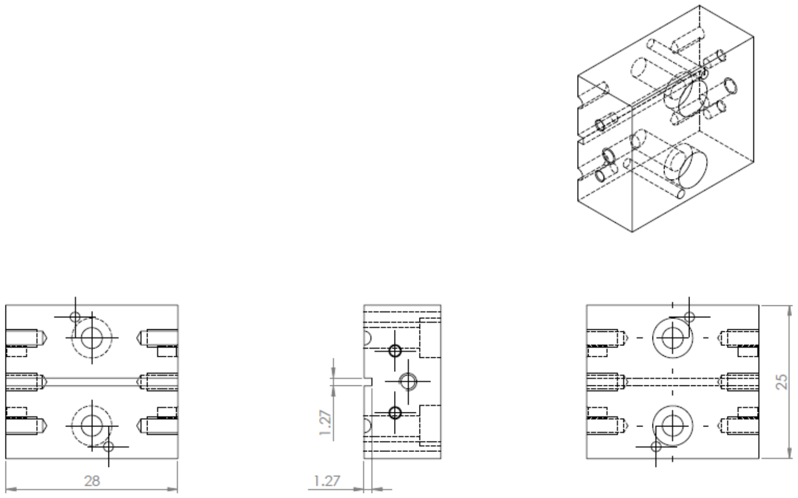

Figure V.2: The right split-block used for W-band transition based on 50µm substrate quartz thickness.

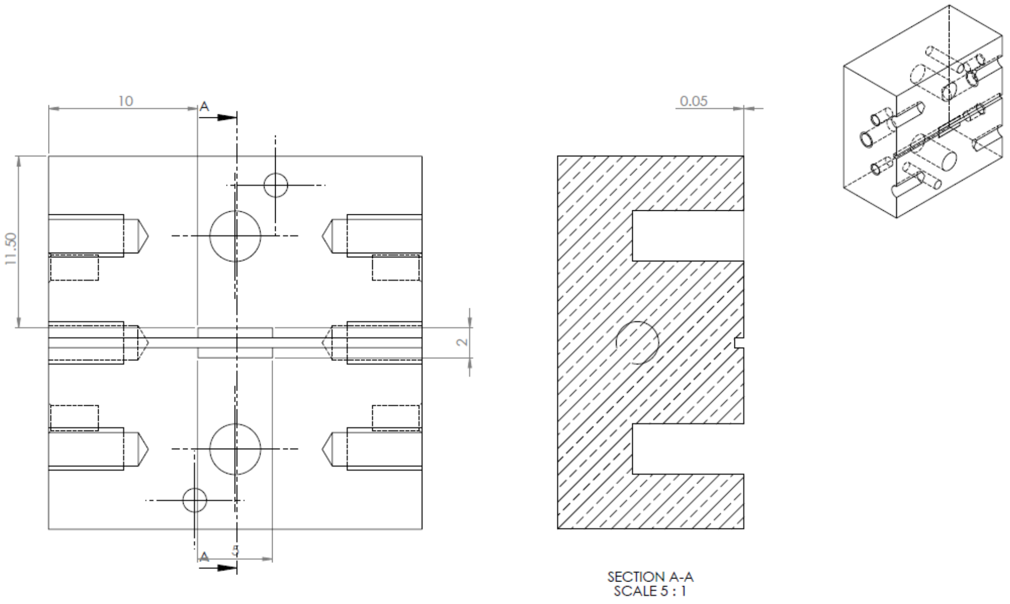

Figure V.3: The left split-block used for G-band transition based on 50µm substrate quartz thickness.

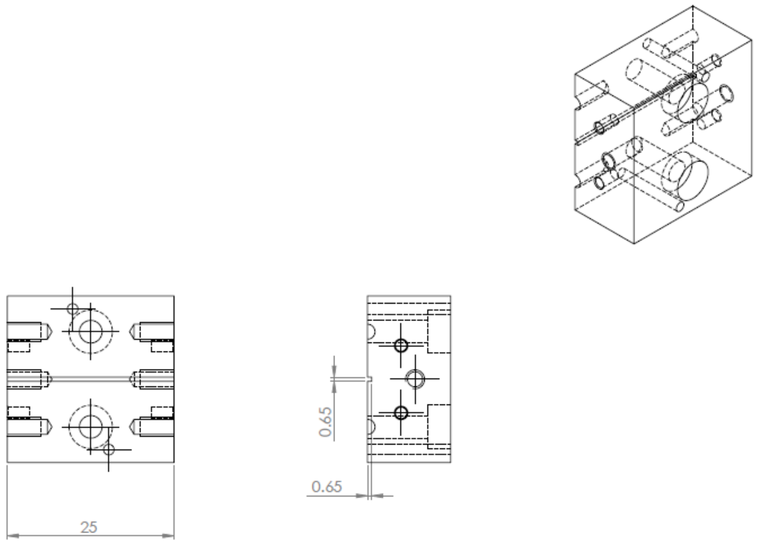

Figure V.4: The right split-block used for G-band transition based on 50µm substrate quartz thickness.

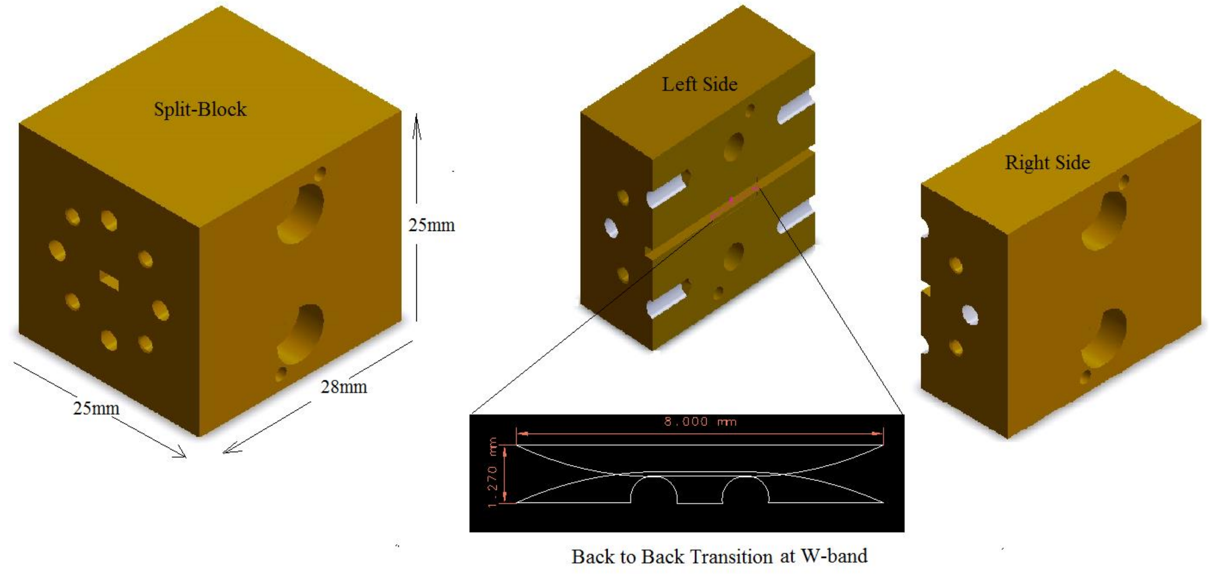

Figure V.5: A 3D view of W-band back to back transition mounted in split-block.

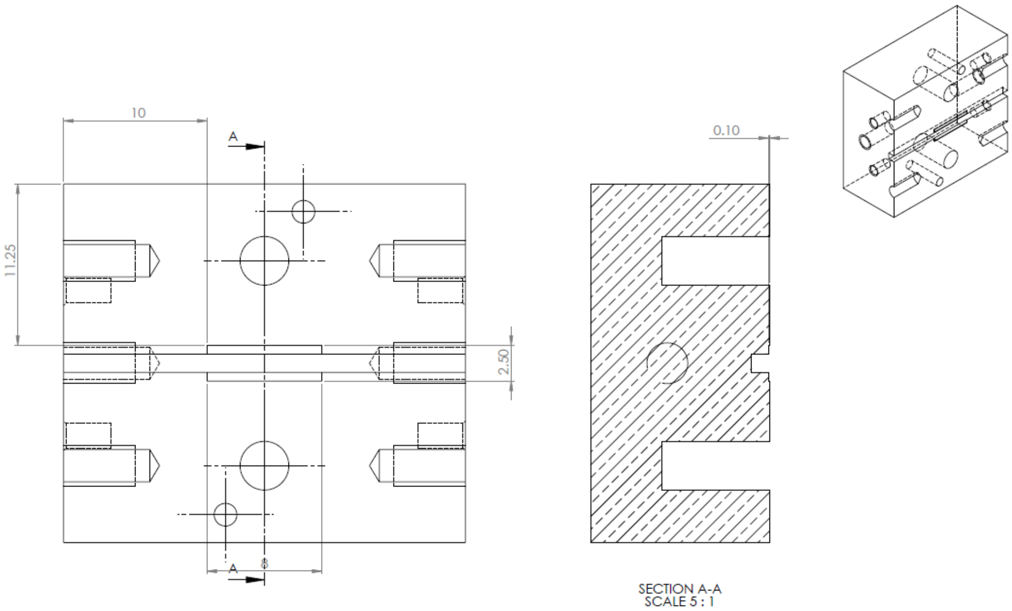

Figure V.6: The left split-block used for W-band transition (LO signal port) based on 100µm substrate quartz thickness.

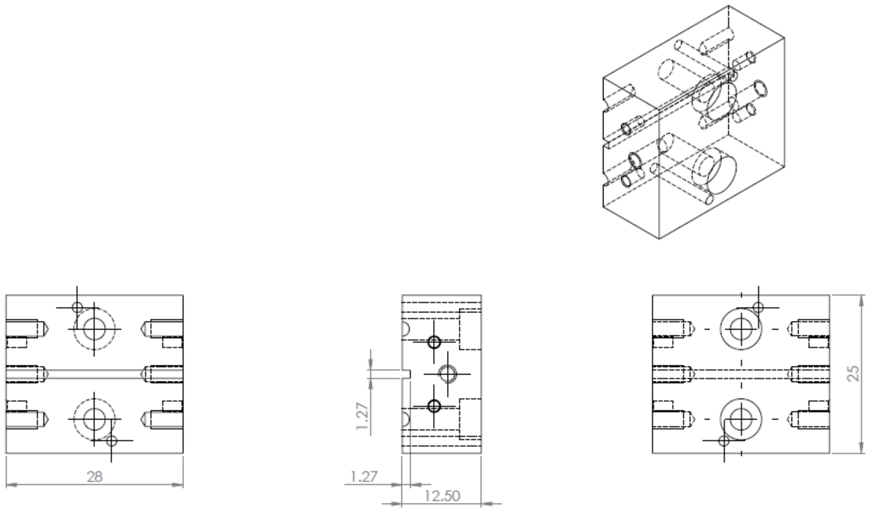

Figure V.7: The right split-block used for W-band transition (LO signal port) based on 100µm substrate quartz thickness.

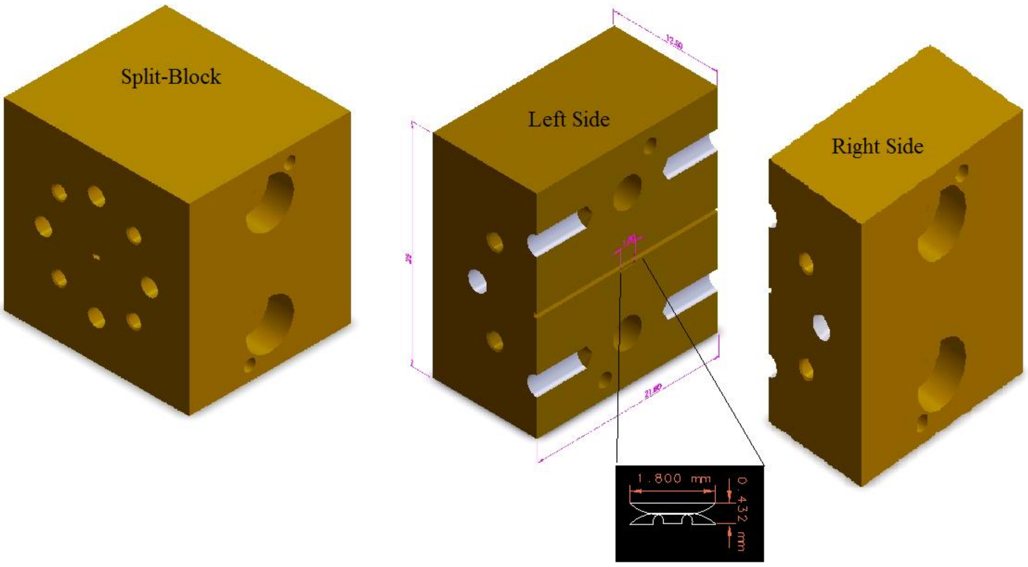

Figure V.8: A 3D view of 320GHz back to back transition mounted in split-block.

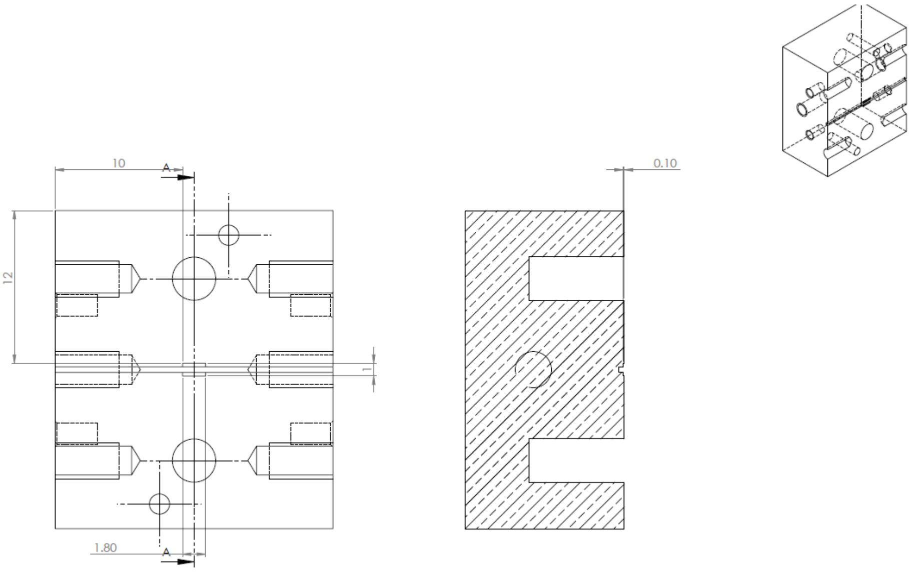

Figure V.9: The left split-block used for 320GHz RF signal transition based on 100µm substrate quartz thickness.

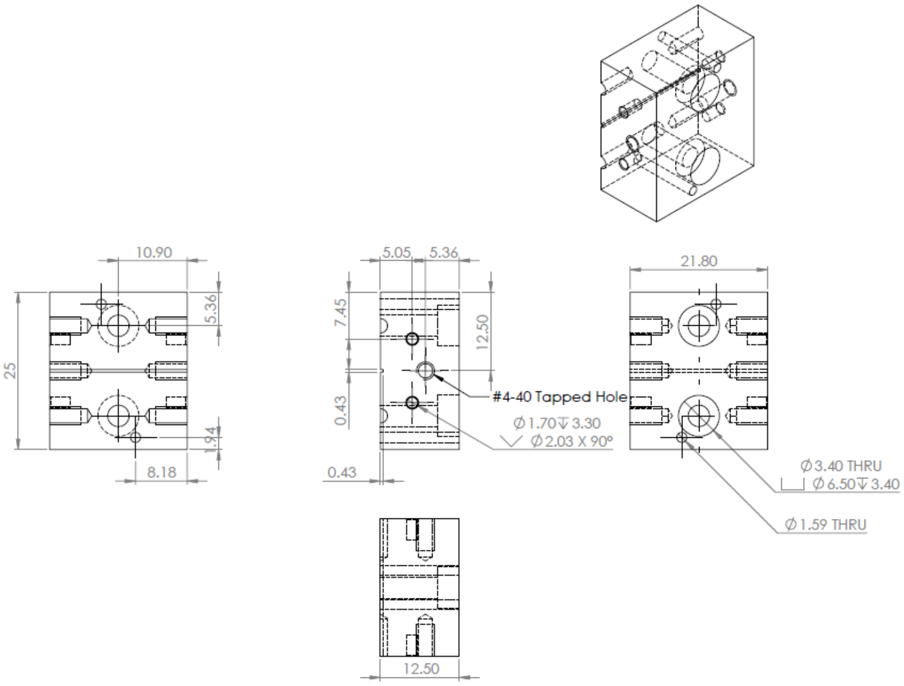

Figure V.10: The right split-block used for 320GHz RF signal transition based on 100µm substrate quartz thickness.

References

[1] A. H. Khan, M. A. Qadeer, J. A. Ansari, and S. Waheed, "4G as a next generation wireless network," in *Future Computer and Communication, 2009. ICFCC 2009. International Conference on*, 2009, pp. 334-338.

[2] C. H. Doan, S. Emami, D. A. Sobel, A. M. Niknejad, and R. W. Brodersen, "Design considerations for 60 GHz CMOS radios," *Communications Magazine, IEEE,* vol. 42, pp. 132-140, 2004.

[3] Y. T. Lo and S. Lee, *Antenna Handbook: Volume III Applications*: Springer Science & Business Media, 2012.

[4] I. Uchendu and J. R. Kelly, "Survey of Beam Steering Techniques Available for Millimeter Wave Applications," *Progress In Electromagnetics Research B,* vol. 68, pp. 35-54, 2016.

[5] G. E. Weibel and H. O. Dressel, "Propagation studies in millimeter-wave link systems," *Proceedings of the IEEE,* vol. 55, pp. 497-513, 1967.

[6] S.-C. Hsin, "Design and analysis of key components for manufacturable and low-power CMOS millimeter-wave receiver front end," 2012.

[7] T. Kürner and S. Priebe, "Towards THz communications-status in research, standardization and regulation," *Journal of Infrared, Millimeter, and Terahertz Waves,* vol. 35, pp. 53-62, 2014.

[8] J. Yang, W.-L. Shan, S. Shi, Q. Yao, Y. Zuo, S. Chen*, et al.*, "The superconducting spectroscopic array receiver (SSAR) for millimeter-wave radio astronomy," in *Millimeter Waves, 2008. GSMM 2008. Global Symposium on*, 2008, pp. 177-179.

[9] D. Vavriv, "MM-wave meteoradars: development, design, and research data," in *Applied Electromagnetics and Communications, 2003. ICECom 2003. 17th International Conference on*, 2003, pp. 13-17.

[10] K. S. J. Murphy, R. Appleby, G. Sinclair, A. McClumpha, K. Tatlock, R. Doney*, et al.*, "Millimetre wave aviation security scanner," in *Security Technology, 2002. Proceedings. 36th Annual 2002 International Carnahan Conference on*, 2002, pp. 162-166.

[11] F. Lin, W. Hu, and A. Li, "Millimeter-wave technology for medical applications," in *Microwave Workshop Series on Millimeter Wave Wireless Technology and Applications (IMWS), 2012 IEEE MTT-S International*, 2012, pp. 1-1.

[12] P. R. Berman and V. S. Malinovsky, *Principles of laser spectroscopy and quantum optics*: Princeton University Press, 2010.

[13] L.-H. Xu, R. M. Lees, E. C. Vasconcellos, S. C. Zerbetto, L. R. Zink, and K. M. Evenson, "Methanol and the optically pumped far-infrared laser," *Quantum Electronics, IEEE Journal of,* vol. 32, pp. 392-399, 1996.

[14] G. Gallerano and S. Biedron, "Overview of terahertz radiation sources," in *Proceedings of the 2004 FEL Conference*, 2004, pp. 216-221.

[15] B. Williams, S. Kumar, Q. Hu, and J. Reno, "Resonant-phonon terahertz quantum-cascade laser operating at 2.1 THz (λ≃ 141 μm)," *Electronics Letters,* vol. 40, pp. 431-433, 2004.

[16] S. H. Gold and G. S. Nusinovich, "Review of high-power microwave source research," *Review of Scientific instruments,* vol. 68, pp. 3945-3974, 1997.

[17] Y.-S. Lee, *Principles of terahertz science and technology* vol. 170: Springer Science & Business Media, 2009.

[18] A. Maestrini, J. Ward, J. Gill, G. Chattopadhyay, F. Maiwald, K. Ellis*, et al.*, "A planar-diode frequency tripler at 1.9 THz," in *Microwave Symposium Digest, 2003 IEEE MTT-S International*, 2003, pp. 747-750.

[19] F. Maiwald, E. Schlecht, J. Ward, R. Lin, R. Leon, J. Pearson*, et al.*, *Design and operational considerations for robust planar GaAs varactors: A reliability study*: Pasadena, CA: Jet Propulsion Laboratory, National Aeronautics and Space Administration, 2003.

[20] H. Eisele, A. Rydberg, and G. I. Haddad, "Recent advances in the performance of InP Gunn devices and GaAs TUNNETT diodes for the 100-300-GHz frequency range and above," *Microwave Theory and Techniques, IEEE Transactions on,* vol. 48, pp. 626-631, 2000.

[21] H. Eisele, "Active two-terminal devices for terahertz power generation by multiplication," in *Terahertz Sources and Systems*, ed: Springer, 2001, pp. 69-86.

[22] V. Radisic, X. Mei, W. Deal, W. Yoshida, P. Liu, J. Uyeda*, et al.*, "Demonstration of sub-millimeter wave fundamental oscillators using 35-nm InP HEMT technology," *Microwave and Wireless Components Letters, IEEE,* vol. 17, pp. 223-225, 2007.

[23] V. Radisic, D. Sawdai, D. Scott, W. R. Deal, L. Dang, D. Li*, et al.*, "Demonstration of a 311-GHz fundamental oscillator using InP HBT technology," *Microwave Theory and Techniques, IEEE Transactions on,* vol. 55, pp. 2329-2335, 2007.

[24] G. Chattopadhyay, E. Schlecht, J. S. Ward, J. J. Gill, H. H. Javadi, F. Maiwald*, et al.*, "An all-solid-state broad-band frequency multiplier chain at 1500 GHz," *Microwave Theory and Techniques, IEEE Transactions on,* vol. 52, pp. 1538-1547, 2004.

[25] A. Srivastava, "Microfabricated Terahertz Vacuum Electron Devices: Technology, Capabilities and Performance Overview," *European Journal of Advances in Engineering and Technology,* vol. 2, pp. 54-64, 2015.

[26] Q. Lu, N. Bandyopadhyay, S. Slivken, Y. Bai, and M. Razeghi, "Continuous operation of a monolithic semiconductor terahertz source at room temperature," *Applied Physics Letters,* vol. 104, p. 221105, 2014.

[27] H.-J. Song and N. Tadao, "Handbook of Terahertz Technologies: Devices and Applications," 2015.

[28] T. Sollner, W. Goodhue, P. Tannenwald, C. Parker, and D. Peck, "Resonant tunneling through quantum wells at frequencies up to 2.5 THz," *Applied Physics Letters,* vol. 43, pp. 588-590, 1983.

[29] J. Scott, J. Kaminski, M. Wanke, S. Allen, D. Chow, M. Lui*, et al.*, "Terahertz frequency response of an In0. 53Ga0. 47As/AlAs resonant-tunneling diode," *Applied physics letters,* vol. 64, pp. 1995-1997, 1994.

[30] E. Brown, T. Sollner, W. Goodhue, and C. Parker, "Millimeter-band oscillations based on resonant tunneling in a double-barrier diode at room temperature," *Applied physics letters,* vol. 50, pp. 83-85, 1987.

[31] E. Brown, J. Söderström, C. Parker, L. Mahoney, K. Molvar, and T. McGill, "Oscillations up to 712 GHz in InAs/AlSb resonant-tunneling diodes," *Applied Physics Letters,* vol. 58, pp. 2291-2293, 1991.

[32] S. Suzuki, M. Asada, A. Teranishi, H. Sugiyama, and H. Yokoyama, "Fundamental oscillation of resonant tunneling diodes above 1 THz at room temperature," *Applied Physics Letters,* vol. 97, p. 242102, 2010.

[33] M. Feiginov, C. Sydlo, O. Cojocari, and P. Meissner, "Resonant-tunnelling-diode oscillators operating at frequencies above 1.1 THz," *Applied Physics Letters,* vol. 99, p. 233506, 2011.

[34] H. Kanaya, H. Shibayama, R. Sogabe, S. Suzuki, and M. Asada, "Fundamental oscillation up to 1.31 THz in resonant tunneling diodes with thin well and barriers," *Applied Physics Express,* vol. 5, p. 124101, 2012.

[35] H. Kanaya, R. Sogabe, T. Maekawa, S. Suzuki, and M. Asada, "Fundamental oscillation up to 1.42 THz in resonant tunneling diodes by optimized collector spacer thickness," *Journal of Infrared, Millimeter, and Terahertz Waves,* vol. 35, pp. 425-431, 2014.

[36] T. Maekawa, H. Kanaya, S. Suzuki, and M. Asada, "Oscillation up to 1.92 THz in resonant tunneling diode by reduced conduction loss," *Applied Physics Express,* vol. 9, p. 024101, 2016.

[37] J. W. Kooi, A. Kovács, M. C. Sumner, G. Chattopadhyay, R. Ceria, D. Miller*, et al.*, "A 275–425-GHz tunerless waveguide receiver based on AlN-barrier SIS technology," *Microwave Theory and Techniques, IEEE Transactions on,* vol. 55, pp. 2086-2096, 2007.

[38] A. D. Semenov, H.-W. Hübers, H. Richter, M. Birk, M. Krocka, U. Mair*, et al.*, "Superconducting hot-electron bolometer mixer for terahertz heterodyne receivers," *Applied Superconductivity, IEEE Transactions on,* vol. 13, pp. 168-171, 2003.

[39] A. Dayem and R. Martin, "Quantum interaction of microwave radiation with tunneling between superconductors," *Physical Review Letters,* vol. 8, p. 246, 1962.

[40] J. Zmuidzinas and P. L. Richards, "Superconducting detectors and mixers for millimeter and submillimeter astrophysics," *Proceedings of the IEEE,* vol. 92, pp. 1597-1616, 2004.

[41] J. Gao, M. Hajenius, Z. Yang, J. Baselmans, P. Khosropanah, R. Barends*, et al.*, "Terahertz superconducting hot electron bolometer heterodyne receivers," *Applied Superconductivity, IEEE Transactions on,* vol. 17, pp. 252-258, 2007.

[42] P. Khosropanah, J. Gao, W. Laauwen, M. Hajenius, and T. Klapwijk, "Low noise NbN hot electron bolometer mixer at 4.3 THz," *Applied Physics Letters, 91 (22), 2007,* 2007.

[43] A. Betz and R. Boreiko, "A practical Schottky mixer for 5 THz (Part II)," in *Proc. of the 7th Int. Symp. on Space THz Technology*, 1996.

[44] G. Chattopadhyay, I. Mehdi, J. S. Ward, E. Schlecht, A. Skalare, and P. H. Siegel, "Development of multi-pixel heterodyne array instruments at submillimeter wavelengths," in *Invited Paper–in Proceedings of the Asia Pacific Microwave Conference*, 2004, pp. 15-18.

[45] M. C. Gaidis, H. M. Pickett, C. Smith, S. C. Martin, R. P. Smith, and P. H. Siegel, "A 2.5-THz receiver front end for spaceborne applications," *Microwave Theory and Techniques, IEEE Transactions on,* vol. 48, pp. 733-739, 2000.

[46] R. Boreiko and A. Betz, "Heterodyne spectroscopy of the 63 μm OI line in M42," *The Astrophysical Journal Letters,* vol. 464, p. L83, 1996.

[47] T.-H. Lee, C.-Y. Chi, J. R. East, G. M. Rebeiz, and G. I. Haddad, "A quasi-optical subharmonically-pumped receiver using separately biased Schottky diode pairs," in *Microwave Symposium Digest, 1994., IEEE MTT-S International*, 1994, pp. 783-786.

[48] M. A. Morgan, "Millimeter-wave MMICs and applications," California Institute of Technology, 2003.

[49] Z. Wang, Y. Zhang, X. Xie, and W. Zhao, "Design of 215–225 GHz subharmonic mixer using planar Schottky diodes," in *Microwave and Millimeter Wave Technology (ICMMT), 2012 International Conference on*, 2012, pp. 1-4.

[50] P. H. Siegel, R. J. Dengler, I. Mehdi, J. E. Oswald, W. L. Bishop, T. W. Crowe*, et al.*, "Measurements on a 215-GHz subharmonically pumped waveguide mixer using planar back-to-back air-bridge Schottky diodes," *Microwave Theory and Techniques, IEEE Transactions on,* vol. 41, pp. 1913-1921, 1993.

[51] I. Mehdi, P. Siegel, D. Humphrey, T. Lee, R. Dengler, J. Oswald*, et al.*, "An all solid-state 640 GHz subharmonic mixer," in *Microwave Symposium Digest, 1998 IEEE MTT-S International*, 1998, pp. 403-406.

[52] B. Thomas, A. Maestrini, and G. Beaudin, "A low-noise fixed-tuned 300-360-GHz sub-harmonic mixer using planar Schottky diodes," *Microwave and Wireless Components Letters, IEEE,* vol. 15, pp. 865-867, 2005.

[53] J. Treuttel, A. Maestrini, B. Alderman, H. Wang, D. Matheson, and P. De Maagt, "Design of a combined tripler-subharmonic mixer at 330 GHz for multipixel application using European Schottky diodes," in *Proceedings of the 21st International Symposium on Space Terahertz Technology, Oxford, UK*, 2010.

[54] L. Miao, J. Jiang, C. Wang, X.-J. Deng, and B. Lu, "A 340GHz sub-harmonic mixer based on planar Schottky diodes," in *Infrared, Millimeter, and Terahertz waves (IRMMW-THz), 2014 39th International Conference on*, 2014, pp. 1-2.

[55] Y. He, M. Yu, and W. Mao, "Simulation design of submillimeter wave subharmonic mixer," in *Microwave Technology and Computational Electromagnetics, 2009. ICMTCE. International Conference on*, 2009, pp. 231-234.

[56] T. Waliwander, M. Crowley, M. Fehilly, D. Lederer, J. Pike, L. Floyd*, et al.*, "Sub-millimeter Wave 183 GHz and 366 GHz MMIC membrane sub-harmonic mixers," in *Microwave Symposium Digest (MTT), 2011 IEEE MTT-S International*, 2011, pp. 1-4.

[57] B. Thomas, B. Alderman, D. Matheson, and P. De Maagt, "A combined 380 GHz mixer/doubler circuit based on planar Schottky diodes," *Microwave and Wireless Components Letters, IEEE,* vol. 18, pp. 353-355, 2008.

[58] J. L. Hesler, K. Hui, S. He, and T. W. Crowe, "A Fixed tuned 400 GHz Subharmonic Mixer Using Planar Schottky Diodes," in *invited talk) in Proc. 1999 Int. Symp. On Space THz Tech., Charlottesville, VA*, 1999, pp. 95-99.

[59] B. Thomas, J. Gill, A. Maestrini, C. Lee, R. Lin, S. Sin*, et al.*, "An integrated 520–600 GHz sub-harmonic mixer and tripler combination based on GaAs MMIC membrane planar Schottky diodes," in *Infrared Millimeter and Terahertz Waves (IRMMW-THz), 2010 35th International Conference on*, 2010, pp. 1-2.

[60] E. Schlecht, J. Gill, R. Dengler, R. Lin, R. Tsang, and I. Mehdi, "A unique 520–590 GHz biased subharmonically-pumped Schottky mixer," *Microwave and Wireless Components Letters, IEEE,* vol. 17, pp. 879-881, 2007.

[61] J. Schür, M. Ruf, and L.-P. Schmidt, "Design of a 4 th harmonic Schottky diode mixer for THz frequencies," in *Infrared and Millimeter Waves, 2007 and the 2007 15th International Conference on Terahertz Electronics. IRMMW-THz. Joint 32nd International Conference on*, 2007, pp. 756-757.

[62] J. V. Siles, J. Grajal, and V. Krozer, "Design of subharmonically pumped schottky mixers for submillimetre-wave applications," in *European Microwave Integrated Circuits Conference, 2006. The 1st*, 2006, pp. 145-148.

[63] L. Esaki, "Solid State Physics in Electronics and Telecommunications," in *Proceedings of an International Conference held in Brussels, June*, 1960, pp. 2-7.

[64] R. Tsu and L. Esaki, "Tunneling in a finite superlattice," *Applied Physics Letters,* vol. 22, pp. 562-564, 1973.

[65] L. L. Chang, L. Esaki, and R. Tsu, "Resonant tunneling in semiconductor double barriers," *Applied Physics Letters,* vol. 24, pp. 593-595, 1974.

[66] L. De Broglie, "Waves and quanta," *Nature,* vol. 112, p. 540, 1923.

[67] J. Bean, "Materials and technologies," ed: John Wiley & Sons, New York, 1990, p. 13.

[68] R. Dingle, W. Wiegmann, and C. H. Henry, "Quantum states of confined carriers in very thin Al x Ga 1− x As-GaAs-Al x Ga 1− x As heterostructures," *Physical Review Letters,* vol. 33, p. 827, 1974.

[69] V. Doychinov, "Quantum Barrier Devices for Sub-Millimetre Wave Detection," PhD thesis, University of Leeds, 2015.

[70] J. P. Sun, G. I. Haddad, P. Mazumder, and J. N. Schulman, "Resonant tunneling diodes: models and properties," *Proceedings of the IEEE,* vol. 86, pp. 641-660, 1998.

[71] X. Wang and H. Xue, "Characterization and modeling of 18–40GHz mm-wave tunneling diode detector," in *Computer Research and Development (ICCRD), 2011 3rd International Conference on*, 2011, pp. 362-365.

[72] M. S. Tyagi, *Introduction to semiconductor materials and devices*: John Wiley & Sons, 2008.

[73] S. Sze and K. K. Ng, "Metal-semiconductor contacts," *Physics of Semiconductor Devices,* pp. 134-196, 2006.

[74] H. Mizuta and T. Tanoue, *The physics and applications of resonant tunnelling diodes* vol. 2: Cambridge University Press, 2006.

[75] M. Tsuchiya and H. Sakaki, "Precise control of resonant tunneling current in AlAs/GaAs/AlAs double barrier diodes with atomically-controlled barrier widths," *Japanese journal of applied physics,* vol. 25, p. L185, 1986.

[76] M. Tsuchiya and H. Sakaki, "Dependence of resonant tunneling current on well widths in AlAs/GaAs/AlAs double barrier diode structures," *Applied physics letters,* vol. 49, pp. 88-90, 1986.

[77] S. Takada and H. Nakamura, "Wentzel–Kramers–Brillouin theory of multidimensional tunneling: General theory for energy splitting," *The Journal of chemical physics,* vol. 100, pp. 98-113, 1994.

[78] S. Mohan, J. P. Sun, P. Mazumder, and G. I. Haddad, "Device and circuit simulation of quantum electronic devices," *Computer-Aided Design of Integrated Circuits and Systems, IEEE Transactions on,* vol. 14, pp. 653-662, 1995.

[79] D. Neculoiu and T. Tebeanu, "SPICE implementation of double barrier resonant tunnel diode model," in *Semiconductor Conference, 1996., International*, 1996, pp. 181-184.

[80] J. Gering, D. Crim, D. G. Morgan, P. Coleman, W. Kopp, and H. Morkoc, "A small-signal equivalent-circuit model for GaAs-AlxGa1− xAs resonant tunneling heterostructures at microwave frequencies," *Journal of applied physics,* vol. 61, pp. 271-276, 1987.

[81] E. Brown, C. Parker, and T. Sollner, "Effect of quasibound-state lifetime on the oscillation power of resonant tunneling diodes," *Applied Physics Letters,* vol. 54, pp. 934-936, 1989.

[82] R. Miles, G. Millington, R. Pollard, D. Steenson, J. Chamberlain, and M. Henini, "Accurate equivalent circuit model of resonant tunnelling diodes," *Electronics letters,* vol. 27, pp. 427-428, 1991.

[83] T. Wei, S. Stapleton, and E. Berolo, "Equivalent circuit and capacitance of double barrier resonant tunneling diode," *Journal of applied physics,* vol. 73, pp. 829-834, 1993.

[84] T. De Roer, M. Hendriks, W. Magnus, M. Henini, H. Heyker, M. Kwaspen*, et al.*, "Accurate Modeling of Double Barrier Resonant Tunneling Diodes," in *Solid State Device Research Conference, 1995. ESSDERC'95. Proceedings of the 25th European*, 1995, pp. 715-718.

[85] J. Schulman, H. De Los Santos, and D. Chow, "Physics-based RTD current-voltage equation," *Electron Device Letters, IEEE,* vol. 17, pp. 220-222, 1996.

[86] D. Neculoiu, T. Tebeanu, and I. Sztojanov, "A new large-signal model for double barrier resonant tunneling diodes for frequency multiplier applications," in *Semiconductor Conference, 1997. CAS'97 Proceedings., 1997 International*, 1997, pp. 349-352.

[87] J. Mattia, A. McWhorter, R. Aggarwal, F. Rana, E. Brown, and P. Maki, "Comparison of a rate-equation model with experiment for the resonant tunneling diode in the scattering-dominated regime," *Journal of applied physics,* vol. 84, pp. 1140-1148, 1998.

[88] M. N. Feiginov, "Displacement currents and the real part of high-frequency conductance of the resonant-tunneling diode," *Applied Physics Letters,* vol. 78, pp. 3301-3303, 2001.

[89] P. Zhao, H. L. Cui, D. L. Woolard, K. L. Jensen, and F. Buot, "Equivalent circuit parameters of resonant tunneling diodes extracted from self-consistent Wigner-Poisson simulation," *Electron Devices, IEEE Transactions on,* vol. 48, pp. 614-627, 2001.

[90] N. Alkeyev, Y. I. Golant, and A. Pashkovskiy, "Computer analysis of resonant tunneling diode structures for subharmonic mixers," in *Microwave and Telecommunication Technology, 2003. CriMiCo 2003. 13th International Crimean Conference*, 2003, pp. 528-529.

[91] M. Long, H. Ying-Long, Z. Yang, W. Liang-Chen, Y. Fu-Hua, and Z. Yi-Ping, "A Small Signal Equivalent Circuit Model for Resonant Tunnelling Diode," *Chinese Physics Letters,* vol. 23, p. 2292, 2006.

[92] D. Deslandes and K. Wu, "Integrated microstrip and rectangular waveguide in planar form," *Microwave and Wireless Components Letters, IEEE,* vol. 11, pp. 68-70, 2001.

[93] D. Liu, U. Pfeiffer, J. Grzyb, and B. Gaucher, *Advanced millimeter-wave technologies: antennas, packaging and circuits*: John Wiley & Sons, 2009.

[94] A. Ø. Olsen, "E-plane circuits for HBV multiliers at 90-140 GHz," PhD, School of Electronic and Electrical Engin, Univeristy of Leeds, 2002.

[95] D. F. Williams, C. Wang, and U. Arz, "An optimal multiline TRL calibration algorithm," in *IEEE MTT S INTERNATIONAL MICROWAVE SYMPOSIUM DIGEST*, 2003, pp. 1819-1822.

[96] A. V. Räisänen, *Experimental studies on cooled millimeter wave mixers*: Helsinki University of Technology, 1980.

[97] A. Maestrini, B. Thomas, H. Wang, C. Jung, J. Treuttel, Y. Jin*, et al.*, "Schottky diode-based terahertz frequency multipliers and mixers," *Comptes Rendus Physique,* vol. 11, pp. 480-495, 2010.

[98] B. Razavi and R. Behzad, *RF microelectronics* vol. 2: Prentice Hall New Jersey, 1998.

[99] S. A. Maas, *The RF and microwave circuit design cookbook*: Artech House, 1998.

[100] W. Liu and D. P. Steenson, "Investigation of subharmonic mixer based on a quantum barrier device," *Microwave Theory and Techniques, IEEE Transactions on,* vol. 48, pp. 757-763, 2000.

[101] T. W. Crowe, R. J. Mattauch, H. P. Röser, W. L. Bishop, W. C. Peatman, and X. Liu, "GaAs Schottky diodes for THz mixing applications," *Proceedings of the IEEE,* vol. 80, pp. 1827-1841, 1992.

[102] R. S. Michaelsen, T. K. Johansen, and V. Krozer, "Design of a× 4 subharmonic sub-millimeter wave diode mixer, based on an analytic expression for small-signal conversion admittance parameters," in *Microwave & Optoelectronics Conference (IMOC), 2013 SBMO/IEEE MTT-S International*, 2013, pp. 1-4.

[103] B. Zhang, Y. Fan, X. Yang, F. Zhong, Z. Chen, S. Zhang*, et al.*, "The design of a 310–350-GHz sub-harmonic mixer with planar schottky diodes," in *Signals Systems and Electronics (ISSSE), 2010 International Symposium on*, 2010, pp. 1-3.

[104] M. Fretz, "Flip chip bonding technologies for hybrid integration," Université de Neuchâtel, 2009.

[105] V. Valenta, T. Spreng, S. Yuan, W. Winkler, V. Ziegler, D. Dancila*, et al.*, "Design and experimental evaluation of compensated bondwire interconnects above 100 GHz," *International Journal of Microwave and Wireless Technologies,* vol. 7, pp. 261-270, 2015.

[106] P. Elenius and L. Levine, "Comparing flip-chip and wire-bond interconnection technologies," *Chip Scale Review,* vol. 4, 2000.

[107] S. Gurbinder and M. Othman, "Effect of Conduction Pre-heating in Au-Al Thermosonic Wire Bonding," *Journal of Surface Engineered Materials and Advanced Technology,* vol. 2011, 2011.

[108] S. Lee, M. J. Yim, R. N. Master, C. Wong, and D. F. Baldwin, "Void formation study of flip chip in package using no-flow underfill," *IEEE Transactions on Electronics Packaging Manufacturing,* vol. 31, pp. 297-305, 2008.

[109] C. A. Palesko and E. J. Vardaman, "Cost comparison for flip chip, gold wire bond, and copper wire bond packaging," in *2010 Proceedings 60th Electronic Components and Technology Conference (ECTC)*, 2010, pp. 10-13.

[110] H. Patel, "Fabrication and Optimisation of Resonant Tunnelling Diode's (RTD's)," MSc, school of electronic and electrical engineering, University of Leeds, school of electronic and electrical engineering, 2013.

[111] R. Li, T. G. Lim, and S. W. Ho, "273-GHz 2X subharmonic up-conversion mixer for system-on-package applications," *Components, Packaging and Manufacturing Technology, IEEE Transactions on,* vol. 2, pp. 1980-1984, 2012.

[112] C. Mishra, U. Pfeiffer, R. Rassel, and S. Reynolds, "Silicon Schottky diode power converters beyond 100 GHz," in *Radio Frequency Integrated Circuits (RFIC) Symposium, 2007 IEEE*, 2007, pp. 547-550.

[113] U. R. Pfeiffer, C. Mishra, R. M. Rassel, S. Pinkett, and S. K. Reynolds, "Schottky barrier diode circuits in silicon for future millimeter-wave and terahertz applications," *Microwave Theory and Techniques, IEEE Transactions on,* vol. 56, pp. 364-371, 2008.

[114] H.-C. Yeh, C.-C. Chiong, M.-T. Chen, and H. Wang, "Review of Millimeter-Wave MMIC Mixers," *Design & Test, IEEE,* vol. 31, pp. 38-45, 2014.